Strong Wintertime Ozone Events in the Upper Green River Basin, Wyoming

Bernhard Rappenglück[1, *], Luis Ackermann[1], Sergio Alvarez[1], Julia Golovko[1], Martin Buhr[2], Robert Field[3], Jeff Soltis[3], Derek C. Montague[3], Bill Hauze[4], Scott Adamson[4], Dan Risch[4], George Wilkerson[4], David Bush[5], Till Stoeckenius[6], Cara Keslar[7]

[1] Department of Earth and Atmospheric Sciences, University of Houston, Houston, Texas, USA

[2] Air Quality Design, Boulder/CO, USA

[3] University of Wyoming, Laramie/WY, USA

[4] Meteorological Solutions Inc., Salt Lake City/UT, USA

[5] T&B Systems, Santa Rosa/CA, USA

[6] Environ, Novato/CA, USA

[7] Wyoming Department of Environmental Quality, Cheyenne/WY, USA

[*] Corresponding author: University of Houston, Department of Earth and Atmospheric Sciences, 4800 Calhoun Rd, Houston, TX 77204-5007,
Tel.: 713-893-1298, Fax: 713-748-7906, e-mail: brappenglueck@uh.edu

Abstract

During recent years, elevated ozone (O_3) values have been observed repeatedly in the Upper Green River Basin (UGRB), Wyoming during wintertime. This paper presents an analysis of high ozone days in late winter 2011 (1-hour average up to 166 ppbv). Intensive Operational Periods (IOPs) of ambient monitoring were performed which included comprehensive surface and boundary layer measurements. On IOP days, maximum O_3 values are restricted to a very shallow surface layer. Low wind speeds in combination with low mixing layer heights (~50 m above ground level around noontime) are essential for accumulation of pollutants within the UGRB. Air masses contain substantial amounts of reactive nitrogen (NO_x) and non-methane hydrocarbons (NMHC) emitted from fossil fuel exploration activities in the Pinedale Anticline. On IOP days in the morning hours in particular, reactive nitrogen (up to 69%), aromatics and alkanes (~10-15%; mostly ethane and propane) are major contributors to the hydroxyl (OH) reactivity. Measurements at the Boulder monitoring site during these time periods under SW wind flow conditions show the lowest NMHC/NO_x ratios (~50), reflecting a relatively low reactive NMHC mixture, and a change from a NO_x-limited regime towards a NMHC limited regime as indicated by photochemical indicators, e.g. O_3/NO_y, O_3/NO_z, and O_3/HNO_3 and the EOR (Extent of Reaction). OH production on IOP days is mainly due to nitrous acid (HONO). On a 24-hr basis HONO photolysis on IOP days can contribute ~83% to OH production on average, followed by alkene ozonolysis (~9%). Photolysis by ozone and HCHO photolysis contributes about 4% each to hydroxyl formation. High HONO levels (maximum hourly median on IOP days: 1,096 pptv) are favored by a combination of shallow boundary layer conditions and enhanced photolysis rates due to the high albedo of the snow surface. HONO is most likely formed through (i) abundant nitric acid (HNO_3) produced in atmospheric oxidation of NO_x, deposited onto the snow surface and undergoing photo-enhanced heterogeneous conversion to HONO (estimated HONO production: 10,206 pptv/hr) and (ii) combustion related emission of HONO (estimated HONO production: ~70 pptv/hr). HONO production is confined to the lowermost 10 m of the boundary layer. HONO, serves as the most important precursor for OH, strongly enhanced due to the high albedo of the snow cover (HONO photolysis rate 10,276 pptv/hr). OH radicals will oxidize NMHCs, mostly aromatics (toluene, xylenes) and alkanes (ethane, propane), eventually leading to an increase in ozone.

Deleted: Until noon on IOP days, HONO photolysis contributes between 74-98% of the entire OH-production.

Deleted: Ozone photolysis (contributing 2-24%) is second to HONO photolysis. However, both reach about the same magnitude in the early afternoon (close to 50%). Photolysis of formaldehyde (HCHO) is not important (2-7%).

Deleted: 2

Deleted: 50

Deleted: 585

Deleted: 2

Deleted: 900

Key word index: wintertime ozone, Upper Green River Basin, HONO, oil and gas production

1 Introduction

The Upper Green River Basin (UGRB) has one of the largest natural gas reserves of the United States (US). In 2009, the proven gas reserves for the Jonah field (11.1 billion cubic meters) ranked seventh and for the Pinedale Anticline field (13.8 billion cubic meters) ranked third among the top 100 natural gas fields in the US (EIA, 2009). Oil and Gas extraction including drill rigs, production equipment and compressor stations are operating continuously and represent the only significant emission source in the UGRB with overall emissions of 9.9 metric tons/day of reactive nitrogen (NO_x) and 41.7 metric tons/day of volatile organic compounds (VOC) (WDEQ, 2011).

The UGRB is a high plateau located about 2,000 m above sea level (asl). It is surrounded by mountain ranges which reach heights up to 3,500 m asl to the West (Wyoming Peak) and 4,200 m asl to the Northeast (Gannett Peak). Winters are usually cold and frequently associated with snow cover. During recent years, elevated hourly ozone values above 150 ppbv have been observed in the UGRB during wintertime (Schnell et al., 2009; Carter and Seinfeld, 2012). As of July 2012, the U.S. Environmental Protection Agency (EPA) declared the UGRB as a non-attainment area for the 2008 ground-level 8-hour ozone standard, which is 75 ppbv. Recent publications have focused on some observational findings in the UGRB in the year 2008 (Schnell et al., 2009) or sensitivity analysis using a box model approach together with VOC (Volatile Organic Compound) incremental reactivities for selected ozone episodes in 2008 and 2011 (Carter and Seinfeld, 2012). Still, there are major uncertainties in our understanding of the occurrence of high ozone levels in the UGRB under wintertime conditions. Apart from specific meteorological conditions for the UGRB (i.e. low mixing layer heights, light winds, extensive snow cover, at times recirculation of air masses), these include processes in the nitrogen oxide (NO_x) and VOC cycles, such as the role of nitric acid (HNO_3) and the radical precursors such as formaldehyde (HCHO) and nitrous acid (HONO). In particular, high daytime HONO levels were found (Rappenglück, 2010 and 2011). Although HCHO levels were moderate, the sources and role of HCHO in the UGRB is not fully understood, particularly with regard to the overall relatively low alkene reactivity as shown by Carter and Seinfeld (2012). A better quantification of these hydroxyl (OH) sources is needed to improve the description of ozone chemistry in the UGRB, which is required to develop efficient strategies to reduce pollution in that area.

In this paper we analyze high ozone days in late winter 2011 (1-hour average up to 166 ppbv) observed in the area of the Boulder station and describe the meteorological and chemical

processes leading to these extreme events using the comprehensive surface and boundary layer measurements collected during the Upper Green Winter Ozone Study (UGWOS) 2011 (MSI, 2011).

2 Methods

Surface air quality data used in this paper were collected continuously at the Boulder site and Boulder South Road site from January - March 2011 (for Boulder South Road site data see also Field et al., 2011). Boundary layer measurements including radiosonde and ozonesonde launches were performed at the Boulder site during Intensive Operational Periods (IOPs). Data from the tethered balloon were obtained at the "Tethered Balloon" site. S1 lists the details of the instrumentation and Figure 1 shows the location of these sites in the UGRB including the locations of oil and gas wells.

Surface measurements included routine measurements for ozone (O_3), reactive nitrogen compounds ($NO/NO_2/NO_x$), total non-methane hydrocarbon (NMHC), methane (CH_4) and trace level measurements for nitrogen monoxide (NO), nitrogen dioxide (NO_2), and total reactive nitrogen (NO_y). Additional measurements included nitric acid (HNO_3), nitrous acid (HONO), formaldehyde (HCHO), carbon monoxide (CO) and online speciated NMHC. If not otherwise indicated the term NMHC denotes total, i.e. non-speciated NMHC measured at the Boulder or "Tethered Balloon" site. A specific measurement design was applied for the HONO measurements. The sampling unit for the HONO measurements was attached to a small tower. The sampling unit stayed at the surface (10 cm above the ground) for 15 min, then moved to the top of the tower (1.80 m above the ground), where it stayed for another 15 min, afterwards the unit returned back to the surface and resumed a new cycle. Upward and downward motions lasted 2 min and were accomplished by a step motor. The purpose was to explore whether HONO gradients close to the surface could be detected. Note: for comparison of HONO data with any ancillary chemistry and meteorological data obtained in this study (e.g. as shown in table S2), HONO data collected at 1.80 m above the surface was used.

At all sites, basic meteorological measurements were made. Additional details beyond the information provided in S1 can be found in MSI, 2011. Here we briefly describe the methodology for the HONO measurements. For the UGWOS 2011 study a commercially available LOPAP® (Long Path Absorption Photometry) instrument was used (QUMA Elektronik & Analytik GmbH, Wuppertal, Germany). The LOPAP® is described thoroughly in Heland et al. (2001) and Kleffmann et al. (2002). It is a wet-chemical in situ instrument

which consists of an external sampling unit where ambient gaseous HONO is directly sampled in a stripping coil using a mixture of sulfanilamide in hydrochloric acid. No sampling lines are used thus minimizing sampling artifacts on surfaces. The stripping reagent is transferred through an insulated transfer line (length: 3 m; outer diameter 5 cm; kept at 20°C) to the instrument where it is converted to an azodye by the reaction with N-naphtylethylendiamine-dihydrochloride. The absorption, more precisely the logarithm of the ratio between the spectral intensity at 650 nm and 550 nm, is measured in long path absorption tubes made of Teflon AF2400 using a two channel minispectrometer (Ocean Optics S2000). In the external sampling unit two stripping coils are used in series. In the first channel HONO as well as possible interferences are determined, while in the second channel only the interferences are quantified. The difference of these two channels yields the HONO signal.

For routine zeroing ultra-high purity nitrogen (UHP N2) was applied every 8 hrs for 30 min directly to the inlet of the external sampling unit by a 1/32" PFA tubing which was partially inserted into the tip of the stripping coil. A linear (or polynomial) fit was calculated for the stable reading and used as the zero baseline. Calibrations were always preceded by zero-measurements. For calibration itself the stripping solution was replaced by 0.01 mg NO_2- per liter stripping solution, while UHP N2 was flowing into the inlet of the external sampling unit. Final calibration values were calculated using the calibration standard concentration and the measured gas and liquid flow rates.

The sampling time is 30 s. The response time, i.e. the time it takes for the signal to go from 100% to 10% of the initial value or from 0% to 90% of the final value, changes every time a new set of peristaltic pump tubing is installed, yet is stable for any given set of tubings. The response time was determined for each set of tubing and ranged between 3.45 - 6.15 min. The time correction used to create the time stamp reported was equal to the sum of the time delay and half the response time, which ranged accordingly between 6.67 - 10.08 min. This time stamp was used to properly allocate air samples to the bottom or up position of the small tower.

The LOPAP® instrument has been tested against DOAS measurements both in smog chamber studies as well as in field campaigns (Kleffmann et al., 2006). Excellent agreement was obtained between these techniques during daytime as well as nighttime. The UH LOPAP instrument recently participated in a large intercomparison chamber instrument (Ródenas et al., 2011) and in a recent field intercomparison (Pinto et al., 2013). So far, interferences were

found to be negligible in most atmospheric air masses (Heland et al., 2001; Kleffmann et al., 2002). Some interferences were found for nitrites (Ródenas et al, 2013), however at nitrite levels orders of magnitude above atmospheric concentrations. The instrument has been tested under polar conditions (Kleffmann and Wiesen, 2008; Villena et al., 2011). Interferences with peroxynitric acid (HO_2NO_2) were found to be less than 0.5% (Ammann, 2013).

3 Results and discussion

3.1. General observations

The Upper Green River Basin had continuous snow cover throughout the winter months January-March 2011. Figure 2 shows that ambient temperature was below freezing most of time, ranging from -28.0°C in early February to +5.1°C in mid-March. Also displayed in the same figure are ambient ozone observations. A slight increase in background ozone from 45 ppbv in January to about 50 ppbv in March is discernible. Apart from this longer term variation, it can clearly be seen that at times significant day-to-day variations in the ozone mixing ratios may occur. While decreases of ozone are reflecting NO titration effects, strong increases of ozone well above the ozone background level are likely due to a combination of dynamic and photochemical processes. During the time frames February 28 - March 02 and March 9 - 12, 2011, the highest hourly ozone readings were observed with up to 166 ppbv at the Boulder surface site on March 02. IOPs were performed during these two periods (IOP#1: 02/28-03/02; IOP#2: 03/09-03/12), which included additional information about the vertical distribution of meteorological parameters as well as some selected trace gases. The following discussions will focus on the time period 2/28 – 3/16/2011. This time period includes the two IOPs and has the most complete data availability with regard to continuous as well as discrete measurements. The non-IOP days during this time frame will be used as reference days.

Figures 3a and b display mean diurnal variations of O_3, NO, NO_x,NMHC, CH_4, NO_y, HNO_3, HONO, and HCHO split into IOP and non-IOP days. Most species show 2-3 times higher mixing ratios on IOP days compared with non-IOP days throughout the day. Ozone shows this enhancement during the afternoon and early evening only. Primarily emitted species like NO show maximum values during the time frame 9:00-12:00 MST (Mountain Standard Time). Species which also can be formed secondarily (e.g. NO_y, HNO_3, HONO, and HCHO) exhibit enhanced levels during sunlit daytime hours from about 07:00 - 18:00 MST, in particular on IOP days. Ozone mixing ratios start to increase by 09:00 MST, reach maximum levels around 15:00 MST and remain at higher levels until early evening. Quite surprisingly,

HONO mixing ratios are high during the daytime on non-IOP days and even higher on IOP days (maximum median around noontime 1,096 pptv) which, compared to other locations, is quite unusual (see e.g. Stutz et al., 2010a). Conventional thinking suggests that HONO levels would instead decrease due to both photolysis and to increased mixing in the boundary layer during the day. The median HONO levels on IOP days are similar to those observed at a highly frequented Houston highway junction (Rappenglück et al., 2013).

A statistical summary for IOP and non-IOP days is given in S2. In the following discussion, we refer to median values. It shows that in the morning hours (0500-0900 MST), the median mixing ratios of most species are enhanced by a factor of 2 on IOP days vs non-IOP days. Some are almost unchanged (e.g. HNO_3, NO_y, ozone). During photochemically active daytime periods (11:00-17:00 MST), the median of most compounds is enhanced by 50-100%, HCHO is enhanced by 171% and HONO by as much as 278%, which hints to significant secondary daytime formation of these species. During the nighttime period, NO_x (mostly composed of NO_2) and HNO_3 show the highest enhancements on IOP days (121% and 138%, respectively). HONO and HCHO are also enhanced (98% and 64%, respectively). Overall, on IOP days trace gases relevant to O_3 formation are all significantly enhanced throughout the day compared with non-IOP days.

The only major anthropogenic emissions in the remotely located UGRB are associated with oil and gas extraction. As a benchmark for this study we compare some results to a highly polluted urban area. Luke et al. (2010) report results of reactive nitrogen compounds for Houston, Texas, a city exposed to complex emissions including emissions from large petrochemical sources (e.g. Parrish et al., 2009; Lefer and Rappenglück, 2010; Olaguer et al., 2013). An investigation of the same daytime periods shows that, while NO_x is significantly higher in the urban air of Houston (about 2-4 times higher when compared to IOP days at Boulder), the picture is different for NO_y. Although NO_y is higher in Houston in the morning and during the night (275% and 186%, respectively), it is lower in Houston than in Boulder during daytime on IOP days. These differences are largely due to HONO and HNO_3. While HONO is slightly lower in the morning and during the night, it is about three times higher during the daytime on IOP days. HNO_3 on the other hand is higher throughout the day on IOP days in Boulder compared to the Houston case. On non-IOP days at Boulder, HONO and HNO_3 levels are mostly lower than in Houston. The HNO_3 fraction of NO_y is around 18% during daytime on non-IOP days, while it is around 22% during daytime on IOP days (Luke et al., 2010, report an overall daytime HNO_3 fraction of 15.7% of NO_y in Houston). For HONO

Deleted: emissons

the corresponding numbers are around 2% (non-IOP days) and 4.5% (IOP days), while Luke et al. report an overall daytime HONO fraction of 1.7% of NO_y.

Luke et al. (2010) also report temporally highly resolved data for particulate nitrate NO_3^- (p-NO_3^-). Median values were 0.234 ppbv (05:00-09:00 CST), 0.091 (11:00-17:00 CST), and 0.135 ppbv for nighttime (21:00-05:00 CST). At Boulder, 24 hour samples were collected. Although not exactly comparable, it may provide us with some estimate. On IOP days, the median value for p- NO_3^- was equivalent to 0.58 ppbv (maximum equivalent to 1.54 ppbv), while on non-IOP days the corresponding values were equivalent to 0.47 ppbv and 0.74 ppbv, respectively, which indicates that p- NO_3^- may be higher at the Boulder site than in Houston.

S3 shows a comparison of NO_y measurements versus individual NO_y compounds for the Boulder site. Particulate data was only collected on a 24 hour basis. Therefore this data set only comprises a small number of observations. The deviation from the 1:1 line is within the accuracy of the NO_y and the combined individual NO_y measurements (see S1) for ranges above 20 ppbv. For NO_y values below 20 ppbv, NO_y tends to be larger than the sum of the individually measured NO_y components. According to S3, still some fraction of NO_y compounds may be missing, even when particulate NO_3 was included. Potential candidates for this NO_y deficit include the nitrate radical (NO_3), dinitrogen pentoxide (N_2O_5), nitrylchloride ($ClNO_2$), peroxy acetylnitrate (PAN) and alkyl nitrates. While NO_3, N_2O_5, and $ClNO_2$ would be present at nighttime (e.g. McLaren et al., 2004; Edwards et al., 2013), PAN and alkyl nitrates are produced photochemically and tend to reach maximum values during daytime (e.g. Hayden et al. 2003; Sommariva et al., 2008 and references therein). No measurements of these species were performed at the Boulder site, however some assumptions can be made. Maximum NO_3 and N_2O_5 levels typically range from about 50 pptv and 300 pptv, respectively, in polluted continental air masses (McLaren et al., 2004) to about 150 pptv and 500 pptv, respectively, in urban areas (Stutz et al., 2010b). NO_3 and N_2O_5 can constitute 7-30% of NO_y (McLaren et al., 2004 and references therein). NO_3 is formed through the reaction of NO_2 with O_3. It is likely that this reaction may be efficient at the Boulder site due to the observed appreciable ambient levels of NO_2 and O_3 (see S2 and Figure 2). Loss mechanisms for NO_3 include reactions with alkenes and biogenic hydrocarbons, and reaction with NO_2 to form N_2O_5. As alkenes and biogenic hydrocarbons are found at low levels in the UGRB (Field et al. 2012a; 2012b), while abundant NO_2 is present, the latter reaction to form N_2O_5 is likely the dominant removal process for NO_3. In addition, low ambient temperatures would favor this process. The homogeneous and heterogeneous

hydrolysis of N_2O_5 may ultimately lead to appreciable amounts of gaseous HNO_3 and particulate nitrate according to McLaren et al, 2004. While no direct measurements of $ClNO_2$ were performed at the Boulder site, particulate chloride (Cl^-) data show low median levels of 0.015 $\mu g/m^3$ (based on 6 24-hr filter samples). This may indicate that Cl^- is not abundantly available to form $ClNO_2$ in appreciable amounts, likely less than 600-800 pptv found in the Uintah Basin in Utah (Edwards et al., 2013). Earlier studies in the UGRB also included PAN measurements (Environ, 2010). The results showed up to 1 ppbv PAN during daytime and up to 400 pptv as an estimated 24 hour average, while corresponding ozone values were 85 ppbv and 51 ppbv, respectively, i.e. PAN was ~1% of the ozone mixing ratios, which lies in the range observed in remote areas (e.g. Rappenglück et al., 2003). Most important precursor candidates for PAN in the UGRB will be ethane, toluene and xylenes. As high PAN values would also coincide with high NO_y values, we assume that PAN would only account for a negligible amount of around 1% percent of the NO_y budget based on the results shown in S3. Alkyl nitrates may account for about 10% of NO_y (Sommariva et al., 2008 and references therein). As alkyl nitrates have an atmospheric lifetime of more than a week they may accumulate under favorable meteorological conditions and contribute to the NO_y budget not only during the day, but also at night. We predominantly found lower values for NO_y at night (see Figure 3b), i.e. at a time when the missing NO_y components NO_3, N_2O_5, $ClNO_2$, and also alkyl nitrates would contribute most to the NO_y budget. This may explain the deficit found in the NO_y budget at NO_y mixing ratios below 20 ppbv.

Deleted: MSI, 2009

Deleted: .

Corresponding analysis for NO_x oxidation products NO_z ($NO_z = NO_y - NO_x$) versus the sum of individual NO_z compounds NO_{zi}, i.e. HNO_3, HONO and p-NO_3^- based on a 24 hour data base yielded NO_z [ppbv] = ΣNO_{zi} [ppbv] * 1.09 - 0.38 ppbv (r^2=0.87) for IOP days and NO_z [ppbv] = ΣNO_{zi} [ppbv] * 1.12 + 0.28 ppbv (r^2=0.82) for non-IOP days, which is of similar magnitude as found in Houston (Luke et al., 2010), for instance. Luke et al. point out that higher nighttime NO_z/NO_{zi} ratios and the magnitude of NO_z - NO_{zi} differences may point to the presence of nighttime $ClNO_2$. Based on our limited data we cannot make similar statements, but cannot rule out this possibility. Our measurements did not include PAN. Using our previous assumptions of about 400 pptv as an estimated 24 hour average value, PAN could contribute up to 5% of the NO_z budget. The atmospheric lifetime of PAN (τ_{pan}) is primarily determined by the following reactions:

$$CH_3C(O)OONO_2 \rightarrow CH_3C(O)OO + NO_2 \qquad (1)$$

$CH_3C(O)OO + NO_2 \rightarrow CH_3C(O)OONO_2$ (2)

$CH_3C(O)OO + NO \rightarrow CH_3C(O)O + NO_2$ (3)

The atmospheric lifetime of PAN thus critically depends on the NO_2/NO ratio and also the ambient temperature, since reaction constant k_1 is proportional to exp(-1/T). Based on reactions (1)-(3), τ_{pan} can be calculated according to Ridley et al. (1990):

$$\tau_{PAN} = \frac{1}{k_1}(1 + \frac{k_2[NO_2]}{k_3[NO]}) \quad (4)$$

For the Boulder site, the shortest τ_{pan} for IOP#1 was 10.6 days and for IOP#2 2.6 days and reached almost 1 day on the last day of the field study (March 16) when temperature reached +5.1°C. It is thus unlikely that PAN may serve as a NO_2 source and contribute to ozone formation under the environmental conditions found during the study. However, it can serve as a reservoir for NO_x and radicals and remove NO_x and radicals out of the UGRB.

Deleted: reservoir

3.2. Role of Meteorological Parameters

3.2.1 Dependence on Wind Direction

S4 and b display daytime and nighttime wind roses of O_3, primarily emitted pollutants NO_x, NMHC, CH_4, and trace gases that may have both primary and secondary sources, i.e. NO_y, HNO_3, HONO, and HCHO. S4a and b include both IOP and non-IOP days in order to obtain larger and more representative data sets. Regardless of IOP and non-IOP days, night-time data will most likely be useful to point to potential emission sources as photochemical processes are at a minimum.

The daytime ozone wind rose clearly shows enhanced mixing ratios for SSW to WSW and SE/ESE directions (median 64-73 ppbv). During nighttime, maximum median ozone of about 60 ppbv occurs under NNE-ENE wind directions. These wind directions only have small amounts of NO_2 (median about 1.5 ppbv; not shown) and are likely more aged air masses. Primarily emitted NO_x, NMHC, and CH_4 display pronounced enhancements during the daytime in the similar directions as for O_3. During nighttime there are significant peaks under SW-W wind directions. While NO_x and NMHC are distinctly enhanced (NO_x ~10 ppbv, NMHC ~900 pptv), still CH_4 with about 4 ppm is a factor of 2 above its background levels.

This hints to sources which emit nitrogen oxides, NMHC and CH_4 or different sources located in the same area which may overlap. This is likely consistent with locations of compressors and drill rigs operating during January – March 2011 (which emit primarily NO_x) relative to well head production equipment (which emits primarily CH_4 and NMHC).

NO_y, HNO_3, HONO, and HCHO (S4b) largely follow the same directional pattern as NO_x and hydrocarbons (S4a). However, contrary to the primarily emitted pollutants NO_x, NMHC, and CH_4, species which may be formed secondarily, i.e. HNO_3, HONO, and HCHO, generally show higher values during daytimes. It is known that HCHO may be emitted primarily from incomplete combustion in either mobile or stationary sources (Zweidinger et al., 1988; Altshuller, 1993; Chen et al., 2004; Dasgupta et al., 2005; Rappenglück et al., 2013). Also, HONO can be emitted primarily from various combustion processes (Kirchstetter et al., 1996; Kurtenbach et al., 2001; Rappenglück et al., 2013) with traffic emissions being an important contribution to ambient HONO (Sarwar et al., 2008).

NO_y behaves somewhat similarly to the primary pollutants, most likely due to the large fraction of NO_x in NO_y (see S2). Interestingly, HONO clearly shows an anisotropic dependence on wind direction, both during night- and daytime, which indicates a point source rather than an area source like the surface. During daytime, HONO mixing ratios are highest from WSW to SSW (median 477 pptv to 545 pptv, respectively), while at night maximum mixing ratios occur under WSW wind direction (median 347 pptv). While the nighttime HONO peak for WSW flow is in accordance with those for other trace gases and hints at a point source, the high daytime HONO levels (see also S2) are at odds with the conventional understanding of HONO diurnal variability, suggesting that additional processes other than point source emissions (e.g. Czader et al., 2012 and references therein) may be important.

Deleted: also

Deleted: This indicates their dual nature, i.e. primarily emitted (as reflected in the nighttime data) and, in addition, secondarily formed (as seen in the daytime data).

Deleted: similarily

3.2.2 Backward Trajectories

For further analysis, we calculated HYSPLIT (HYbrid Single-Particle Lagrangian Integrated Trajectory) backward trajectories (Draxler and Hess, 2013, Rolph, 2013) based on 12 km resolution meteorological data provided by NAM (North American Mesoscale model). Uncertainties stated by Draxler and Hess are in the range of 15-30% of the travel distance. As an additional test, we calculated back and forward trajectories within the UGRB for the times of interest and found only negligible difference among those. Although, there might be some limitations associated with the accuracy of backward trajectories, they at least may provide information about major regimes. The results of trajectory calculations are shown in Figure 4

and they indicate three major regimes during the 2/28 – 3/16/2011 period. Non-IOP days mostly showed consistent air mass flows out of the NW wind sector (example shown 3/8/2011). Also, they are associated with higher wind speeds and enhanced atmospheric dispersion. This coincides with the generally low to modest levels of pollutants (S4a and b). The days with the highest ozone levels during each IOP may show recirculation processes during the day (as for March 03, 2011); however, they are usually characterized by the fact that at least once during the day, trajectories eventually pass through the area Southwest of Boulder before arriving at Boulder. According to Figure 1, air masses would then pass the oil and gas well locations of the Pinedale Anticline and also a large number of compressor facilities (Figure 5). According to the trajectories on March 12, air masses would have passed this sector at the most 1-2 hours before arrival at Boulder and would have stayed in that region for about 1 hour. As seen in S4a and b, air masses coming from the SW quadrant carry maximum amounts of both primary and secondary pollutants. As shown later, they are also associated with the highest VOC reactivity and a change of NO_x sensitivity towards a VOC sensitivity regime.

3.2.3 Boundary Layer Height

Tethersonde data taken on IOP days indicate very shallow boundary layer heights. Based on the data in S5 and using approaches by Stull (1988), average morning boundary layer heights (09:00-11:00 MST) would be estimated to be about 35 m above ground level (agl) around noon (11:00-13:00 MST), around 50 m agl in the early afternoon (13:00-15:00 MST), reach a daily maximum around 80 m agl, and in the late afternoon (15:00-17:00 MST) decrease to around 45 m agl. This is largely in agreement with SODAR data (not shown). Figure 6 shows vertical profiles of ozone and wind direction on IOP days. Generally, IOP days were characterized by W to NW flows above 600 m agl and appreciable temporal and spatial changes in wind direction below this level. These lower level changes are also reflected in the backward trajectories previously shown in Figure 4. Below 600 m agl, windspeed was generally less than 5 m/s. Above 600 m agl, wind speed rapidly increased above 10 m/s (not shown). The strong changes in atmospheric flow around 600 m agl certainly helps to maintain inversions and stable boundary layer conditions beneath this layer throughout IOP days. Since surrounding mountain ranges of the UGRB reach heights up to 3,500 m asl to the West (Wyoming Peak) and 4,200 m asl to the Northeast (Gannett Peak), the boundary layer air masses are easily trapped within the basin and recirculation processes as shown for March 02

in Figure 4 are likely. This is in accordance with earlier wintertime meteorological studies in similar areas of the Rocky Mountains (Yu and Pielke, 1986).

Figure 6 shows that ozone exhibits a distinct behaviour associated with the atmospheric dynamic pattern: above 600 m agl, ozone mixing levels are quite stable around 60 ppbv regardless of the day and time of the day. It represents background ozone levels in the well mixed lower troposphere. Below 600 m agl, ozone mixing ratios clearly show diurnal changes with lower than background values in the early morning and strongly enhanced values in the afternoon. The maximum deviations are clearly restricted to a very shallow surface layer. There is no evidence of ozone carry over from previous days. Ozone deposition over dry surfaces is about 0.4 cm/s (Hauglustaine et al., 1994); however, it is about 0.07 cm/s over snow surfaces (Hauglustaine et al. 1994), i.e. ozone removal through turbulent diffusion is significantly reduced. Recent studies over polar snow indicate even lower deposition velocities in the range of 0.01-0.07 cm/s (Helmig et al., 2009). As deposition may play a minor role during snow covered periods in the UGRB, the ozone deviation from the background ozone level is instead determined by removal (e.g. nighttime titration) and daytime in-situ formation processes.

As an example, Figure 7 shows selected data obtained by the tethersonde system for the IOP day March 02, 2011. The results for ΔT (Delta-T in the plot) indicate well defined inversion and stable conditions in levels with $\Delta T > 0$ °C. Again, it can be seen that highest ozone levels are restricted to the surface levels. Precursors such as NO_2 and NHMC may exhibit a layered distribution. Highest levels may occur close to the mixing layer height as defined by ΔT. This hints to pollution plumes which may have originated from either elevated sources and/or sources which show some plume rise due to higher than ambient temperatures. Potential ozone O_x, as expressed by the sum of O_3 and NO_2 provides information about the potential presence of O_3 formation processes. Using the tethersonde data and segregating it into time frames like in S5, we obtain S6. This figure shows two main features: (i) formation of O_3 from early morning to the afternoon throughout the surface layer and (ii) apart from the late afternoon, a tendency towards higher O_x values in higher layers of the surface layers. Highest O_x mixing ratios at the surface occur only in the late afternoon.

In an attempt to investigate other trace gases for which no vertically resolved data is available, we segregated surface data into 5 m bins of hourly SODAR mixing layer height (MLH) data and split it into day- and nighttime observations. Results are shown in S7. For ozone, daytime data is clearly higher than nighttime data regardless of the MLH. However, during daytime,

maximum ozone levels are observed under lowest MLH. Speciated NMHC data obtained at the Boulder South Road site generally show enhanced values under MLH < 40 m agl and decreasing concentrations with increasing MLHs regardless of the time of day. However, while higher nighttime concentrations of speciated NMHC classes are found at lower MLHs, during daytime, the lowest MLHs are associated with lower concentrations of NMHC classes. Assuming NMHC sources which do not change emission strength during the day, this points to photochemical degradation of NMHCs in the lowermost surface layers. The change in the median values is about -20% for alkanes, - 45% for alkenes, and almost -50% for aromatics. CO does not change significantly with MLH and time of day. NO_x shows significantly higher values during daytime and, contrary to NMHC classes, there is no change at lowermost MLHs when comparing daytime with nighttime observations. However, nighttime data clearly shows decreasing NO_x levels with increasing MLHs. Both HCHO and HONO show higher values during the daytime than nighttime regardless of MLHs. In accordance with other primary pollutants like NMHC and NO_x, HCHO and HONO exhibit a trend towards lower mixing ratios with increasing MLHs during nighttime.

In general, results from IOP days, such as March 02 and 12, indicate that slightly variable wind directions (including recirculation) and low wind speeds in combination with low boundary layer heights are essential for accumulation of both primary and secondary pollutants. The occurrence of low boundary layer heights in presence of snow cover in mountainous regions is in accordance with previous model simulations (Bader and McKee, 1985). These studies also showed that these conditions can hold a stable layer until very late in the day.

Deleted: reciruclation

3.2.4 HONO and relationships with radiation and relative humidity

Some photo-enhanced heterogeneous reactions are currently being discussed as likely daytime HONO sources (Kleffmann, 2007). S8 shows a comparison of HONO data obtained close to the surface (10 cm above the surface) and at about 1.80 m above the surface. The plot contains all data of the 2/28-3/16/2011 period, as segregation into IOP and non-IOP days would have resulted into patchier time series with larger intermittent data gaps. To some extent S8 may provide some general characterization. S8 reflects the main results of Figure 3b with higher HONO levels during the daytime. However, two additional observations are evident: (i) scatter in the HONO data is greater at the 1.80 m level, where maximum concentrations are found in the morning and early afternoon. The absence of these early morning high levels in

Deleted: It

the surface data suggest that the observed maximum at 1.80 m may be due to transport of HONO rather than a surface source most likely due to the stratified properties of the planetary boundary layer (PBL) with suppressed vertical mixing during these times (see chapter 3.6), (ii) The median HONO values at the surface show a significant increase around noon coinciding with the strongest solar irradiation, and surpass those at the 1.80 m level. This suggests a strong surface source of HONO which is most efficient around noontime. According to Villena et al. (2011), HONO photolysis can be the most important OH radical source in polar regions under clean conditions (e.g. in polar regions), in particular when HONO was not correlated to CO and NO_x, which would otherwise hint to direct emissions. From S8 and S4b, it is evident that daytime photochemical processes contribute to HONO formation at the Boulder site, while transport is important throughout the day. Potential direct combustion related emissions will be discussed later.

Deleted: .

As pointed out by Stutz et al. (2004), relative humidity may be favorable for HONO formation, at least in urban environments. S9 shows that on IOP and non-IOP days, HONO levels are higher during the day than at night, regardless whether the measurements were taken close to the surface or at 1.80 m agl. During nighttime, photochemical processes are at a minimum. A trend towards higher HONO levels with increasing higher relative humidity can be discerned, with a maximum around 80%,. Again, this does not seem to depend on the measurement height. A dependency of the $HONO/NO_2$ ratio on relative humidity as described by Stutz et al. (2004) could not be identified in our data set, likely due to the fact that the snow cover itself provided a constant amount of water, which would be in line with observations by Wojtal et al. (2011) for aqueous surfaces.

3.3. Role of Emissions and Chemistry

3.3.1 Potential combustion emissions for radical precursors HCHO and HONO

Primary sources for HCHO and HONO are important sources for the hydroxyl radical (e.g. Ren et al., 2013; Czader et al., 2013). While HCHO may have a variety of primary sources, its secondary formation during daytime usually exceeds primary HCHO emissions significantly (e.g. Rappenglück et al., 2010 and references therein). This is also reflected in the Boulder site data when comparing daytime HCHO data on IOP vs. non-IOP days (see S2 and Figure 3b). However, secondarily produced HCHO does not provide a net OH source as the formation of OH already consumed OH.

Unfortunately, there were no CO measurements taken at the Boulder site, but linear regression analysis of CO versus NO_x calculated for the Boulder South Road site indicate CO [ppbv] = 6.14 × NO_x [ppbv] + 140 [ppbv] (r^2=0.55) over all wind directions for the entire time period 2/28-3/16/2011. The slope is very close to values obtained for urban traffic rush hour, which is 6.01±0.15 ppbvv CO / 1 ppbv NO_x (Rappenglück et al., 2013). While the correlation coefficient is significantly weaker than found in the Rappenglück et al. (2013) study (r^2=0.91), which may be due to higher degree of mixing of different air masses, it indicates the presence of combustion sources; under remote unpolluted conditions CO and NO_x would be almost unrelated (see e.g. Villena et al., 2011).

As previously mentioned, compressors and drill rigs were operating during January – March 2011 in the area located upwind of the Boulder site under SW flow conditions. These units emit primarily NO_x relative to well head production equipment which primarily emits CH_4 and NMHC. As indicated in S4a and b, enhanced levels of primary pollutants occur under SSW-W flows during daytimes and under SW-W flows during the night. In an attempt to identify potential emission sources for HCHO and HONO, we performed correlation analyses with various other trace gases measured at the Boulder site focusing on nighttime data, to exclude daytime photochemical processes and SW-W wind directions which showed peak values for all species in accordance with S4a and b. NO_z/NO_y ratios were around 0.35 under these wind flow conditions and thus, significantly less than 0.6, indicating freshly emitted pollutants.

Deleted: focussing

S10 clearly shows the close relationship between HONO and NO_2, NO_x, and HNO_3 as observed at the Boulder site. The good, although somewhat weaker, correlation of HONO with total NMHC at the Boulder site is most likely due to the fact that emission sources which emit NO_x may be located close to NMHC sources. HCHO shows overall weaker correlations with NO_x, total NMHC, and CH_4 compared with HONO. HCHO has a longer atmospheric lifetime than HONO (~6-7 hrs for HCHO vs. ~5-7 min for HONO at local noontime conditions during the UGRB study) and thus some appreciable background, which may also include remnants of previous day formation of HCHO. This background may get mixed into freshly emitted plumes and cause higher data scatter. In any case, according to S10, HCHO shows stronger correlation with total NMHC and CH_4 than with NO_x, while for HONO it is the opposite behaviour. This hints to different source categories for HONO and HCHO.

Based on the CO/NO_x observations at the Boulder South Road, we assume that NO_x at the Boulder site would also be primarily related to combustion sources. In a recent traffic related

emission study, measurements of HONO versus NO_x yielded a slope of 15.86±0.82 pptv HONO / 1 ppbv NO_x (r^2=0.75) and a slope of 25.00±1.06 pptv HCHO / 1 ppbv NO_x (r^2=0.80) for HCHO versus NO_x (Rappenglück et al., 2013). The slopes of HONO versus NO_x for the Boulder nighttime data under wind direction 180°-270° and the Houston traffic related measurements are almost identical. In the traffic emissions study, Rappenglück et al. argued that the high HONO/NO_x emission ratios were likely due to heavy duty vehicles. In the case of the Upper Green River Basin, stationary diesel powered compressors may act similarly. This may likely be favored in addition by altitude effects, as it has been demonstrated for diesel vehicles up to an altitude of 2,400 m asl (e.g. Bishop et al., 2001; Wang et al., 2013) In particular it seems that NO_2 emissions increase at the expense of NO emissions (Yin et al., 2013). For HCHO versus NO_x, the slopes are significantly lower than found in traffic related combustion emissions. The correlation coefficient is also weaker. It is likely that different emission sources overlap. Since HCHO shows a closer correlation with total NMHC at the Boulder site and even closer with CH_4 as shown in S10, it is likely that well head equipment, in addition to co-located compressors, may contribute to HCHO emissions. Interestingly, contrary to HCHO, HONO displays a stronger correlation with total NMHC than with CH_4. This may further support the ideas that HONO emissions are more related to combustion (compressors) and HCHO has some overlapping emissions originating from drill rig operations.

3.4. NMHC versus NO_x limitation of ozone production

Observation based methods like photochemical indicators such as O_3/NO_y, O_3/NO_z, and O_3/HNO_3 and the EOR (Extent of Reaction) can be used to evaluate whether ozone production at a given location may be VOC or NO_x limited (Sillman, 2002; Sillman and He, 2002). The EOR is defined as:

$$EOR = \left(1 - \frac{NO_x}{1.3 \cdot NO_y}\right)^{0.67} \qquad (5)$$

Sillman and He (2002) point out that the photochemical indicators also depend on the chemical environment, in particular for O_3/NO_z (which may not be applicable for highly polluted scenarios). They classified relatively clean environments (O_3 < 80 ppbv), moderately polluted (100 - 200 ppbv O_3) and highly polluted environments (O_3 > 200 ppbv). According to

Sillman and He, photochemical indicators would tend to increase with decreasing ozone values. It is not certain, if these photochemical indicators can be applied to the environment found in the UGRB without modifications, as the radical pool is largely dominated by the photolysis of HONO, at least in the lowermost layer of the PBL (see discussion in chapter 3.6). While there might be some limitations to this concept, we followed this approach in an attempt to explore whether an ensemble of photochemical indicators would at least point towards common tendencies with regard to VOC and NO_x limitation. S11 lists ranges of indicator values which are representative of different regimes. We calculated the photochemical indicators for the Boulder site. For this analysis, we focus on the IOP days, as those were the days with maximum ozone levels. As shown in Figure 3a ozone mixing ratios are usually below 80 ppbv before 11:00 MST and afterwards above 80 ppbv. It is common to all photochemical indicators that they display significant changes throughout the day depending on the wind direction (Figure 8). While there are no consistent patterns throughout the day among all photochemical indicators, some general tendencies for the most critical time periods with regard to regulatory purposes can be deduced. In most cases during morning hours (07:00-11:00 MST; O_3 < 80 ppbv) and/or under SW flow conditions, all indicators reach minimum values. S12 shows that O_3/NO_y, O_3/NO_z and the EOR would indicate VOC limitation; the values of O_3/HNO_3 would fall into the transitional regime according to S11, if not in the VOC limited regime assuming that photochemical indicators would be higher in the case where O_3 < 80 ppbv. From 13:00-15:00 MST, i.e. the time period with O_3 > 80 ppbv, all indicators either point towards a NO_x limited or a transitional regime. Any change from a VOC-limited regime towards a NO_x limited regime or vice versa implies passing the transitional regime, where ozone production can be most efficient and can reach maximum values as shown by Mao et al. (2010). The periods with the lowest values for photochemical indicators generally coincide with minimum values of the NMHC/NO_x ratio as observed at the Boulder site (Figure 9). This minimum value is about 50 and represents a relatively high value compared to urban areas (Mao et al., 2010). This could be due to relatively low NMHC reactivity, either caused by low temperatures or a NMHC mixture which is mostly composed of slow reacting hydrocarbons (e.g. alkanes such as ethane and propane), or a combination of both. Carter and Seinfeld (2012) found that regimes sensitive to VOC or NO_x may vary from year to year and depend on the specific location in the UGRB. For the Boulder site in 2011 they determined a VOC sensitive regime, which largely agrees with our analysis for the morning hours on IOP days. Carter and Seinfeld also state that under such conditions

Deleted: Generally, median values of all indicators would point towards NO_x limitation of ozone production, which would be expected for rural areas. However,

Deleted: i

Deleted:

Deleted: the other indicator values

Deleted: On non-IOP days, the values for the photochemical indicators would be slightly higher but still show a similar diurnal and wind directional pattern. C

Deleted: NO_x

Deleted: VOC

Deleted: reaching or

additional OH generated by an increased level of HONO would favor O_3 formation, while NO_x saturation would also have the potential to cause additional HONO formation. Carter and Seinfeld (2012) modeled the Boulder 2011 case based on the HONO data presented in this paper and found much better simulations of O_3 compared to the baseline scenario, when HONO was added, which is very encouraging. In addition to the Carter and Seinfeld analysis our paper also considers diurnal variations of the NMHC/NO_x ratio, including any fluctuations in the NMHC mix, which is also subject to wind directional changes, at least for the Boulder site. As mentioned above, our data shows that there is likely a transition phase after the morning NO_x saturation conditions towards a VOC saturation regime, which is not described by Carter and Seinfeld and would require diversified speciated regulatory mitigation strategies.

3.5. OH reactivity

In order to describe the importance of individual or classes of trace gases with regard to photochemical processes, it is important to consider both the reactivity and the amount of these trace gases in ambient air. One way to do this is to calculate the propene equivalent *J* as proposed by Chameides et al. (1992):

$$J = C_J \frac{k_{OH}(J)}{k_{OH}(C_3H_6)} \qquad (6)$$

with C_j being the mixing ratio of hydrocarbon compound J in ppbC or any other compound J in ppbv, the reaction rate of this compound with OH (k_{OH}) and normalized to the reaction rate of propene with OH ($k_{OH}(C_3H_6)$). This approach expresses any individual or classes of trace gases in terms of propene units. However, it is an approximation as reactions other than with OH, i.e. with O_3, NO_3, and Cl, are neglected. In our approach, we merge data from the Boulder South Road site (speciated NMHC, CH_4, CO, NO_x) with data collected at the Boulder site (HCHO, HONO) to have a most comprehensive data set. During the winters of 2011 and 2012 nineteen canister surveys of speciated NMHC were performed at sites throughout the UGRB. Boulder and Boulder South Road are located three miles from each other. The Boulder site is closer to the spine of the Pinedale Anticline development and concentrations at this site are generally slightly higher than Boulder South Road. While the r^2 for the comparison of data from these two sites for each of four surveys during February and March

2011 were each greater than 0.97, there is some variation of slope between the two sites with values ranging from 1.2 to 1.7. The two Boulder sites share the characteristic of measuring air that is influenced by a wide range of oil and gas emission sources (Field et al. 2012a; 2012b) with similar contributions between NMHC classes. When considering speciated NMHC alkanes are most correlated and aromatic are least correlated. Although there might be slight differences in the atmospheric chemistry settings of both sites, we believe that this will not have major impacts on the general findings. Figure 10 displays the diurnal variation of the fractions of the propene-equivalent on IOP days. Within the speciated NMHC obtained at the Boulder South Road site, the most important contributions to the overall OH reactivity stem from aromatics (50-60%), alkanes (30-40%) and the remaining ~10% alkenes. As expected, the contribution from alkynes and isoprene is negligible due to their low reactivity (alkynes) and low mixing ratios (isoprene). Although CH_4 accounts for the largest fraction of all hydrocarbons (ranging from 90% around noon to 95% in the morning hours on a ppb basis), its propene-equivalent fraction is quite modest with 1-2% due its low reactivity. This pattern does not change much throughout the day and is not much different on non-IOP days (not shown). It should be noted that in terms of absolute propene-equivalents, OH-reactivity on IOP days reaches up to 48 ppbC before noon compared to 31 ppbC around the same time on non-IOP days. While alkanes contribute to the propene-equivalent about twice as much on IOP days than on non-IOP days, the contribution by aromatics increases by about 30%, whereas the contribution by alkenes stays about the same. When other compounds are included (CO, NO_x, HCHO, HONO), it becomes apparent that NO_x plays an important role both in terms of contribution to reactivity as well as to the diurnal change of contributions. On IOP days aromatics contribute about 35-40%, alkanes 20-30%, NO_x 20-40%, and alkenes about 5-10% to the overall propene-equivalent. The remaining ~5% are due to CO, HONO, HCHO, alkynes, and CH_4. The contribution from NO_x reaches its maximum from 05:00 - 09:00 MST. The picture is different on non-IOP days, where NO_x contributions are significantly lower throughout the day. More specifically, the contributions to the propene-equivalent on non-IOP days would be: aromatics 40-60%, alkanes, 20-40%, NO_x 10-35%, alkenes 5-10%, and ~5% for the remaining trace gases CO, HONO, HCHO, alkynes, and CH_4.

Figure 11 displays OH reactivity based on the sum of the reaction rate coefficients multiplied by the mixing ratios of reactants with OH (Mao et al., 2010):

$$k_{OH} = \sum k_{OH+VOC_i}[VOC_i] + k_{OH+CO}[CO] + k_{OH+NO}[NO] + k_{OH+NO_2}[NO_2] + k_{OH+HNO_3}[HNO_3] + \ldots \quad (7)$$

Figure 11 clearly shows that on IOP days OH reactivity is higher than on non-IOP days by a factor of 2. During the daytime on IOP days, the magnitude of OH reactivity is comparable to that found in direct OH measurements for urban air in Houston, Texas (Mao et al., 2010) or in Mexico City (Sheehy et al., 2010) . Contrary to the urban Houston case, where NO_x may contribute up to 50% to OH reactivity during the rush hour, for the Boulder case NO_x may contribute up to 69% throughout the day. This may be due to NO_x emission sources in the Boulder area whose emissions strength does not change much throughout the day (e.g. compressors). Another distinction is that, at Boulder, alkenes may contribute around 5% to the overall OH reactivity while for the Houston case, it can be up to 35%. The contribution from alkanes is in the 10-15% range at Boulder, while in Houston it is about 5-10%. The contribution of aromatics is about the same for both cases (10-15%).

Deleted: On

In accordance with S4a and b, also the absolute propene-equivalent displays similar distribution with highest values under SW wind directions. The reactivity mix does not change that much with wind direction (i.e. mostly aromatics, alkanes, and NO_x), mostly from SW. Figure 12 shows that while alkanes contribute 80-85%, aromatics around 10-15%, and alkenes less than ~5% of NMHCs on a mass basis, aromatics contribute 50% and alkanes around 45% to the propene-equivalent as observed at the Boulder South Road site. Still, contributions by alkenes are low. Contributions from CH_4 and isoprene are negligible.

The major finding is that on IOP days in the morning hours in particular, NO_x (and to some extent HONO as it is closely associated with NO_x), aromatics and alkanes (the latter ones largely dominated by ethane and propane) are major contributors to the OH reactivity and propene equivalent at Boulder. Highest reactivities are found in air masses arriving at the Boulder site under SW flow conditions. This time period and wind flow condition largely coincide with the lowest NMHC/NO_x ratios observed at the Boulder site and a switch from NO_x limited to transitional, if not VOC limited regime, with the largest ozone production efficiency as described in the previous chapter 3.4. Under VOC limited conditions, it is likely that highly reactive aromatics, such as toluene and xylenes, may be most efficiently competing with other NMHCs in reactions with OH. NO_x reactions with OH in turn will cause substantial formation of HNO_3.

3.6. Role of HONO

As discussed, major removal processes for OH at the Boulder site involve reactions with NO_x, aromatics, and alkanes. Sources for OH are photolysis processes of O_3, aldehydes (foremost HCHO), H_2O_2, $ClNO_2$, and HONO. Alkene ozonolysis may also contribute to OH formation. Recent studies suggest that major OH formation occurs through HONO photolysis in the morning, HCHO photolysis in late morning, and O_3 photolysis throughout the day, whereas photolysis of H_2O_2 and alkene ozonolysis are of minor importance during the day (Elshorbany et al., 2009; Ren et al., 2013; Czader et al., 2013). According to an analysis by Elshorbany et al. (2009), HONO photolysis can contribute to about 52% of radicals on a 24-h average, followed by alkene ozonolysis (about 20%), HCHO photolysis (about 15%) and ozone photolysis (about 4%) in an urban area. On the other hand, in unpolluted polar regions HONO is suggested to be a major radical source (98%) and ozone photolysis would account for the remaining 2% (Villena et al., 2011). Mao et al. (2010) report that contributions to the radical pool from HONO photolysis may be highest in high NO_x environments.

Deleted: Nighttime a

Deleted: For the Boulder site, we suspect that nighttime alkene ozonolysis is negligible. Median values for ethene and propene are about 25% and 7% of those found in urban areas like Houston (Leuchner and Rappenglück, 2010) and thus may play an even lower role than in Houston where it was found to be of least importance (Ren et al., 2013). As mentioned earlier we presume that $ClNO_2$ may not be present in appreciable amounts based on the low levels of particulate chloride. However, ozone and HONO (see also S2) at the Boulder site can exceed values found in urban areas.

The primary production of hydroxyl radicals from the photolysis of O_3, $P(OH)_{prim\_O_3}$, the photolysis of HCHO, $P(HO_2)_{prim\_HCHO}$, the photolysis of HONO, $P(OH)_{prim\_HONO}$, and from alkene ozonolysis, $P(OH)_{prim\_alkenes}$ can be calculated as follows (see also Elshorbany et al., 2009; Sörgel et al., 2011):

$$P(OH)_{prim\_O_3} = \frac{2 \cdot J_{O(^1D)}[O_3] \cdot k_{O(^1D)+H_2O}[H_2O]}{k_{O(^1D)+H_2O}[H_2O] + k_{O(^1D)+O_2}[O_2] + k_{O(^1D)+N_2}[N_2]} \quad (8)$$

$$P(HO_2)_{prim\_HCHO} = 2 \cdot J_{HCHO}[HCHO] \quad (9)$$

$$P(OH)_{prim\_HONO} = J_{HONO}[HONO] - k_{OH+NO}[NO] \cdot [OH] - k_{HONO+NO}[HONO] \cdot [OH] \quad (10)$$

$$P(OH)_{prim\_alkenes} = \sum k_{O_3+alkene}[alkene] \cdot [O_3] \cdot \Phi_{OH} \quad (11)$$

where photolysis rates for photolysis of $O(^1D)$ ($J_{O(1D)}$), HCHO (J_{HCHO}), and HONO (J_{HONO}), temperature dependant reaction rates (Atkinson et al., 2004; 2006) and Φ_{OH}, the OH yield of gas-phase reactions of ozone with alkenes, are used (Rickard et al., 1999).

Figure 13 displays results of calculation of OH-productions due to the above processes for IOP and non-IOP days. Photolysis of $ClNO_2$ is not included. As mentioned earlier we presume that $ClNO_2$ may not be present in appreciable amounts based on the low levels of particulate chloride. In Figure 13, median data for ozone, HCHO, HONO, and alkenes were taken. The results clearly indicate that OH production on IOP days is mainly due to HONO. Between 9:30-15:30 MST, HONO photolysis contributes between 83-94% of the entire OH-production, i.e. slightly less than observed in polar areas (Villena et al., 2011), whereas the contributions by other processes range between 2-7% each. On a 24-hr basis HONO photolysis on IOP days can contribute ~83% to OH production on average, followed by alkene ozonolysis (~9%). Photolysis by ozone and HCHO photolysis contributes about 4% each to hydroxyl formation. On non-IOP days the picture is different and more closely resembles the results by Elshorbany et al. (2009) for an urban area. The contributions to hydroxyl formation on non-IOP days were as follows: HONO photolysis (~54%), alkene ozonolysis (~28%), ozone photolysis (~13%), and HCHO photolysis (~5%). It is worth noting that the calculated OH-production due to HCHO photolysis represents an upper limit as we did not distinguish between primary and secondary HCHO in these calculations. These results are different from the simulation analyses for a site in the Uintah Basin, Utah (Edwards et al., 2013). Potential reasons may include that Edwards et al. assumed a uniform increase of O_3 precursors by a factor of 2 under cold pool events, that the site may have been exposed to a different ambient chemical matrix (e.g. HCHO is significantly higher, while HONO is significantly lower at the Horse Pool site/UT compared to the Boulder site/WY) and that they assumed a primary fraction of 50% of the observed daily integrated HCHO mixing ratio.

In environments with a significant amount of NO_x the dominant terminal loss mechanism for OH is the reaction with NO_2, leading to the formation of HNO_3:

$$NO_2 + OH + M \rightarrow HNO_3 + M \qquad (M = N_2, O_2) \qquad (12)$$

which translates into:

$$L(OH) = k_{NO_2+OH}[NO_2] \qquad (13)$$

Thus a photostationary state OH concentration can be calculated as follows:

Deleted: photolysis of ozone, HCHO, and HONO

Deleted: M

Deleted: and

Deleted: While a surface albedo of 80% for snow cover was considered, the data do not take into account the altitude of the Boulder site (2,000 m above sea level). Thus OH -production may actually be even higher than shown in the plots. Nevertheless, t

Deleted: Until noon

Deleted: 74

Deleted: 8

Deleted: . Ozone photolysis (2-24%) is second to HONO photolysis

Deleted: However, both reach about the same magnitude in the early afternoon (close to 50%). The picture is different on non-IOP days, where HONO surpasses the OH-contribution by ozone photolysis in the early morning hours only. The absolute contribution to OH-production caused by ozone photolysis and HCHO photolysis on IOP days does not differ much from non-IOP days. In both cases the photolysis of HCHO contributes mostly less than 10% (on IOP days 2-7%) to the overall OH-production and is thus not important.

$$[OH]_{PSS} = \frac{P(OH)_{prim\_O_3} + P(OH)_{prim\_HONO} + P(OH)_{prim\_alkenes} + P(HO_2)_{prim\_HCHO}}{L(OH)} \quad (14)$$

Figure 14 shows that OH concentrations can reach very high values during the time period 11:00-16:00 MST on IOP days. These are in the ranges found in New York City (Ren et al., 2003), Houston (Mao et al., 2010), Mexico City (Sheehy et al., 2010) and in the River Pearl Delta (Lu et al., 2012), and at times exceed those. On non-IOP days maximum OH mixing ratios are significantly lower, and are confined to noontime. The OH chain length ranges between 10 and 13 between 12:00-15:00 MST on IOP days, which is of a similar magnitude as found in Houston and Mexico City, and significantly higher than in New York City (Mao et al., 2010). Figure S13 clearly shows that the OH net production occurs around noontime and is on the order of 4×10^7 molecules cm^{-3} s^{-1}. In urban areas the peak OH net production occurs during morning rush hours (Mao et al., 2010) at similar or higher magnitude than in our study, and decreases significantly afterwards. In NO_x rich environments such as New York City the OH net production is maintained around noontime, albeit lower than during rush-hours and slightly lower than in our study.

Based on the calculated OH concentrations it is possible to determine the photostationary state concentration of HONO using the following equation:

$$[HONO]_{PSS} = \frac{k_{OH+NO}[OH]\cdot[NO]}{J_{HONO} + k_{OH+HONO}[OH]} \quad (15)$$

$[HONO]_{PSS}$ was ~26% of the observed ambient HONO mixing ratios on IOP days and 44% on non-IOP days during 11:30-15:30 MST, when $P(OH)_{prim\_HONO}$ was at a maximum, which is significantly less than observed in the urban area of Santiago de Chile, for instance (~66%; Elshorbany et al., 2009). These low fractions of $[HONO]_{PSS}$ indicate that a strong daytime source for HONO must be present. High daytime $HONO/NO_x$ ratios are also usually considered an indicator for strong additional photochemical HONO sources (Elshorbany et al., 2009). Figure 15 shows that the $HONO/NO_x$ ratio is about the same value for IOP and non-IOP days throughout the nighttime. In particular, in the morning hours from 05:00 - 09:00 MST, when maximum levels of primary pollutants are present (Figure 3a), the $HONO/NO_x$ ratio tends to be at a minimum and is between 2-5% in both cases, which is similar to other locations. However, it increases significantly from 12:00-14:00 MST on non-IOP days

Deleted: For the Boulder site, it is the photolysis of HONO, which makes a significant difference from non-IOP days to IOP days, as it is 6 times higher on IOP days. The high OH-production rate of 2,900 pptv/hr by HONO-photolysis must be balanced by HONO sources of the same magnitude.¶
At the Boulder site no speciated photolysis rates measurements were available. As a surrogate, we plotted measured incoming ultraviolet (UV) radiation in Figure 14. On IOP days, incoming UV radiation was on the order of 10% higher than on non-IOP days. Data in Figure 14 shows that HONO increases as incoming UV radiation increases. T

767 (median values ~10%) and from 11:00-16:00 on IOP days (median values up to 30%).
768 According to Villena et al. (2011) the magnitude of the HONO/NO_x ratio is similar to the
769 magnitude of the ratio of the corresponding atmospheric lifetimes. Based on the calculated
770 J_{HONO} photolysis rates an atmospheric lifetime for HONO of about 5-7 min between 11:30-
771 15:30 MST on IOP days can be deduced. Using the calculated OH concentrations and
772 temperature dependant reaction rates for reactions with OH and O_3 a corresponding
773 atmospheric lifetime of ~19 min for NO_2 can be retrieved, which translates into a ratio of both
774 lifetimes on the order of ~26, which is close to the observed average median HONO/NO_x
775 ratios for that time period, which is ~21. On non-IOP days, the atmospheric lifetime of NO_x is
776 much longer (almost 1 hr), the ratio of the HONO and NO_x lifetimes is ~12, the observed
777 HONO/NO_x ratio is ~9. This indicates that more HONO is being formed in photochemical
778 processes, most likely through NO_2 conversion, on IOP days during these time periods. At the
779 same time, NO_x levels decrease (Figure 3a). As meteorological conditions (PBL height; SW
780 wind flow) do not vary much during this time of the day on IOP days, and NO_x deposition
781 velocity onto snow surfaces is low (Hauglustaine et al., 1994), rapid oxidation of NO_x leads
782 to a decrease in NO_x mixing ratios. Reactions of NO_2 with OH and O_3 will lead to the
783 formation of HNO_3 accelerated through the enhanced availability of radicals due to the strong
784 HONO photolysis source. This decrease in ambient NO_x levels indicate that these removal
785 processes exceed other sources for NO_x, e.g. through photolysis of HONO.
786 For the Boulder site, it is the photolysis of HONO, which makes a significant difference to
787 hydroxyl formation, as it is up to a magnitude higher on IOP days than on non-IOP days
788 around noontime and the overall 24-hr production of OH due to HONO photolysis is 6 times
789 higher on IOP days versus non-IOP days. While also the contribution by HCHO photolysis to
790 hydroxyl formation is enhanced by 3-5 times, the contribution by ozone photolysis and alkene
791 ozonolysis remains at the same level.
792 The high OH-production rate of 10,726 pptv/hr by HONO-photolysis must be balanced by
793 HONO sources of the same magnitude. At the Boulder site no speciated photolysis rates
794 measurements were available. As a surrogate, we plotted measured incoming ultraviolet (UV)
795 radiation in Figure 15. On IOP days, incoming UV radiation was on the order of 10% higher
796 than on non-IOP days. We calculated photolysis rates using the TUV model (for specific
797 details see figure caption of Figure 13). Median noontime levels on IOP days were 3.14×10^{-5}
798 [s^{-1}] for $J_{O(1D)}$, 1.78×10^{-2} [s^{-1}] for J_{NO2}, 7.87×10^{-7} [s^{-1}] for J_{HNO3}, 3.64×10^{-3} [s^{-1}] for J_{HONO}, and
799 4.74×10^{-5} [s^{-1}] for J_{HCHO}. Likewise, photolysis rates were reduced by about 10% on non-IOP

Deleted: During

Deleted: periods

Deleted: nitrogen oxide

Deleted: from non-IOP days to IOP days

Deleted: 6 times

Deleted:

Deleted: 2

Deleted: 900

Deleted: ¶

days. Those high photolysis rates are primarily due to the high snow albedo, already relatively high solar zenith angles in March, high altitude (2,160 m) and relatively low latitude (42.7° N) of the UGRB. Some of these factors differ significantly from conditions found in polar regions. Generally, data in Figure 15 shows that HONO increases as incoming UV radiation increases. Also during the same time periods, O_3 increases as well. It appears likely that HONO is being produced through photo-enhanced formation processes which are most efficient when snow cover is present.

Deleted: This indicates that more HONO is being formed through NO_2 conversion.

It has become evident that ambient HONO concentrations are higher than can be accounted for by direct emissions and that heterogeneous processes on surfaces may lead to enhanced ambient HONO levels. In particular, these processes tend to occur on surfaces with adsorbed water in the dark (Finlayson- Pitts et al., 2003; Jenkin et al., 1988; Kleffmann et al., 1998) based on the following reaction (Goodman et al., 1999; Kleffmann et al., 1998):

$$2NO_{2(ads)} + H_2O_{(ads)} \rightarrow HONO_{(ads)} + HNO_{3(ads)} \qquad (16)$$

Deleted: 8

Recently, an additional nighttime formation of HONO that was not related to NO_2 was reported on aqueous surfaces in the marine boundary layer by Wojtal et al. (2011), assuming a surface nano layer saturated with NO_2 precursors and no irreversible loss of HONO from that layer. Wojtal et al. observed that HONO/NO_2 ratios would increase during the night from 3-30% and even higher on some occasions, with HONO levels about 1 ppbv at night. While we suspect that the snow surface could have been saturated with NO_2 precursors due to appreciable amounts of these compounds in ambient air (see Figures 3a and b), we did not observe increasing HONO/NO_x ratios throughout the night as shown in Figure 15. Also, HONO mixing ratios were 3-10 times lower compared to the Wojtal et al. study.

Deleted: 4

Over the last decade a variety of photo-enhanced HONO formation mechanisms have been discussed to explain observations of elevated daytime HONO levels (Kleffmann, 2007).. These include: (i) the photolysis of surface adsorbed nitrate or nitric acid (Zhou et al., 2001; Zhou et al., 2002; Ramazan et al., 2006), (ii) the photolysis of ortho-nitrophenols (Bejan et al., 2006), (iii) light-induced NO_2 reduction on surface adsorbed humic acid films (Stemmler et al., 2007), (iv) gas-phase reaction of electronically excited NO_2, due to photolysis, with water (Li et al., 2008), and (v) the conversion of HNO_3 to HONO on primary organic aerosol (Ziemba et al., 2010).

As mentioned in chapter 3.1., observations at the Boulder site were characterized by remarkably high ambient levels of HONO, HNO_3, and p-NO_3^- which on IOP days were higher than in urban air measurements, e.g. in Houston, Texas. HONO showed close correlation with HNO_3 not only during nighttimes (S10) but, contrary to NO_2 and NO_x, also during daytime regardless of IOP or non-IOP days with correlation coefficients ranging from 0.73 and 0.80. Contrary to Ziemba et al. (2010), who found that HONO was anticorrelated with HNO_3 during morning traffic rush hours, our observations do not show any anticorrelation during any time period. We thus assume that conversion of HNO_3 to HONO on primary organic aerosol will be negligible in the UGRB. HNO_3 on IOP days formed a higher fraction of NO_y than in Houston (22% vs 16%). Its fraction of NO_z ranged between 30-40%, with maximum values found under SW wind directions. Again, corresponding values in Houston were only about 20% (Luke et al., 2010). Particulate NO_3^- at the Boulder site was closely related to EC, elemental carbon, (r^2=0.85) and OC, organic carbon (r^2=0.73), but only showed poor correlation with sulfur (r^2=0.09) and sulfate (r^2=0.03). This fingerprint is likely associated with fossil fuel combustion in industrial processes (Jacobson, 2012). Björkman et al. (2013) studied dry deposition velocities for HNO_3 and p-NO_3^- onto snow surfaces in the arctic. They found that the dry deposition velocity for particulate NO_3^- critically depends on the particle size; still, for particle sizes around 7 µm, the dry deposition velocity is significantly lower than for HNO_3. Overall, the dry deposition of p-NO_3^- only accounts for 1-7% of the total nitrate dry deposition (Björkman et al., 2013). According to reaction (8) $HNO_{3(ads)}$ can already be formed through $NO_{2(ads)}$. Dry deposition velocity of HNO_3 onto snow surfaces is about 50 times greater than for NO_2 (Hauglustaine et al., 1994). Using median data for NO_2 and HNO_3 mixing ratios as shown in S2 dry deposition flux of HNO_3 onto the snow surface may be about 8 - 65 times greater than for NO_2, with maximum values during daytime, as HNO_3 mixing ratios surpass those of NO_2. While reaction (8) would likely contribute to HONO formation throughout the day as shown by Wojtal et al. (2011) over aqueous surfaces, we assume that deposition of HNO_3 would be of critical importance, in accordance with studies by Zhou et al. (2003).

When adsorbed on a surface, the following reactions may occur (Mack and Bolton, 1999; Zhou et al., 2002; Zhou et al., 2003):

$$HNO_{3(ads)} + h\nu \rightarrow [HNO_3]^*_{(ads)} \quad (17)$$

$$[HNO_3]^*_{(ads)} \rightarrow HNO_{2(ads)} + O(^3P)_{(ads)} \quad (18)$$

Deleted: 9

Deleted: 0

$$[HNO_3]^*_{(ads)} \rightarrow NO_{2(ads)} + OH_{(ads)} \quad (19)$$

Deleted: 1

Reaction (17) requires sunlit daytime conditions. $NO_{2(ads)}$ formed in (19) may then further react according to reaction (16) and subsequently form HONO. According to Zhou et al. (2003), the production yield of HONO from surface HNO_3 photolysis is almost independent of relative humidity between 20%-80%, although some moisture is necessary. Thus snow cover would provide a favorable substrate. On the other hand, the negligible dependence on relative humidity may explain, at least partly, why we did not find a clear correlation of HONO with relative humidity.

Deleted: 9

Deleted: 1

Deleted: 8

Figure S14 shows that generally the HONO extra source, which balances the OH production rate due to HONO photolysis (dOH/dt -HONO; see Figure 13) correlates better with $J_{O(1D)}$ (R^2_{IOP}=0.86; $R^2_{non-IOP}$=0.85) and J_{HNO3} (R^2_{IOP}=0.82; $R^2_{non-IOP}$=0.88) than with J_{NO2} (R^2_{IOP}=0.71; $R^2_{non-IOP}$=0.85). According to Villena et al. (2010) and Elshorbany et al. (2012) a better correlation of the daytime HONO extra source with $J_{O(1D)}$ would point to photolysis of HNO_3 as a potential HONO source, whereas a better correlation with J_{NO2} would point to photosensitized conversion of NO_2 on humic acid surfaces.

Following the approach by Villena et al. (2010) we determined the correlation of the HONO extra source with photolysis rates for each day. In our case we used photolysis rates based on TUV calculation. In Figure S15 the slopes m of each daily correlation of the HONO extra source versus J_{NO2} (mJ_{NO2}) are plotted against median daytime NO_2 mixing ratios for the same time periods. For these plots any days with daily median NO mixing ratios > 500 pptv were excluded to avoid potential bias due to freshly polluted air masses. The results are segregated for IOP and non-IOP days. A similar approach is shown for mJ_{HNO3} against median daytime HNO_3 mixing ratios. The following observations can be deduced: (i) in both cases IOP days show higher $mJ_{NO2, HNO3}$ values, (ii) the slopes of $mJ_{NO2, HNO3}$ are steeper on IOP days than on non-IOP days, and (iii) correlation coefficients R^2 of $mJ_{NO2, HNO3}$ versus NO_2 and HNO_3, respectively, are higher on IOP than non-IOP days. While this indicates photo-enhanced HONO formation on IOP days, the stronger correlation coefficients in the case of mJ_{HNO3} versus HNO_3 mixing ratios (R^2_{IOP}=0.97; $R^2_{non-IOP}$=0.89) compared with the case of mJ_{NO2} versus NO_2 mixing ratios (R^2_{IOP}=0.84; $R^2_{non-IOP}$=0.39) would indicate that photolysis of HNO_3 may play an important role for HONO formation. According to Villena et

al. (2010) the correlation of mJ_{NO2} against the product of [NO_2]×1/v (v being the horizontal windspeed) used as an indication for turbulent vertical mixing, was even stronger, suggesting a ground surface source. In our study, correlations of mJ_{HNO3} versus HNO_3 mixing ratios ($R^2_{IOP\_v}$=0.98; $R^2_{non-IOP\_v}$=0.97) as well as mJ_{NO2} versus NO_2 mixing ratios ($R^2_{IOP\_v}$=0.95; $R^2_{non-IOP\_v}$=0.85) also became stronger when windspeed was included.

As mentioned earlier Figure S8 provides some general characterization of HONO mixing ratios obtained at 1.80 m above the ground versus HONO mixing ratios obtained 10 cm above the ground. Quantitative flux measurements were not performed based on the small tower measurements. However, some additional estimates on PBL properties can be deduced based on meteorological measurements obtained at the Tall Tower site located about 10 km Southeast of the Boulder site (2,149 m; 42.4241°N; -109.5609°W; see Figure 1). For describing atmospheric stability the Bulk Richardson number R_B can be applied (Stull, 1988):

$$R_B = \frac{g\Delta\overline{\Theta_v}\Delta z}{\overline{\Theta_v}\left[\left(\Delta\overline{U}\right)^2 + \left(\Delta\overline{V}\right)^2\right]} \qquad (20)$$

where $\overline{\Theta_v}$ is the virtual potential temperature averaged over a given time interval, Δz the difference between two altitudes, $\Delta\overline{\Theta_v}$ the difference of the virtual potential temperature over Δz, averaged over a given time interval, $\Delta\overline{U}$ and $\Delta\overline{V}$ the differences of the windspeed in u direction and v direction, respectively, over Δz averaged over a given time interval, and g the gravitational constant. The Bulk Richardson number relates the thermal buoyancy to mechanical shear. For our calculations we used the meteorological data obtained at the 3 m and 25 m level. In the absence of relative humidity measurements at the 25 m level we calculated R_B using potential temperature instead of virtual potential temperature. Figure 14 indicates that on IOP days most of the time the PBL is stable and behaves like a laminar stratified flow. This likely explains why figure S8 does not indicate a vertical gradient of HONO mixing ratios and that the layers seem to be decoupled from each other. It is only during the time frame 11:00-16:00 MST that the PBL becomes turbulent. During this time frame also the mixing layer height tends to increase, albeit slightly, until the maximum atmospheric instability is reached. More importantly, this time frame also coincides with the

time period of maximum OH mixing ratios as shown in Figure 14 and the development of a vertical gradient in HONO mixing ratios as indicated in Figure S8. This is the time frame when vertical exchange processes from the surface may occur. During other times of the day these processes are largely suppressed.

The distribution of trace gases within the atmosphere depends on their atmospheric lifetime and the atmospheric turbulent diffusion. The turbulent diffusion time Δt is determined by:

$$\Delta t = \frac{(\Delta z)^2}{2K_z} \qquad (21)$$

Likewise, a diffusion distance can be defined:

$$\Delta z = \sqrt{2K_z \cdot \Delta t} \qquad (22)$$

where Δz is the vertical distance traveled by an eddy and K_z is the turbulent diffusion coefficient or eddy diffusivity. K_z relates vertical fluxes of matter with properties of the PBL (e.g. Stull, 1988 and references therein):

$$F = -K_z \frac{\partial C}{\partial z} = -\frac{k u_* z}{\Phi_M} \frac{\partial C}{\partial z} \qquad (23)$$

where F is the vertical flux, C the mixing ratio of a trace gas, $k = 0.4$ the von Kármán constant, u_* the friction velocity, and Φ_M an empirically derived stability function. Φ_M can be described as a function of the Bulk Richardson number for specific cases (Arya, 1998):

$$\Phi_M = 1 - R_B \qquad 0.25 < R_B < 1 \qquad (24)$$

$$\Phi_M = (1 - 15 \cdot R_B)^{\frac{1}{4}} \qquad R_B < 0.25 \qquad (25)$$

In our study K_z can only be calculated for cases $R_B < 1$, i.e. for the time frame 11:00-16:00 MST (see Figure 14). For this time frame and for a height of 3 m the median K_z was 348 cm^{-2} s^{-1}, ranging from 253-840 cm^{-2} s^{-1}, which is about 5-10 less than observed above the

snowpack at Summit, Greenland (Honrath et al., 2002), but of the same magnitude found in Alert, Canada (Zhou et al., 2001). Given the maximum mixing layer height of about 58 m (Figure 14) this translates into a turbulent diffusion time of more than 13 hrs likely causing the development of vertical gradients of trace gases whose atmospheric lifetime is shorter than 13 hrs. Given an atmospheric lifetime of 5-7 min for HONO around noontime, when turbulent mixing is present, HONO mixing ratios may have decreased due to photolysis by 15% by the time it reaches the 1.80 m sampling level and by 63%, when it reaches about 4.40 m, which is significantly lower than found in Alert, which was 11 m (Zhou et al., 2001). At Boulder HONO will almost be completely removed (by 99.6%) when it reaches 10 m above the surface level. This means that OH formation due to HONO is likely confined to the lowermost 10% of the PBL, while other OH formation processes due to photolysis of HCHO, O_3 and alkene ozonolysis may be active throughout the PBL. HONO measurements were taken at 10 cm and 1.80 m above the ground, which translates into turbulent diffusion times from the ground of 0.15 s and 46.5 s, respectively. During the time frame 11-13:00 MST of Figure S8 a vertical HONO gradient is visible. The average HONO photolysis rate during that time frame is 3.44×10^{-3} s^{-1}. Considering an average HONO mixing ratio at 10 cm of ~700 pptv and a vertical turbulent diffusion time of 46.35 s from the bottom sampling location to the 1.80 m sampling location an average HONO mixing ratio of ~600 pptv at the 1.80 m level would be expected, a decrease of ~14%. The data of S8 indicates an average HONO mixing ratio of ~500 pptv, which would imply a doublefold decrease. Given the uncertainties and limitations in our assumptions on the atmospheric stability as retrieved from the "Tall Tower" site, the HONO small tower observations at the Boulder site, and the TUV calculated HONO photolysis rate, the results are reasonable.

Zhou et al. (2003) calculate HONO formation rates based on surface HNO_3 photolysis. We adopted this approach to explore whether this process may balance the median HONO photolysis rate of 10,700 pptv/hr at the Boulder site around noontime on IOP days. According to Zhou et al. the upward flux F_{up} of NO_x and HONO can be described as follows:

$$F_{up} = \alpha \cdot J \cdot v \cdot C \cdot t \qquad (26)$$

where α represents the fraction of the average of the individual median values for the diurnal variation of the UV radiation (Figure 15) versus the noontime maximum value of the UV radiation. This value is about 25% and is used to determine the fraction of deposited HNO_3

Deleted: 2

Deleted: 9

Deleted: 12

Deleted: 4

exposed to noontime photolysis rate J_{HNO3} (s^{-1}). The parameter ν is the average HNO_3 dry deposition velocity, C is the ambient HNO_3 concentration (moles m^{-3}) and t (s) is the accumulation time since the last precipitation. Zhou et al. applied the following values for their calculation: $J_{HNO3} = 2.5\times10^{-5}$ s^{-1}, ν = 2×10^{-2} m s^{-1}, C = 700 pptv = 3.1×10^{-8} moles m^{-3}, and t =24 hrs = 86.400 s. Zhou et al. calculated a HONO production rate of ~150 pptv/hr for a 100 m boundary layer height. For the estimate at the Boulder site, we consider a different HNO_3 concentration and also assume a different photolysis rate J_{HNO3} due to higher albedo. The median HNO_3 mixing ratio on IOP days at Boulder was 2.1 ppbv (which equals 9.37×10^{-8} moles m^{-3}). According to the TUV model J_{HNO3} is ~2.5 times higher over surfaces with 75% albedo (e.g. over snow) compared with standard surfaces. For the Boulder site the effective active layer for HONO is the lowermost 10 m of the PBL. This would result in a HONO emission flux of 10,206 pptv/hr, which is very close to the observed loss of HONO due to its photolysis. Apart from surface emissions combustion related HONO emissions may contribute to the HONO flux. As outlined earlier we found a robust HONO/NO_x emission ratio of 15 pptv HONO / 1 ppbv NO_x during nighttimes under SW flow conditions. In the quadrant southwest of Boulder multiple facilities related to oil and gas drilling activities are distributed over an area of ~300 km^2. According to the WDEQ inventory (WDEQ, 2011), the overall NO_x emission from these facilities is ~1180 kg/hr with about 91% originating from drill rig and completion emissions. The overall NO_x flux in this area would be ~4,000 µg m^{-2} hr^{-1}. Assuming a boundary height of 50 m agl this would result in an increase of ~39 ppbv/hr for NO_x and an increase of ~585 pptv/hr for HONO using the emission ratio of 15 pptv HONO / 1 ppbv NO_x. Given an average windspeed of 1.4 m s^{-1} between 11:00-16:00 MST on IOP days and a distance of about 3-5 km between the Boulder site and most local sources we estimate that photolysis will have removed 85% (for the closest sources) and up to 90% (for the most distant sources) of ambient HONO by the time air masses would reach the Boulder site based on a HONO lifetime of ~5-7 min during the same time period Thus during the transport HONO photolysis may likely have contributed to radical formation. At the Boulder site an estimated HONO production of 70 pptv/hr would still be due to combustion related HONO emissions. Together with the surface HONO flux due to photolysis of HNO_3 adsorbed on the snow surface this would account for a total HONO production rate of 10,276 pptv/hr at around noontime on IOP days, which is in very good agreement with the photolysis rate of HONO of 10,726 pptv/hr. We therefore conclude that ultimately, NO_x emitted into the extremely shallow boundary layer during the wintertime season in the UGRB is causing high

Deleted: Finlayson-Pitts and Pitts (2000) and references therein,

Deleted: photolysis rates for ozone, HCHO, and HONO, which we used to calculate OH-production,

Deleted: are

Deleted: about

Deleted: 80

Deleted: We assume the same magnitude of change for J_{HNO3}. The specific conditions for the Boulder site would lead to ~7.5 times higher HONO emission than found in the Zhou et al. study, i.e. 1,125 pptv/hr. Boundary layer measurements at Boulder were around 50 m agl around noontime on IOP days, which

Deleted: 2

Deleted: 50

Deleted: We assume that these emissions may be transported to the Boulder site

Deleted:

Deleted: and that removal processes may be negligible

Deleted: Both

Deleted: and the combustion related HONO emissions

Deleted: 2

Deleted: 835

Deleted: 2

Deleted: 900

HONO levels. This occurs from two processes: i) HNO_3 produced during atmospheric oxidation of NO_x can be deposited onto the snow surfaces which facilitate subsequent photo-enhanced heterogeneous conversion to HONO and ii) through combustion related emission of HONO. HONO, in turn, will serve as the most important precursor for OH, strongly enhanced due to the high albedo of the snow cover. The first process is the most dominant process.

Deleted: ,

Deleted: The high altitude of the UGRB (2,000 m asl), which we did not consider in our calculations, may likely intensify these processes.

4 Conclusions

During the periods February 28 - March 02 and March 9 - 12, 2011, designated Intensive Operational Periods (IOPs), high hourly ozone readings up to 166 ppbv were observed at the Boulder surface site, located in the Upper Green River Basin, Wyoming. These values were well above the estimated surface background ozone of ~40 ppbv and lower tropospheric ozone background of ~60 ppbv in March. During the IOPs comprehensive surface measurements were performed and observations of vertical distributions of meteorological parameters and selected trace gases were carried out. The observed high ozone levels likely result from a combination of multiple factors.

Deleted: Intensive

Maximum ozone values are restricted to a very shallow surface layer. There is no evidence of ozone carry over from previous days. Ozone levels may remain stable as ozone deposition velocity onto snow surfaces is low. On IOP days, slightly variable wind directions (including recirculation) and low wind speeds in combination with low mixing layer heights (~50 m agl around noontime) are essential for accumulation of both primary and secondary pollutants within the UGRB. IOP days are usually characterized by the fact that, at least once during the day, trajectories eventually pass through the area Southwest of Boulder before arriving at the Boulder site. Recirculation processes within the basin may also occur. Air masses would then pass the oil and gas well locations of the Pinedale Anticline and also a large number of compressor facilities at the most 1-2 hours before arrival at Boulder and would have stayed in that region for about 1 hour. Compressors and drill rigs emit primarily NO_x, relative to well head production equipment, which emits primarily CH_4 and NMHC. While compressors and drill rigs would also emit HONO and to some extent HCHO, well head production equipment would only contribute to emissions of HCHO. This is largely supported in an analysis of nighttime ratios of HONO and HCHO versus NO_x, NMHC, and CH_4 in air masses coming from this area. In general, these air masses contain maximum amounts of both primary and secondary pollutants. They are also associated with the highest VOC reactivity and a change from a NO_x sensitive towards a VOC sensitive regime.

Deleted: reciruclation

Deleted: of

Deleted: ity

Deleted: ity

On IOP days in the morning hours in particular, NO_x (up to 69%), then aromatics and alkanes (~10-15%; mostly ethane and propane) are major contributors to the OH reactivity and propene equivalent at Boulder. Highest OH reactivities (up to 22 s^{-1}) are found in air masses arriving at the Boulder site under SW flow conditions. This time frame (and also wind direction) largely coincides with the lowest NMHC/NO_x ratios at the Boulder site and a change from a NO_x-limited regime towards a VOC limited regime, which implies reaching or passing the transitional regime where ozone production can be most efficient and can reach maximum values. This is supported by photochemical indicators such as O_3/NO_y, O_3/NO_z, and O_3/HNO_3 and the EOR (Extent of Reaction). The NMHC/NO_x at the Boulder site during these periods is ~50 and represents a relatively high value compared to urban areas. This could be due to relatively low NMHC reactivity, either caused by low temperatures or a NMHC mixture which is mostly composed of slow reacting hydrocarbons (e.g. alkanes), or a combination of both. Under VOC limited conditions, it is likely that highly reactive aromatics, such as toluene and xylenes, may be most efficiently competing with other NMHCs in reactions with OH. NO_x reactions with OH in turn will cause substantial formation of HNO_3.

OH production on IOP days is mainly due to HONO. Until noon HONO photolysis contributes between 83-94% of the entire OH-production, whereas the contributions by other processes range between 2-7% each. On a 24-hr basis HONO photolysis on IOP days can contribute ~83% to OH production on average, followed by alkene ozonolysis (~9%). Photolysis by ozone and HCHO photolysis contributes about 4% each to hydroxyl formation. The contributions to hydroxyl formation on non-IOP days were as follows: HONO photolysis (~54%), alkene ozonolysis (~28%), ozone photolysis (~13%), and HCHO photolysis (~5%).

We conclude that ultimately, NO_x emitted into the extremely shallow boundary layer during the wintertime season in the UGRB is causing high HONO levels (maximum hourly median on IOP days: 1,096 pptv) through (i) HNO_3 produced in atmospheric oxidation of NO_x, deposited onto the snow surface and undergoing photo-enhanced heterogeneous conversion to HONO (estimated HONO production: 10,206 pptv/hr) and (ii) combustion related emission of HONO at the Boulder site (estimated HONO production: ~70 pptv/hr). HONO production is confined to the lowermost 10 m of the boundary layer. HONO, in turn, serves as the most important precursor for OH, strongly enhanced due to the high albedo of the snow cover (HONO photolysis rate 10,276 pptv/hr). OH radicals oxidize NMHCs, mostly aromatics (toluene, xylenes) and alkanes (ethane, propane), eventually leading to an increase in ozone. The data do not suggest that relative humidity favors the presence of high levels of HONO.

Deleted: 74

Deleted: 8

Deleted: .

Deleted: Ozone photolysis (2-24%) is second to HONO photolysis. However, both reach about the same magnitude in the early afternoon (close to 50%).

Deleted: On non-IOP days, HONO surpasses the OH-contribution by ozone photolysis only in the early morning hours. The absolute contribution to OH-production caused by ozone photolysis and HCHO photolysis on IOP days does not differ much from non-IOP days. In both cases the photolysis of HCHO contributes mostly less than 10% (on IOP days 2-7%) to the overall OH-production and is thus not important. ¶

Deleted: 2

Deleted: 50

Deleted: 585

Deleted: 2

Deleted: 900

Deleted: es

This may be due to the assumption that the surface HNO_3 photolysis is almost independent of relative humidity (Zhou et al., 2003) or the limitation of our data, which always showed relative humidity well above 50% during nighttimes.

Deleted: s

Deleted: The high altitude of the UGRB (2,000 m asl), which we did not consider in our calculations, may likely intensify these processes.

Acknowledgements

The authors would like to thank the Wyoming Department of Environmental Quality (WDEQ) for their support. Support by MSI, especially by Bill Hauze and Tyler Ward is greatly appreciated.

References

Ammann, M.: priv. comm., *Paul Scherrer Institute (PSI), Villigen, Switzerland*, 2013.

Altshuller, A.P.: Production of aldehydes as primary emissions and from secondary atmospheric reactions of alkenes and alkanes during the night and early morning hours, *Atmos. Environ.*, 27A, 21-32, 1993.

Arya, S.P.: Air Pollution Meteorology and Dispersion, Oxford University Press, USA, 1998.

Atkinson, R., Baulch, D.L., Cox, R.A., Crowley, J.N., Hampson, R.F., Hynes, R.G., Jenkin, M.E., Rossi, M.J., and Troe, J.: Evaluated kinetic and photochemical data for atmospheric chemistry: Volume I – gas phase reactions of O_x, HO_x, NO_x and SO_x species, *Atmos. Chem. Phys.*, 4, 1461-1738, 2004.

Atkinson, R., Baulch, D.L., Cox, R.A., Crowley, J.N., Hampson, R.F., Hynes, R.G., Jenkin, M.E., Rossi, M.J., and Troe, J.: Evaluated kinetic and photochemical data for atmospheric chemistry: Volume II – gas phase reactions of organic species, *Atmos. Chem. Phys.*, 6, 3625-4055, 2006.

Bader, D.C., and McKee, T.B.: Effects of Shear, Stability and Valley Characteristics on the Destruction of Temperature Inversions. *J. Clim. Appl. Meteor.*, 24, 822-832, 1985.

Bejan, I., Abd El Aal, Y., Barnes, I., Benter, T., Bohn, B., Wiesen, P., and Kleffmann, J.: The photolysis of ortho-nitrophenols: an new gas phase source of HONO, *Phys. Chem. Chem. Phys.* 8, 2028 –2035, 2006.

Bishop, G.A., Morris, J.A., Stedman, D.H., Cohen, L.H., Countess, R.J., Countess, S.J., Maly, P., Scherer, S.: The Effects of Altitude on Heavy-Duty Diesel Truck On-Road Emissions, *Environ. Sci. Technol.*, 35, 1574-1578, 2001.

Björkman, M.P., Kühnel, R., Partridge, D.G., Roberts, T.J., Aas, W., Mazzola, M., Viola, A., Hodson, A., Ström, J., and Isaksson, E.: Nitrate dry deposition in Svalbord, *Tellus B*, 65, 19071, http://dx.doi.org/10.3402/tellusb.v.65i0.19071, 1-18, 2013.

Carter, W.P.L., and Seinfeld, J.H.: Winter ozone formation and VOC incremental reactivities in the Upper Green River Basin of Wyoming, *Atmos. Environ.*, 50, 255-266, doi:10.1016/j.atmosenv.2011.12.025, 2012

Chameides, W.L., Fehsenfeld, F., Rodgers, M.O., Cardelino, C., Martinez, J., Parrish, D., Lonneman, W., Lawson, D.R., Rasmussen, R.A., Zimmerman, P., Greenberg, J., Middleton, P., Wang, T.: Ozone precursor relationships in the ambient air, *J. Geophys. Res.*, 97, 6037-6055, 1992.

Chen, J., So S., Lee H., Fraser M.P., Curl R.F., Harman T., and Tittel F.K.: Atmospheric Formaldehyde Monitoring in the Greater Houston Area in 2002, *Appl. Spectrosc.*, 58, 243-247, 2004.

Czader, B.H., Li, X., and Rappenglueck, B.: CMAQ modeling and analysis of radicals, radical precursors and chemical transformations, *J. Geophys. Res.*, doi: 10.1002/jgrd.50807, posted online: 5 Sep 2013, 2013.

Czader, B.H., Rappenglück, B., Percell, P., Byun, D., Ngan, F., and Kim, S.: Modeling nitrous acid and its impact on ozone and hydroxyl radical during the Texas Air Quality Study 2006, *Atmos. Chem. Phys.*, 12, 6939-6951, doi:10.5194/acp-12-6939-2012, 2012.

Dasgupta, P.K., Li J., Zhang G., Luke W.T., McClenny W.A., Stutz J., and Fried A.: Summertime Ambient Formaldehyde in Five U.S. Metropolitan Areas: Nashville, Atlanta, Houston, Philadelphia, and Tampa, *Environ. Sci. Technol.*, 39, 4767-4783, 2005.

Draxler, R.R., and Rolph, G.D.: HYSPLIT (HYbrid Single-Particle Lagrangian Integrated Trajectory) Model access via NOAA ARL READY Website

Deleted: in revision, 2013.

(http://ready.arl.noaa.gov/HYSPLIT.php). NOAA Air Resources Laboratory, Silver Spring, MD, 2013.

Edwards, P. M., Young, C. J., Aikin, K., deGouw, J. A., Dubé, W. P., Geiger, F., Gilman, J. B., Helmig, D., Holloway, J. S., Kercher, J., Lerner, B., Martin, R., McLaren, R., Parrish, D. D., Peischl, J., Roberts, J. M., Ryerson, T. B., Thornton, J., Warneke, C., Williams, E. J., and Brown, S. S.: Ozone photochemistry in an oil and natural gas extraction region during winter: simulations of a snow-free season in the Uintah Basin, Utah, *Atmos. Chem. Phys. Discuss.*, 13, 7503-7552, doi:10.5194/acpd-13-7503-2013, 2013.

EIA (U.S. Energy Information Administration): Top 100 Oil and Gas Fields, http://www.eia.gov/oil_gas/rpd/topfields.pdf, accessed February 2013, 2009.

Elshorbany, Y.F., Kleffmann, J., Hofzumahaus, A., Kurtenbach, R., Wiesen, P., Brauers, T., Bohn, B., Dorn, H.-P., Fuchs, H., Holland, F., Rohrer, F., Tillmann, R., Wegener, R., Wahner, A., Kanaya, Y., Yoshino, A., Nishida, S., Kajii, Y., Martinez, M., Kubistin, D., Harder, H., Lelieveld, J., Elste, T., Plass-Dülmer, C., Stange, G., Berresheim, H., and Schurath, U.: HO_x budgets during HOxComp: A case study of HO_x chemistry under NO_x-limited conditions, *J. Geophys. Res.*, 117, D03307, doi:10.1029/2011JD017008, 2012.

Elshorbany, Y.F., Kurtenbach, R., Wiesen, P., Lissi, E., Rubio, M., Villena, G., Gramsch, E., Rickard, A.R., Pilling, M.J., and Kleffmann, J.: Oxidation capacity of the city air of Santiago de Chile, *Atmos. Chem. Phys.*, 9, 2257-2273, 2009.

Environ: Final Report - 2009 Upper Green River Ozone Study, Report to Wyoming Department of Environmental Quality (WDEQ), Cheyenne, WY, March 2010, available at http://deq.state.wy.us/aqd/downloads/AirMonitor/Wint09_Final_3-2010_a0.pdf, accessed 2013, 2010.

Field, R.A., Soltis, J., and Montague, D.: Pinedale Anticline Spatial Air Quality Assessment (PASQUA), Mobile laboratory monitoring of ozone precursors, Boulder South Road site 10/29/2010 to 05/02/2011. *Summary Report University of Wyoming*, Laramie, Wyoming. Published on line at: http://www-das.uwyo.edu/ozone/index.html, 2011.

Field, R.A., Soltis, J., and Montague, D.: Pinedale Anticline Spatial Air Quality Assessment (PASQUA), 2011-2012 Spatial Distribution Surveys. *Summary Report University of*

Wyoming, Laramie, Wyoming. Published on line at: http://www-das.uwyo.edu/ozone/index.html, 2012a.

Field, R.A., Soltis, J., and Montague, D.: Temporal and Spatial Distributions of Volatile Organic Compounds Associated with Oil and Gas Development in the Upper Green River Basin of Wyoming, Invited in Session: A21J *American Geophysical Union, Fall Meeting*, San Francisco CA/USA, 03.-07.12.2012, 2012b.

Finlayson- Pitts, B. J., Wingen, L.M., Sumner, A.L., Syomin, D., and Ramazan, K.A.: The heterogeneous hydrolysis of NO_2 in laboratory systems and in outdoor and indoor atmospheres: An integrated mechanism, *Phys. Chem. Chem. Phys.*, 5, 223-242, 2003.

Finlayson-Pitts, B.J., and Pitts Jr., J.N.: Chemistry of the upper and lower atmosphere, Academic Press, San Diego, 969 pages, 2000.

Goodman, A. L., Underwood, G.M., and Grassian, V.H.: Heterogeneous reaction of NO_2: Characterization of gas-phase and adsorbed products from the reaction, $2NO_{(2)}(g)+H_2O(a)$-> $HONO(g)+HNO_3(a)$ on hydrated silica particles, *J. Phys. Chem. A*, 103(36), 7217-7223, 1999.

Hauglstaine, D.A., Granier, C., Brasseur, G.P., and Megie, G.: The importance of atmospheric chemistry in the calculation of radiative forcing on the climate system, *J. Geophys. Res.*, 99, 1173-1186, 1994.

Hayden, K.L., Anlauf, K.G., Hastie, D.R., Bottenheim, J.W.: Partitioning of reactive atmospheric nitrogen oxides at an elevated site in southern Quebec, Canada, *J. Geophys. Res.*, 108, 4603, doi:10.1029/2002JD003188, 2003.

Heland, J., Kleffmann, J., Kurtenbach, R., and Wiesen, P.: A new instrument to measure gaseous nitrous acid (HONO) in the atmosphere, *Environ. Sci. Technol.*, 35, 3207-3212, 2001.

Helmig, D., Cohen, L.D., Bocquet, F., Oltmans, S., Grachev, A., and Neff, W.: Spring and summertime diurnal surface ozone fluxes over the polar snow at Summit, Greenland, *Geophys. Res. Lett.*, 36, L08809, doi:10.1029/2008GL036549, 2009.

Honrath, R.E., Lu, Y., Peterson, M.C., Dibb, J.E., Arsenault, M.A., Cullen, N.J., Steffen, K.: Vertical fluxes of NO_x, HONO, and HNO_3 above the snowpack at Summit, Greenland, *Atmos. Environ.*, 36, 2629-2640, 2002.

Jacobson, M.Z.: Air Pollution and Global Warming, History, Science, And Solutions, Cambridge University Press, 406 pages, 2012.

Jenkin, M. I., Cox, R.A., and Williams, D.J.: Laboratory studies of the kinetics of formation of nitrous acid from the thermal reaction of nitrogen dioxide and water vapour, *Atmos. Environ.*, 22, 487-498, 1988.

Kirchstetter, T. W., Harley, R.A., and Littlejohn, D.: Measurement of Nitrous Acid in Motor Vehicle Exhaust, *Environ Sci Technol*, 30(9), 2843-2849, 1996.

Kleffmann, J.: Daytime sources of nitrous acid (HONO) in the atmospheric boundary layer, *Chem. Phys.*, 8(8), 1137-1144, 2007.

Kleffmann, J., Heland, J., Kurtenbach, R., Lörzer, J.C., and Wiesen, P.: A new instrument (LOPAP) for the detection of nitrous acid (HONO), *Environ. Sci. Pollut. Res.*, 9, 48-54, 2002.

Kleffmann, J., Becker, K.H., and Wiesen, P.,: Heterogeneous NO_2 conversion processes on acid surfaces: possible atmospheric implications, *Atmos. Environ.*, 32, 2721 - 2729, 1998.

Kleffmann, J., Lörzer, J.C., Wiesen, P., Kern, C., Trick, S., Volkamer, R., Ródenas, M., and Wirtz, K.: Intercomparison of the DOAS and LOPAP techniques for the detection of nitrous acid (HONO), *Atmos. Environ.*, 40, 3640-3652, 2006.

Kleffmann, J., and Wiesen, P.: Technical Note: Quantification of interferences of wet chemical HONO LOPAP measurements under simulated polar conditions, *Atmos. Chem. Phys.*, 8, 6813-6822, 2008.

Kurtenbach, R., Becker K.H., Gomes J.A.G., Kleffmann J., Lörzer J.C., Spittler M., Wiesen P., Ackermann R., Geyer A., and Platt U.: Investigations of emissions and heterogeneous formation of HONO in a road traffic tunnel, *Atmos. Environ.*, 35(20), 3385-3394, 2001.

Lefer, B., Rappenglück B: The TexAQS-II radical and aerosol measurement project (TRAMP), *Atmos. Environ.*, 44, 3997-4004, doi:10.1016/j.atmosenv.2010.05.053, 2010.

Leuchner, M., and Rappenglück, B.: VOC Source-Receptor Relationships in Houston during TexAQS-II, *Atmos. Environ.*, 44, 4056-4067, doi:10.1016/j.atmosenv.2009.02.029, 2010.

Li, S. P., Matthews, J., and Sinha, A.: Atmospheric hydroxyl radical production from electronically excited NO_2 and H_2O, *Science,* 319(5870), 1657-1660, 2008.

Lu, K.D., Rohrer, F., Holland, F., Fuchs, H., Bohn, B., Brauers, T., Chang, C.C., Häseler, R., Hu, M., Kita, K., Kondo, Y., Li, X., Lou, S.R., Nehr, S., Shao, M., Zeng, M., Wahner, A., Zhang, Y.H., and Hofzumahaus, A.: Observation and modelling of OH and HO2 concentrations in the Pearl River Delta 2006: a missing OH source in a VOC rich atmosphere, *Atmos. Chem. Phys.*, 12, 1541-1569, 2012.

Luke, W.T., Kelley, P., Lefer, B.L., Flynn, J., Rappenglück, B., Leuchner, M., Dibb, J.E., Ziemba, L.D., Anderson, C.H., and Buhr, M.: Measurements of Primary Trace Gases and NO_y Composition in Houston, Texas, *Atmos. Environ.*, 44, 4068-4080, doi:10.1016/j.atmosenv.2009.08.014, 2010.

Mack, J., and Bolton, J.R.: Photochemistry of nitrite and nitrate in aqueous solution: A review, *J. Photochem. Photobiol. A: Chem.*, 128, 1-13, 1999.

Mao, J., Ren, X., Chen, S., Brune, W.H., Chen, Z., Martinez, M., Harder, H., Lefer, B., Rappenglück, B., Flynn, J., and Leuchner, M.: Atmospheric Oxidation Capacity in the Summer of Houston 2006: Comparison with Summer Measurements in Other Metropolitan Studies, *Atmos. Environ.*, 44, 4107-4115, doi:10.1016/j.atmosenv.2009.01.013, 2010.

McLaren, R., Salmon, R. A., Liggio, J., Hayden, K. L., Anlauf, K. G., and Leaitch, W. R., Nighttime chemistry at a rural site in the Lower Fraser Valley, *Atmos. Environ.*, 38, 5837–5848, 2004.

MSI (Meteorological Solutions Inc.): Final Report 2011 Upper Green River Ozone Study, Report to Wyoming Department of Environmental Quality (WDEQ), Cheyenne, WY, October 2011, available at http://deq.state.wy.us/aqd/downloads/AirMonitor/Final_UGWOS_2011_Ozone_Study_Report_Text_and_Appendices.pdf, accessed 2013, 2011.

Olaguer, E.P., Kolb, C.E., Lefer, B., Rappenglück, B., Zhang, R., Pinto, J.P.: Overview of the SHARP campaign: motivation, design, and major outcomes, *J. Geophys. Res.*, accepted, 2013.

Deleted: MSI (Meteorological Solutions Inc.): Final Report - 2009 Upper Green River Ozone Study, Report to Wyoming Department of Environmental Quality (WDEQ), Cheyenne, WY, October 2009, 2009.¶

Parrish, D.D., Allen, D.T., Bates, T.S., Estes, M., Fehsenfeld, F.C., Feingold, G., Ferrare, R. , Hardesty, R.M., Meagher, J.F., Nielsen-Gammon, J.W., Pierce, R.B., Ryerson, T.B., Seinfeld, J.H., Williams, E.J.: Overview of the second Texas air quality study (TexAQS-II) and the Gulf of Mexico atmospheric composition and climate study (GoMACCS). *J. Geophys. Res.* 114, D00F13. doi:10.1029/2009JD011842, 2009.

Pinto J., Dibb J., Lee B., Rappenglück B., Wood E., Zhang R., Lefer B., Ren X., Stutz J., Ackermann L., Golovko J., Herndon S., Levi M., Meng Q., Munger J., Zhaniser M., Zheng J.: Intercomparison of Field Measurements of Nitrous Acid (HONO) during the SHARP Campaign, *J. Geophys. Res.*, submitted, 2013.

Ramazan, K. A., Wingen, L.M., Miller, Y., Chaban, G.M., Gerber, R.B., Xantheas, S.S., and Finlayson-Pitts, B.J.: New Experimental and Theoretical Approach to the Heterogeneous Hydrolysis of NO_2: Key Role of Molecular Nitric Acid and Its Complexes, *J. Phys. Chem.* A 2006 110 (21), 6886-6897, 2006.

Rappenglück, B.: WDEQ UGWOS 2010 HONO Measurements, Report to Meteorological Solutions Inc. Salt Lake City, UT, May 2010, 2010.

Rappenglück, B.: WDEQ UGWOS 2011 HONO Measurements, Report to Meteorological Solutions Inc. Salt Lake City, UT, August 2011, 2011.

Rappenglück, B., Dasgupta, P.K., Leuchner, M., Li, Q., and Luke, W.: Formaldehyde and its relation to CO, PAN, and SO_2 in the Houston-Galveston airshed, *Atmos. Chem. Phys.*, 10, 2413-2424, 2010.

Rappenglück, B., Lubertino, G., Alvarez, S., Golovko, J., Czader, B., and Ackermann, L.,: Radical Precursors and Related Species from Traffic as Observed and Modeled at an Urban Highway Junction, *J. Air Waste Man. Assoc.*, doi: 10.1080/10962247.2013.822438, posted online: 18 Jul 2013, 2013.

Rappenglück, B., Melas, D., and Fabian, P.: Evidence of the impact of urban plumes on remote sites in the Eastern Mediterranean, *Atmos. Environ.*, 37, 1853-1864, 2003.

Deleted: accepted

Reidmiller, D.R., Jaffe, D.A., Fischer, E.V., and Finley, B.: Nitrogen oxides in the boundary layer and free troposphere at the Mt. Bachelor Observatory, *Atmos. Chem. Phys.*, 10, 6043-6062, 2010.

Ren, X., van Duin, D., Cazorla, M., Chen, S., Mao, J., Brune, W.H., Flynn, J.H., Grossberg, N., Lefer, B.L., Rappenglück, B., Wong, K.W., Tsai, C., Stutz, J., Dibb, J.E., Jobson, B.T., Luke, W.T., and Kelley, P.: Atmospheric Oxidation Chemistry and Ozone Production: Results from SHARP 2009 in Houston, Texas, *J. Geophys. Res.*, 118, 5770-5780, doi: 10.1002/jgrd.50342, 2013.

Ren, X., Harder, H., Martinez, M., Lesher, R. L., Oliger, A., Shirley, T., Adams, J., Simpas, J. B., and Brune, W. H.: HO_x concentrations and OH reactivity observations in New York City during PMTACS-NY2001, Atmos. Environ., 37, 3627–3637, 2003.

Rickard, A. R., Johnson, D., McGill, C. D., and Marston, G.: OH yields in the gas-phase reactions of ozone with alkenes, *J. Phys. Chem.*, A103, 7656–7664, 1999.

Ridley, B.A., Shetter, J.D., Gandrug, B.W., Salas, L.J., Singh, H.B., Caroll, M.A., Hübler, G., Albritton, D.L., Hastie, D.R., Schiff, H.I., Mackay, G.I., Karechi, D.R., Davies, D.D., Bradshaw, J.D., Rodgers, M.O., Sandholm, S.T., Torres, A.L., Condon, E.P., Gregory, G.L., and Beck, S.M.: Ratios of peroxyacetylnitrate to active nitrogen observed during aircraft flights over the eastern Pacific oceans and continental United States. *J. Geophys. Res.*, 95, 10179–10192, 1990.

Ródenas, M., Munoz, A., Alacreu, F., Brauers, T., Dorn, H.-P., Kleffmann, J., and Bloss, W.: Assessment of HONO Measurements: the FIONA Campaign at EUPHORE in Disposal of Dangerous Chemicals in Urban Areas and Mega Cities, I. Barnes and K.J. Rudzinski (eds.), *NATO Science for Peace and Security Series C: Environmental Security*, DOI 10.1007/978-94-007-5034-0_4, 2013.

Ródenas, M., Muñoz, A., Alacreu, F., Dorn, H-P., Brauers, T., Kleffmann, J., Mikuška, P., Večeřa, Z., Häseler, R., Ye, C., Ruth, A., Dixneuf, S., Venables, D., Darby, S., Chen, J., Ashu-ayem, E., Elshorbany, Y., Voigt, C., Jessberger, P., Kaufmann, S., Schäuble, D., Mellouki, A., Cazaunau, M., Grosselin, B., Colomb, A., Michoud, V., Miet, K., Ball, S., Daniels, M., Goodall, I., Tan, D., Stickel, R., Case, A., Rappenglück, B., Croxatto, G.,

Deleted: in press,

Deleted: . u

Percival, C., Bacak, A., Mcguillen, M., Dibb, J., Scheuer, E., Zhou, X., Ferm, M., Varma, R., Pilling, M., Clemente, E., Porras, R., Vera, T., Vázquez, M., Borrás, E., Valero, J., and Bloss, W.: The FIONA campaign (EUPHORE): Formal Intercomparison of Observations of Nitrous Acid, *EGU Joint Assembly*, Vienna/Austria, 03.-09.04.2011, 2011.

Rolph, G.D.: Real-time Environmental Applications and Display sYstem (READY) Website (http://ready.arl.noaa.gov). NOAA Air Resources Laboratory, Silver Spring, MD, 2013.

Sarwar, G., Roselle S.J., Mathur R., Appel W., Dennis R.L., and Vogel, B.: A comparison of CMAQ HONO predictions with observations from the Northeast Oxidant and Particle Study, *Atmos. Environ.*, 42, 5760-5770, 2008

Schnell, R.C., Oltmans, S.J., Neely, R.R., Endres, M.S., and Molenar, J.V.,: Rapid photochemical production of ozone at high concentrations in a rural site during winter, *Nat. Geosci.*, 2, 120-123, 2009.

Sheehy, P.M., Volkamer, R., Molina, L.T., and Molina, M.J.: Oxidative capacity of the Mexico City atmosphere - Part 2: A RO_x radical cycling perspective, *Atmos. Chem. Phys.*, 10, 6993-7008, 2010.

Sillman, S.: Observation-based methods (OBMs) for analyzing urban/regional ozone production and Ozone-NO_x-VOC sensitivity, Report to EPA, 1D-57-95-NTEX, available at http://www-personal.umich.edu/~sillman/obm.htm, accessed 2013, 2002.

Sillman, S., and He, D.: Some theoretical results concerning O_3-NO_x-VOC chemistry and NO_x-VOC indicators, *J. Geophys. Res.*, 107, D22, 4659, 2002.

Sörgel, M., Regelin, E., Bozem, H., Diesch, J.-M., Drewnick, F., Fischer, H., Harder, H., Held, A., Hosaynali-Beygi, Z., Martinez, M., and Zetsch, C.: Quantification of the unknown HONO daytime source and its relation to NO_2, *Atmos. Chem. Phys.*, 11, 10433-10447, doi:10.5194/acp-11-10433-2011, 2011.

Sommariva, R., Trainer, M., de Gouw, J.A., Roberts, J.M., Warneke, C., Atlas, E., Flocke, F., Goldan, P.D., Kuster, W.C., Swanson, A.L., Fehsenfeld, F.C., A study of organic nitrates formation in an urban plume using a Master Chemical Mechanism, *Atmos. Environ.*, 42, 5771-5786, 2008.

Stemmler, K., Ndour, M., Elshorbany, Y., Kleffmann, J., D'Anna, B., George, C., Bohn, B., Ammann, M.: Light induced conversion of nitrogen dioxide into nitrous acid on submicron humic acid aerosol, *Atmos. Chem. Phys.*, 7(16), 4237-4248, 2007.

Stull, R.B.: An Introduction to Boundary Layer Meteorology, Springer, 684 pages, 1988.

Deleted: Bounday

Stutz, J., Alicke B., Ackermann R., Geyer A., Wang S., White A.B., Williams E.J., Spicer E.J., and Fast, J.D.: Relative humidity dependence of HONO chemistry in urban areas, *J. Geophys. Res.*, 109, D03307, doi: 10.1029/2003JD004135, 2004.

Stutz, J., Oh, H.-J., Whitlow, S.I., Anderson, C.H., Dibb, J.E., Flynn, J., Rappenglück, B., and Lefer, B.: Simultaneous DOAS and Mist-Chamber IC measurements of HONO in Houston, TX, *Atmos. Environ.*, 44, 4090-4098, doi:10.1016/j.atmosenv.2009.02.003, 2010a.

Stutz, J., Wong, K.W., Lawrence, L., Ziemba, L., Flynn, J.H., Rappenglück, B., and Lefer, B.: Nocturnal NO_3 radical chemistry in Houston, TX, *Atmos. Environ.*, 44, 4099-4106, doi:10.1016/j.atmosenv.2009.03.004, 2010b.

TUV (2010): TUV 5.0 model version 5, November 2010. available at http://cprm.acd.ucar.edu/ Models/TUV/. Madronich, S. and S. Flocke, Theoretical estimation of biologically effective UV radiation at the Earth's surface, in Solar Ultraviolet Radiation - Modeling, Measurements and Effects (Zerefos, C., ed.). NATO ASI Series Vol. I52, Springer-Verlag, Berlin, 1997.

U.S. EPA (U.S. Environmental Protection Agency: Area Designations for 2008 Ground-level Ozone Standards, http://www.epa.gov/ozonedesignations/2008standards/final/region8f.htm, accessed February 2013, 2012.

Villena, G., Wiesen, P., Cantrell, C.A., Flocke, F., Fried, A., Hall, S.R., Hornbrook, R.S, Knapp, D., Kosciuch, E., Mauldin, III R.L., McGrath, J.A., Montzka, D., Richter, D., Ullmann, K., Walega, J., Weibring, P., Weinheimer, A., Staebler, R.M., Liao, J., Huey, L.G., and Kleffman, J.: Nitrous acid (HONO) during polar spring in Barrow, Alaska: a net source of OH radicals?, *J. Geophys. Res.*, 116, D00R07, doi:10.1029/2011JD016643, 2011.

Wang, X., Yin, H., Ge, Y., Yu, L., Xu, Z., Yu, C., Shi, X., Liu, H.: On-vehicle emission measurement of a light-duty diesel van at various speeds at high altitude, *Atmos. Environ.*,, doi: 10.1016/j.atmosenv.2013.09.015, 2013

WDEQ: 2011 Winter Upper Green River Basin Emission Inventory, Wyoming Department of Environmental Quality (WDEQ), Cheyenne, Wyoming, 2011.

Wojtal, P., Halla, J. D., and McLaren, R.: Pseudo steady states of HONO measured in the nocturnal marine boundary layer: a conceptual model for HONO formation on aqueous surfaces, *Atmos. Chem. Phys.*, 11, 3243-3261, doi:10.5194/acp-11-3243-2011, 2011.

Yin, H., Ge, Y., Wang, X., Yu, L., Ji, Z., Chen, W.: Idle emission characteristics of a light-duty diesel van at various altitudes, *Atmos. Environ.*, 70, 117-122, doi:10.1016/j.atmosenv.2013.01.012, 2013

Yu C.-H., and Pielke, R.A.: Mesoscale Air Quality Under Stagnant Synoptic Cold Season Conditions in the Lake Powell Area. *Atmos. Environ.*, 20, 1751-1762, 1986.

Zhou, X., Beine, H.J., Honrath, R.E., Fuentes, J.D., Simpson, W., Shepson, P.B., and Bottenheim, J.W.: Snowpack photochemical production of HONO: a major source of OH in the arctic boundary layer in springtime, *Geophys. Res. Lett.*, 28 (21), 4087-4090, 2001.

Zhou, X., Gao, H., He, Y., and Huang, G.: Nitric acid photolysis on surfaces in low-NO_x environments: significant atmospheric implications, *Geophys. Res. Lett.*, 30(23), doi:10.1029/2003GL018620, 2003.

Zhou, X. L., He Y., Huang G., Thornberry T. D., Carroll M. A., and Bertman, S. B.,: Photochemical production of nitrous acid on glass sample manifold surface, *Geophys. Res. Lett.*, 29(14), doi:10.1029/2002GL015080, 2002.

Ziemba, L.D., Dibb, J.E., Griffin, R.J., Anderson, C.H., Whitlow, S.L., Lefer, B.L., Rappenglück, B., and Flynn, J.: Heterogeneous conversion of nitric acid to nitrous acid on the surface of primary organic aerosol in an urban atmosphere, *Atmos. Environ.*, 44, 4081-4089, doi:10.1016/j.atmosenv.2008.12.024, 2010.

Zweidinger, R.B., Sigsby J.E., Tejada S.B., Stump F.D., Dropkin D.L., Ray W.D., and Duncan J.W.:. Detailed hydrocarbon and aldehyde mobile source emissions from roadway studies, *Environ. Sci. Technol.*, 22, 956-962, 1988

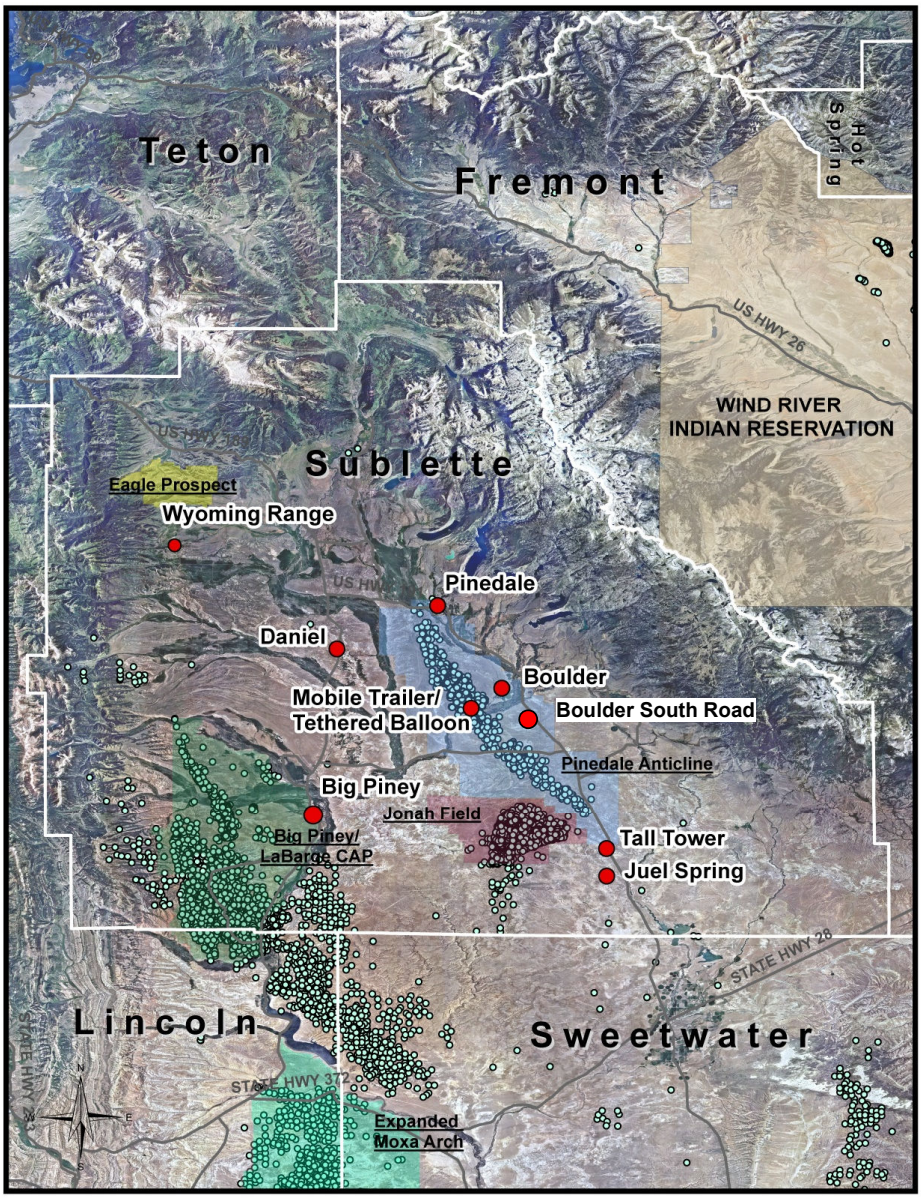

Jan 2010- May 2011 Oil and Gas Well Locations
WDEQ Monitors
Big Piney/LaBarge CAP
Expanded Moxa Arch
Jonah Field
Pinedale Anticline

Fig. 1. The monitoring sites "Boulder", "Boulder South Road", "Tethered Balloon", "Tall Tower" and other WDEQ (Wyoming Department of Environmental Quality) monitoring sites relative to the locations of oil and gas well locations operating during January – March 2011.

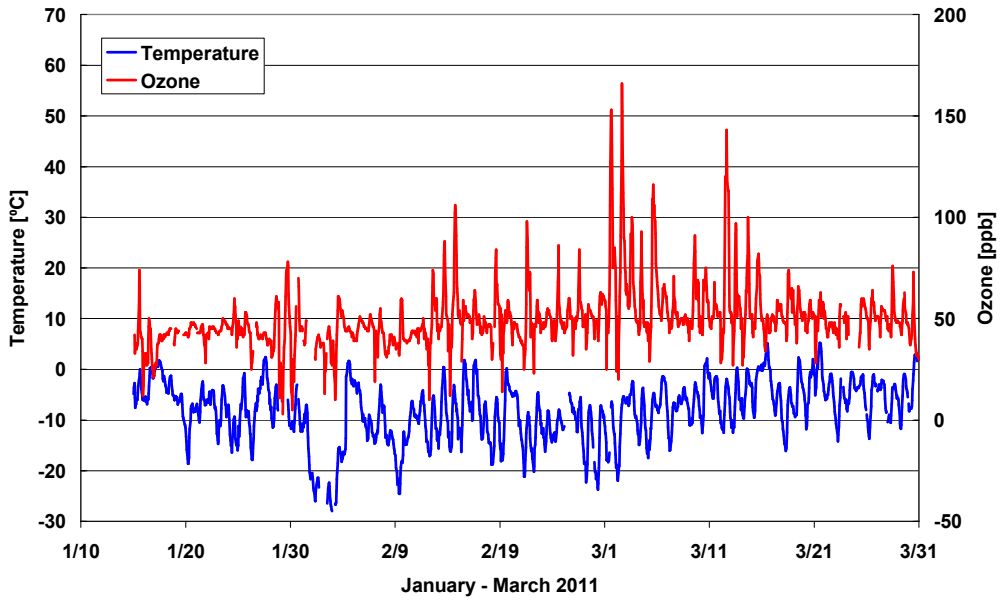

Fig. 2. Time series for ozone and temperature based on hourly data at the Boulder site for January-March 2011.

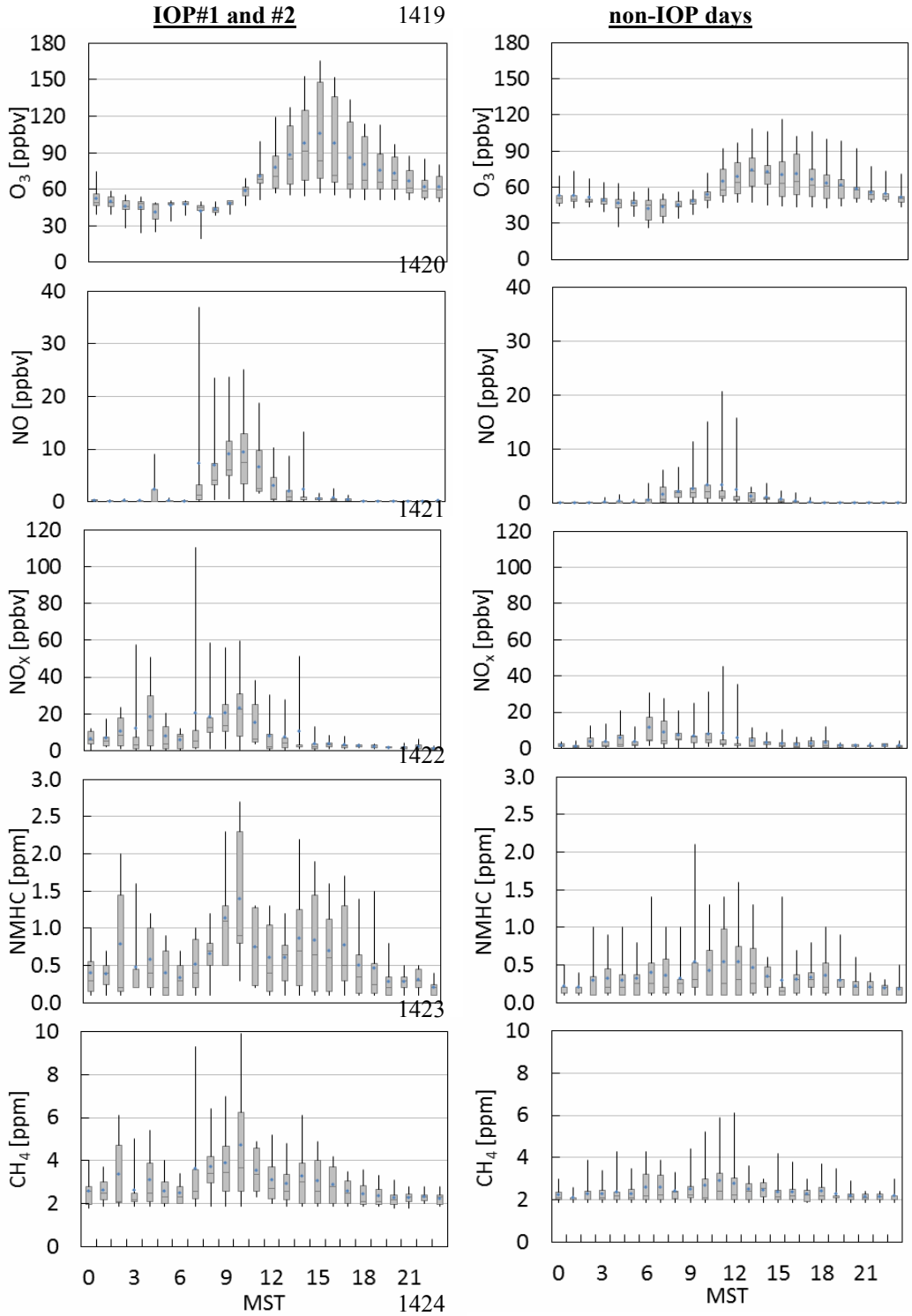

Fig. 3a. Mean diurnal variation of selected trace gases for IOP and non-IOP days.

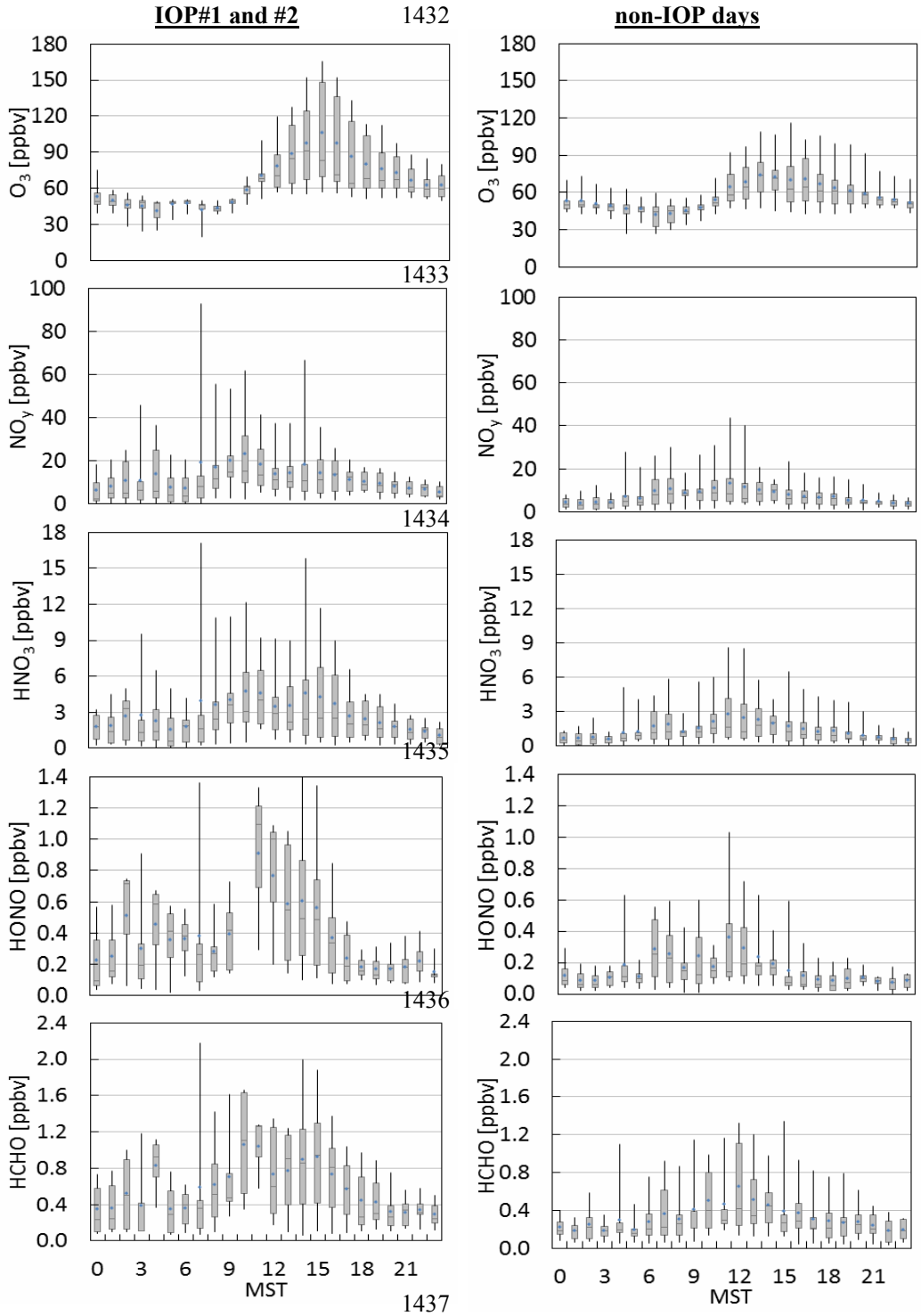

Fig. 3b. Mean diurnal variation of selected trace gases for IOP and non-IOP days.

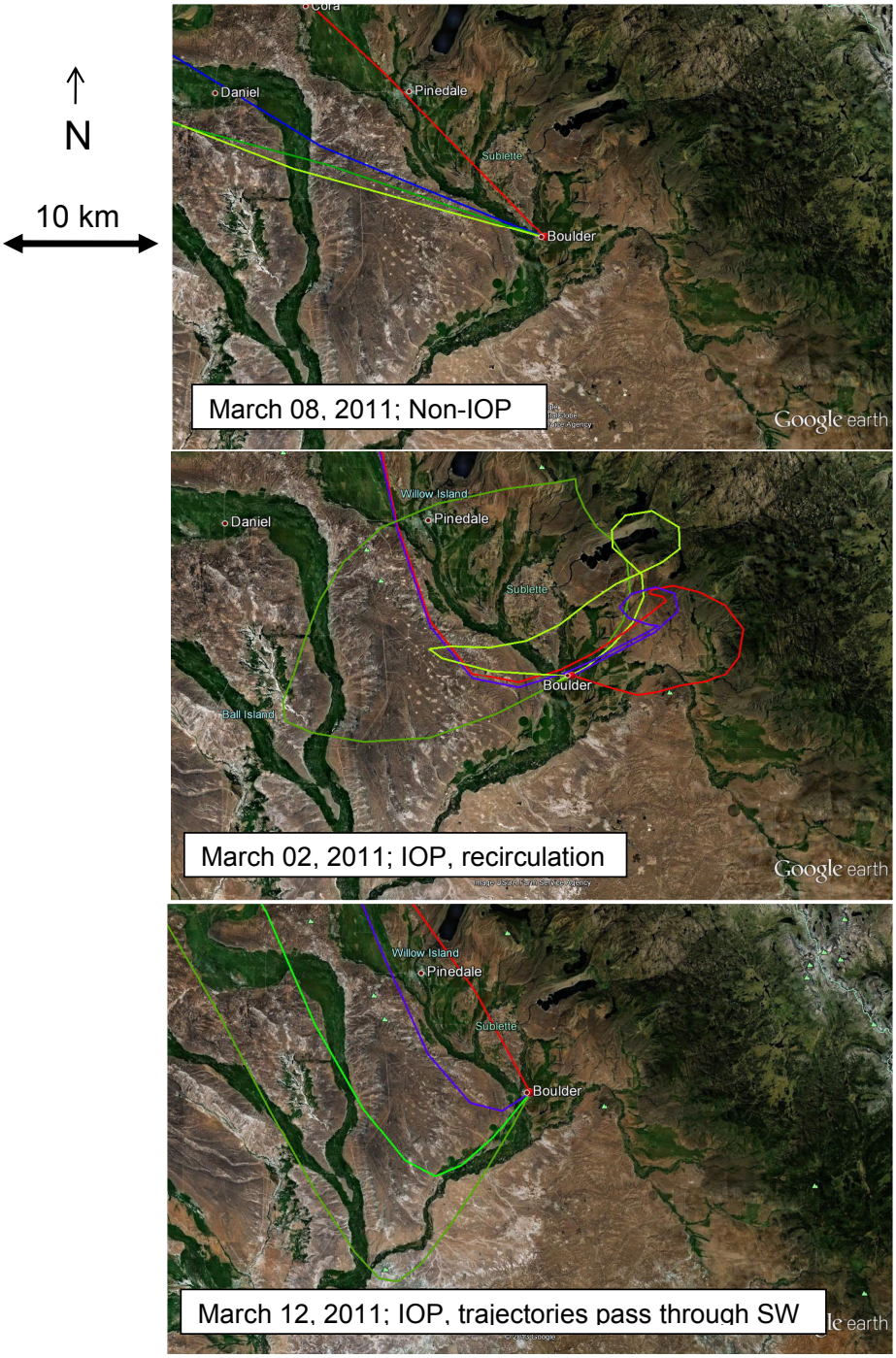

Fig. 4. HYSPLIT backward trajectories calculated for 50 m a.g.l. and for following arrival times at Boulder: 07:00 MST (red), 12:00 MST (blue), 14:00 MST (light green), and 17:00 MST (dark green).

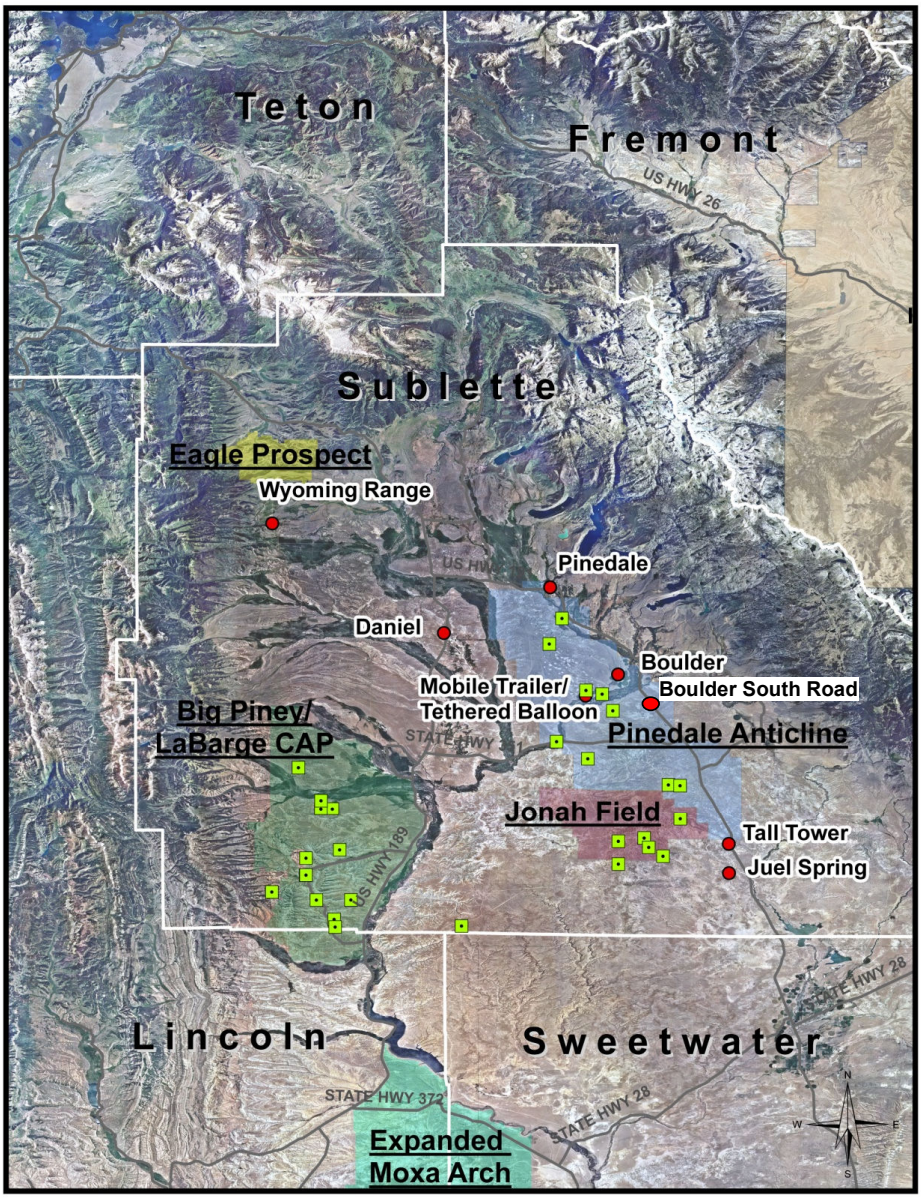

Fig. 5. Locations of compressors (green rectangles) operating during January – March 2011 relative to the Boulder monitoring site.

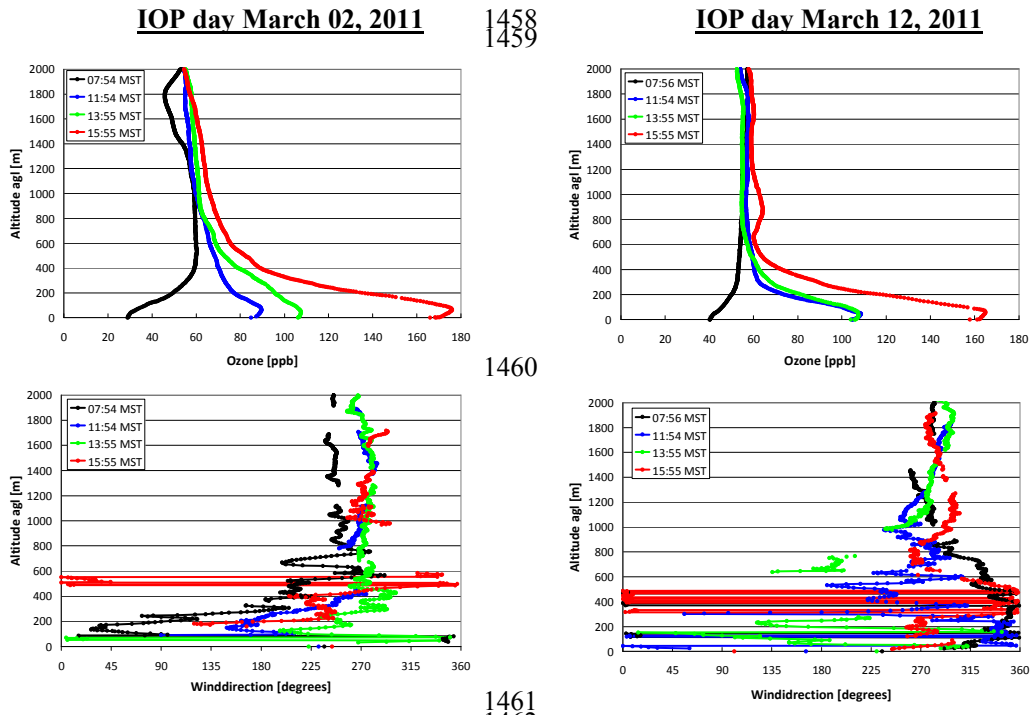

Fig. 6. Profiles of ozone (above) and wind direction (below) on IOP days March 02, 2011 (left) and March 12, 2011 (right).

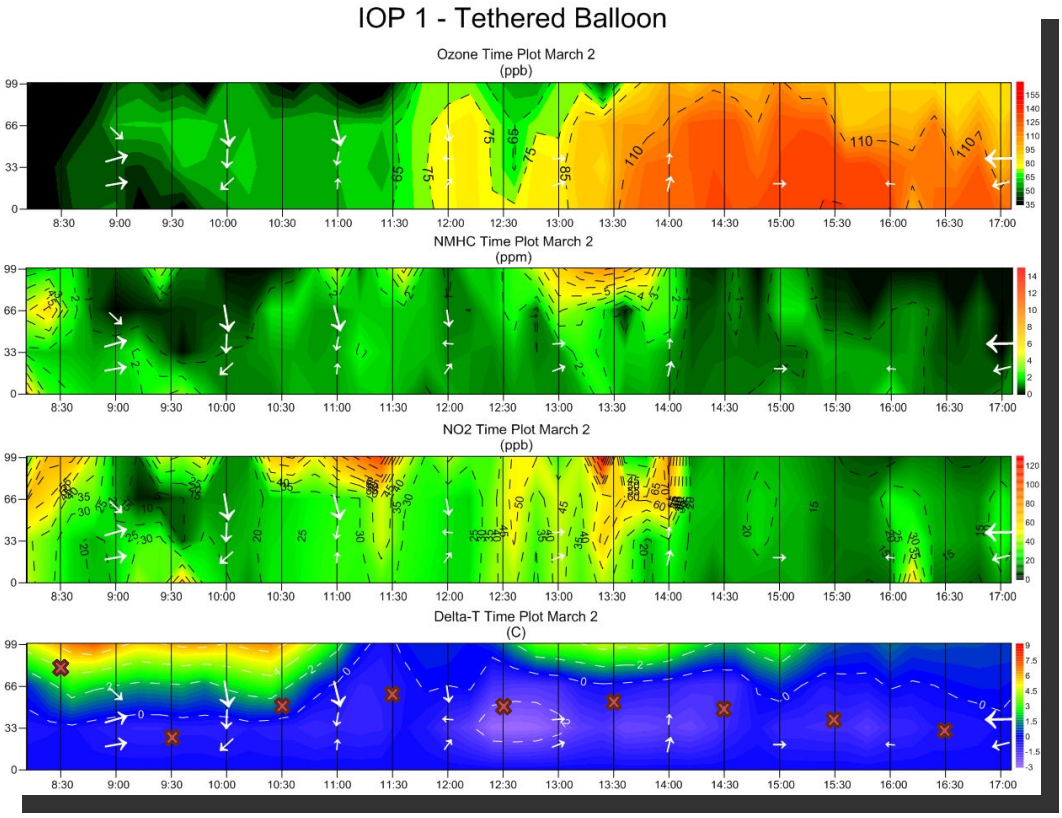

Fig. 7. Results from tethersonde measurements of ozone, NMHC, NO_2, and ΔT (Delta-T) on March 02, 2011. ΔT is defined as the temperature at a given level minus the temperature at the surface. Mixing layer heights as determined by SODAR data are indicated as "x" in the ΔT plot.

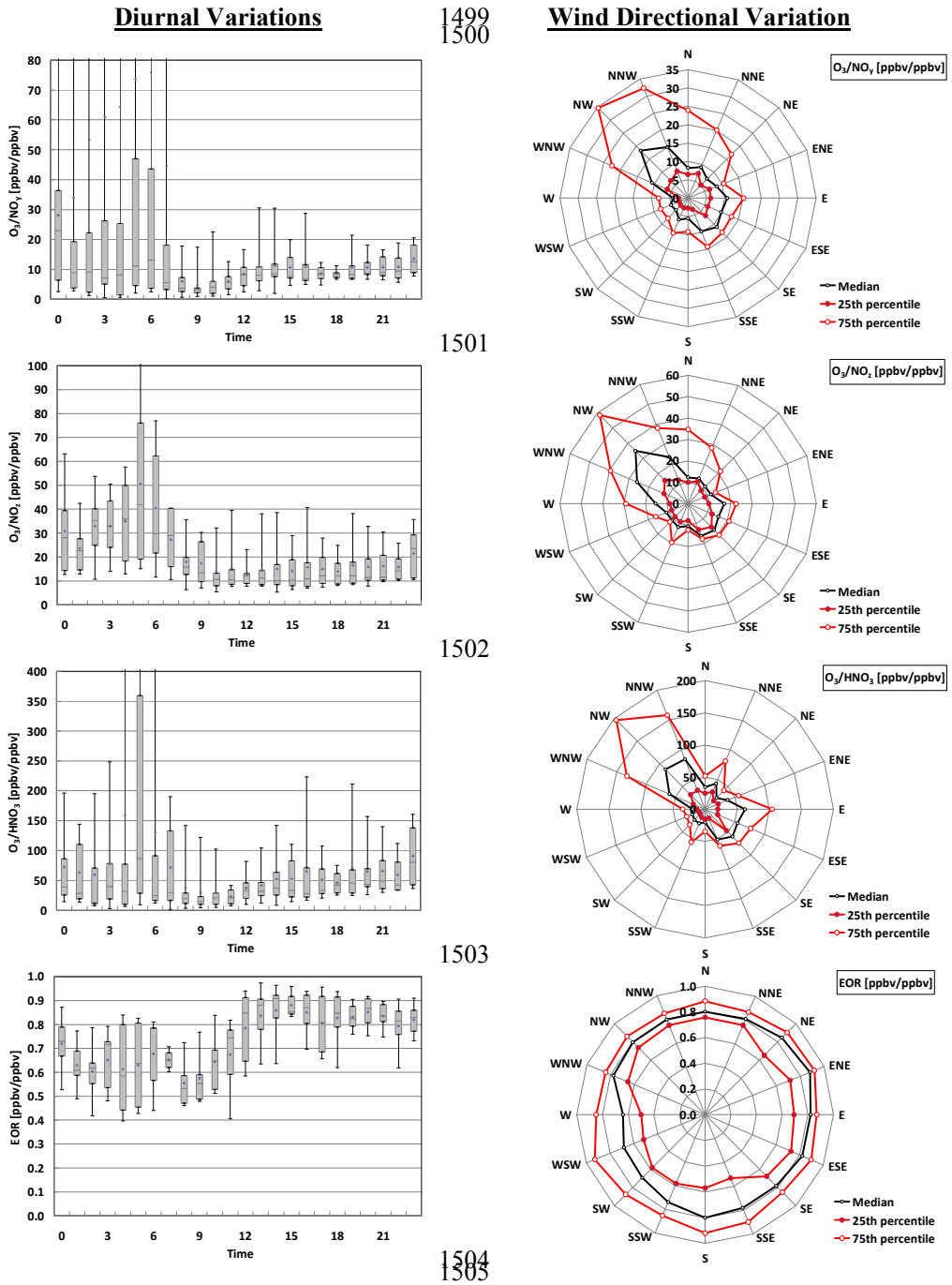

Fig. 8. Diurnal and wind directional variation of photochemical indicators O_3/NO_y, O_3/NO_z, O_3/HNO_3 and EOR on IOP days. Units shown in brackets for the wind directional variation plots refer to the radial direction of the corresponding trace gas plot.

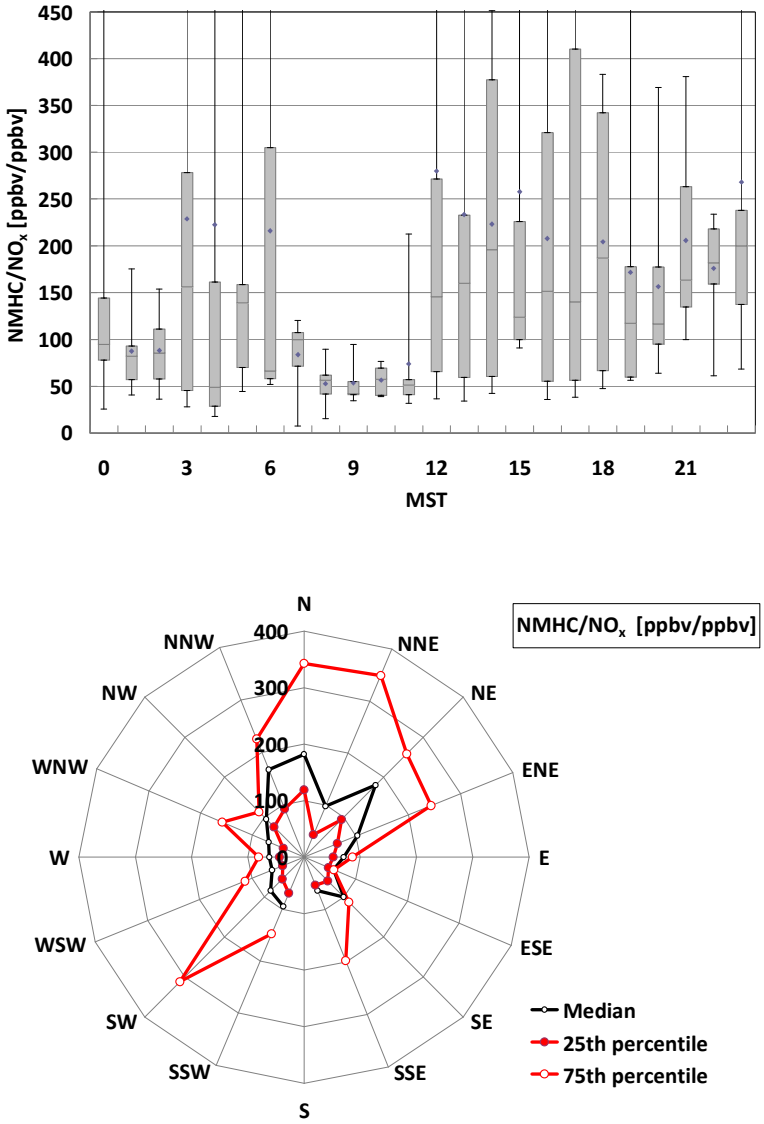

Fig. 9. Diurnal and wind directional variation of the NMHC/NO_x ratio at the Boulder site on IOP days. Units shown in brackets for the wind directional variation plots refer to the radial direction of the corresponding trace gas plot.

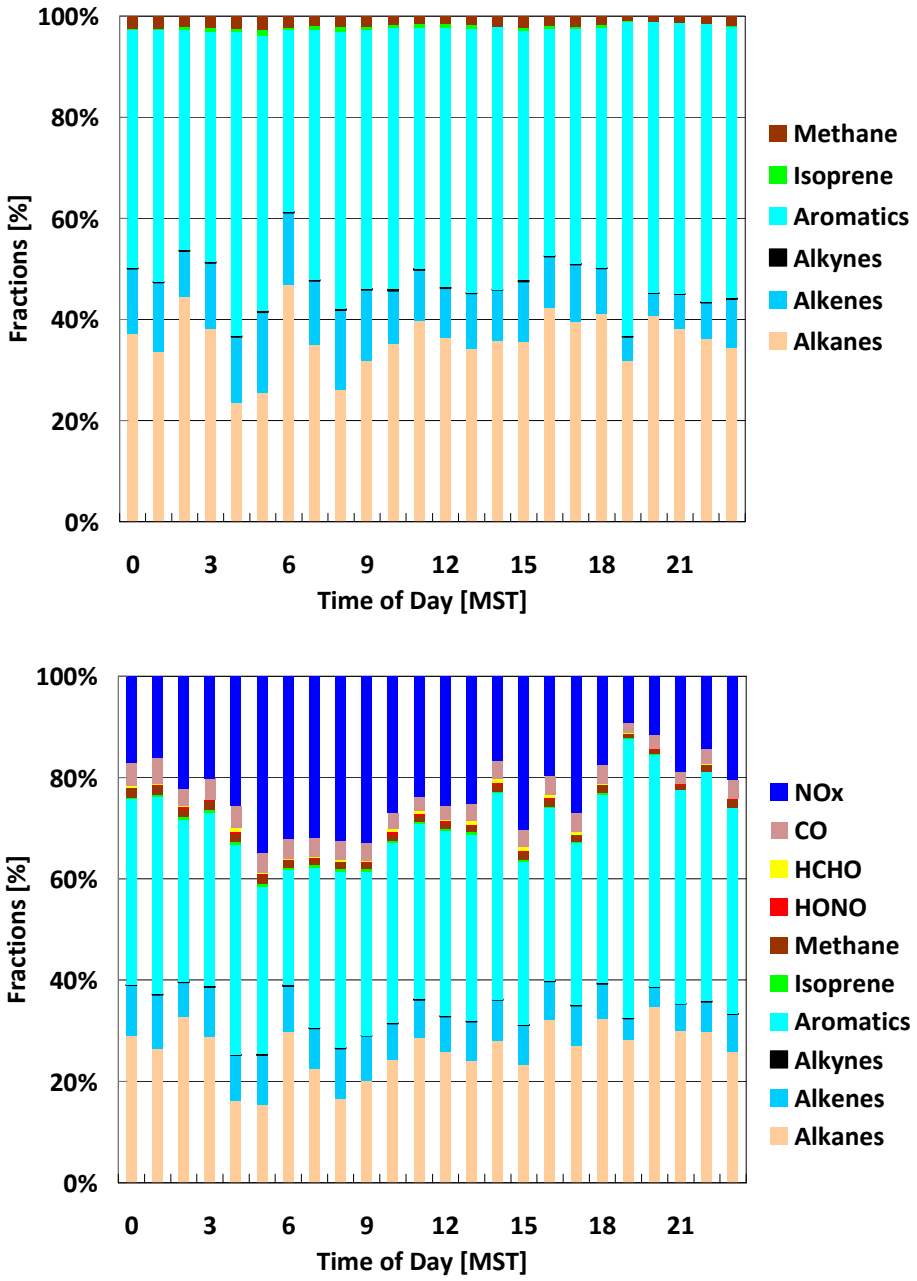

Fig. 10. Diurnal variation of fractions of propene-equivalent on IOP days. Above: NMHC classes and CH_4 only. Below: same as above, but in addition NO_x, CO, HCHO, and HONO. Speciated NMHC, NO_x, and CO data from the Boulder South Road site.

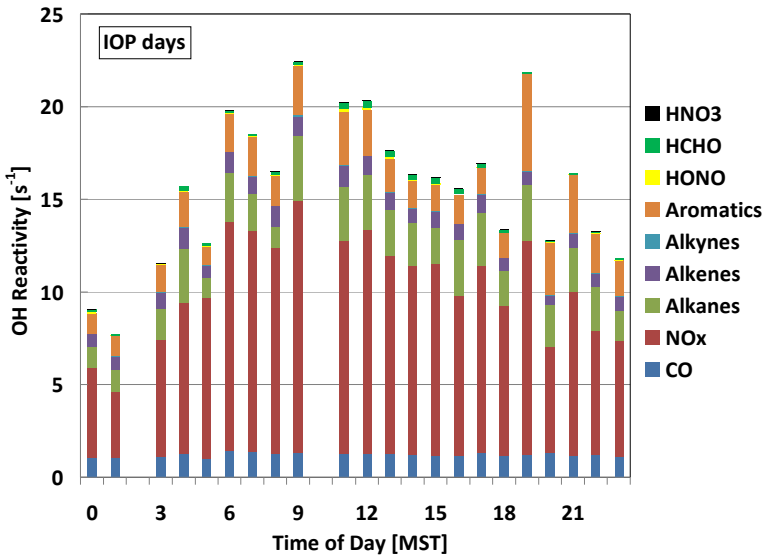

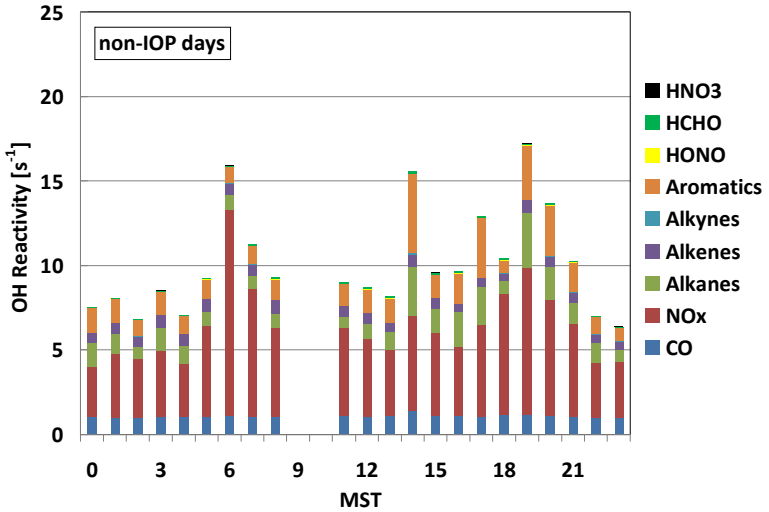

Fig. 11. OH reactivity on IOP days (above) and non-IOP days (below). Speciated NMHC, NO_x, and CO data from the Boulder South Road site.

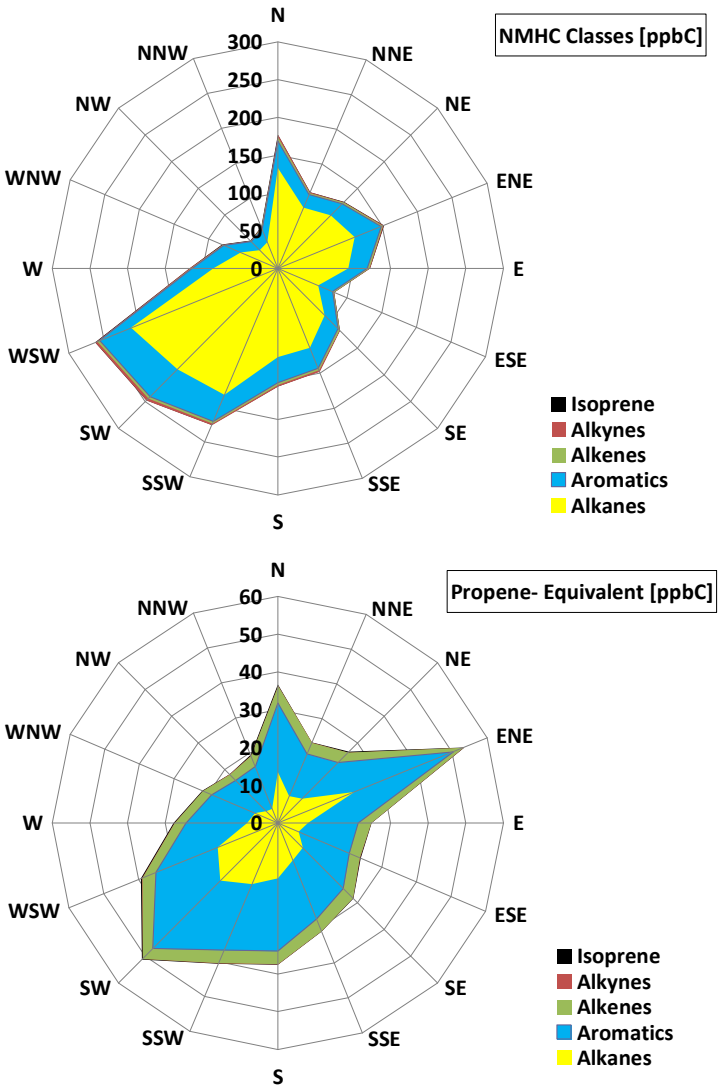

Fig. 12. Wind directional dependence of NMHC classes and the propene equivalent for all days. Speciated NMHC data from the Boulder South Road site. Units shown in brackets refer to the radial direction of the corresponding trace gas plot.

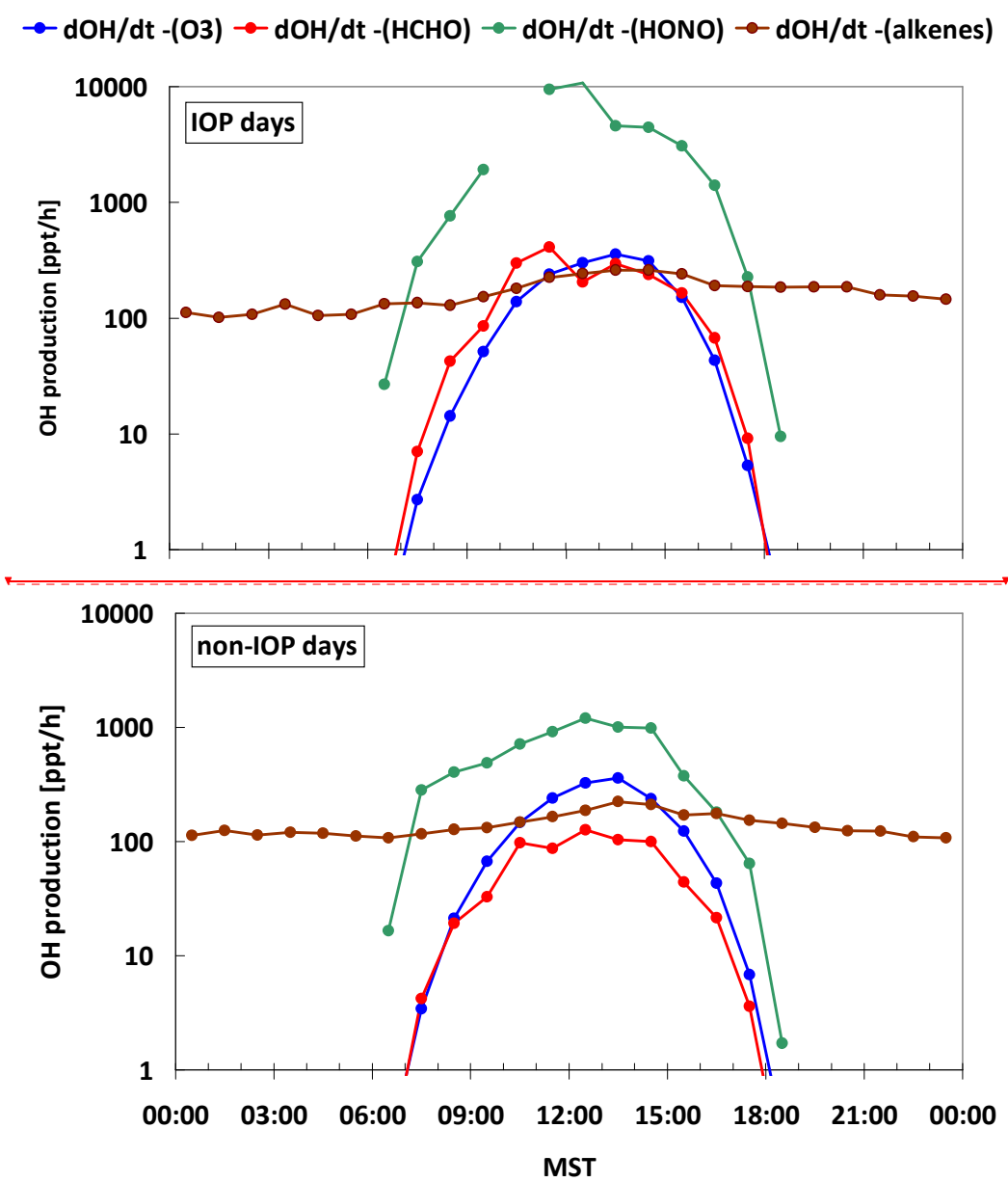

Fig. 13. OH production due to photolysis of O_3, HCHO, HONO, and alkene ozonolysis for IOP and non-IOP days.

Photolysis rates were calculated using the TUV model 5.0 (TUV 2010) considering the altitude of the Boulder site. Data for the snow surface albedo, the total ozone column and the total aerosol optical depth (AOD) at 550 nm for each day of the time frame 2/28 - 3/16/2011 were obtained from the European MAAC model reanalysis (http://data-portal.ecmwf.int/data/d/macc_reanalysis/). The corresponding values ranged from 0.63-0.76 (snow surface albedo), 306-381 Dobson units (total ozone column), and 0.128-0.448 (total AOD). Calculated photolysis rates were further adjusted using the ratio of TUV calculated surface UV radiation versus observed incoming UV radiation at the Boulder site for each hour of the field campaign.

Deleted: ¶

Deleted:

Deleted: ozone

Deleted: and

Deleted: based on latitude 43°N, date March 01, 80% albedo, and cloudless conditions using approaches in Finlayson-Pitts and Pitts (2000) and references therein

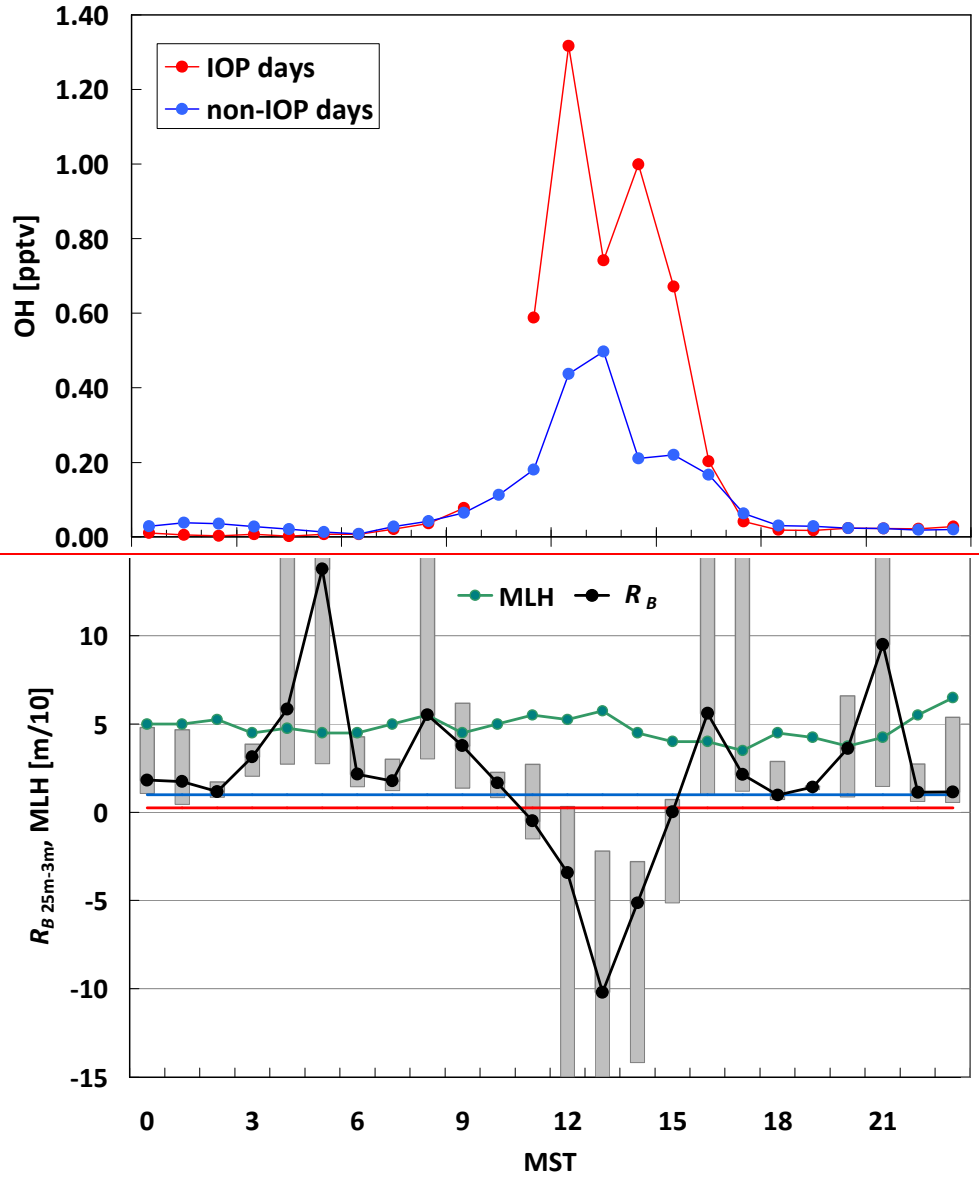

Fig. 14. Above: OH mixing ratios calculated based on equation (14) on IOP and non-IOP days. Below: median diurnal variation of the mixing layer height (MLH) and the Bulk Richardson number on IOP days between the levels 3 m and 25 m above the ground level as obtained at the "Tall Tower" site. The blue line indicates R_B=1, above which the flow is considered to be laminar. The red line indicates R_B=0.25, below which the flow is considered to be turbulent. 0.25 < R_B < 1, indicates a transitional range, where the flow can be either laminar or turbulent depending on its history.

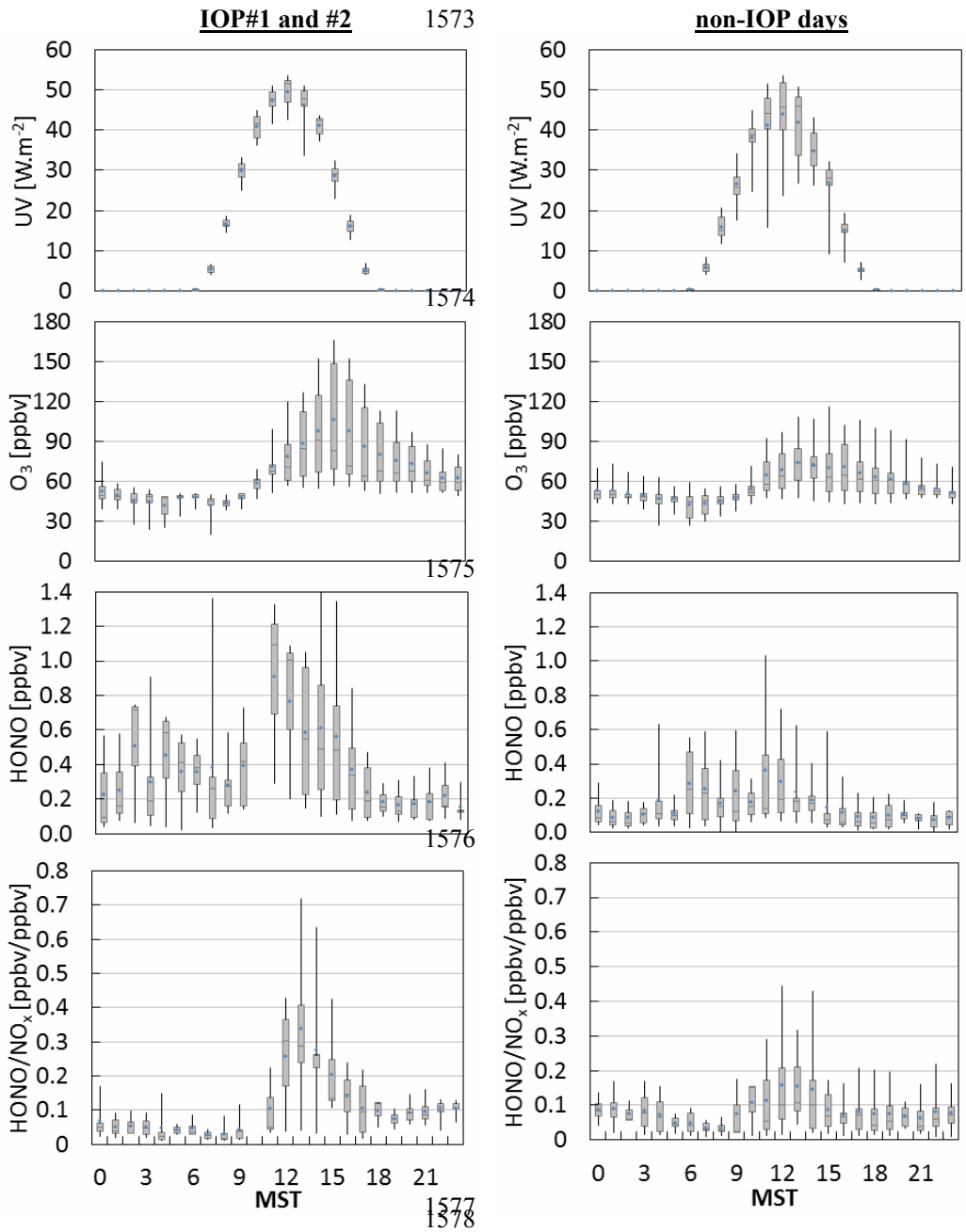

Fig. 15. Mean diurnal variation of incoming UV radiation, ozone, HONO, and the HONO/NO_x ratio for IOP and non-IOP days.

Deleted: 4

S1: Overview of air quality instrumentation used in this study (1-min data available, unless noted otherwise). At all sites standard meteorological systems.

Boulder site 42.7186°N, -109.7531°W; 2,160 m asl	**Method**	**Model**	**Accuracy**	**Precision**	**Detection Limit**
O_3	UV Photometric	T-API 400E		0.5%	0.6 ppbv
NO[*)]	Chemiluminescence	Super Snooper by AQD	± 5.4% +3 pptv		2 pptv
NO_2[*)]	Chemiluminescence	Super Snooper by AQD w/Blue Light Detector	± 13.6% + 6 pptv		2 pptv
NO_y[*)]	Chemiluminescence	Super Snooper by AQD w/molybdenum converter	± 14.8% + 4 pptv		2 pptv
HNO_3	Redox Denuder Difference	home-built instrument by AQD	± 26.9% + 50 pptv		0.1 ppbv
HONO[**)]	Long Path Absorption Photometry	QUMA-LOPAP	± 10%	5%	1-2 pptv
HCHO[***)]	Fluorometric Hantzsch Reaction	AL 4021	± 2%	10%	60 pptv
NMHC/CH_4[1)]	Flame Ionization Detection	Baseline-Mocon Series 9000 NMHC/CH_4 analyzer	± 5%	± 5%	0.1 ppmv
Speciated particulates[2)]	IMPROVE_A/TORTOT Elements: X-ray Fluorescence Major ions: Ion Chromatography	URG-3000N Carbon Sampler Met One SASS Speciation Air Sampler System	Total OC: 2-6 % Total EC: 2-6% < 10%	< 10 % < 10%	0.45 µg/cm^2 0.06 µg/cm^2
Mixing Layer height[3)]	Doppler Sodar	ASC Model 4000 miniSodar			15 m
Radiosondes[3)]	GPS-based Upper Air Sounding System	InterMet iMet-3050 403 MHz GPS	± 0.5 m/s (horiz.) ± 5° (horiz.) ± 0.2°C ± 2%		
Ozone sondes[3)]	Titration of ozone in KI	EN-SCI Corp. KZ-ECC O_3 sondes	± 10%		2-3 ppbv
Boulder South Road 42.6840°N, -109.7083°W; 2139 m asl					
NO_x[1)]	UV Photometric	Thermo Scientific 42i	< ± 5 %	< 5 %	0.4 ppbv
CO[1)]	NDIR	Thermo Scientific 48i TLE	< ± 5 %	< 10 %	0.04 ppmv
Speciated NMHCs [1)]	GC/FID	Perkin Elmer Ozone Precursor Analyzer	< ± 3 %	< 5 %	0.01 ppbv

Tethered Balloon site 42.6822°N, -109.8089°W; 2,143 m asl					
Temperature[3)]		HOBO U23 Pro V.2	± 0.21°C (0° to 50°C) ± 0.28°C (at - 20°C) ± 0.5°C (at - 30°C)		
Relative Humidity[3)]		HOBO U23 Pro V.2	± 2.5 % (10%-90% RH) ± 4.5 % (at 100% RH)		
O_3[3,4)]	UV Photometric	T-API 400E		0.5%	0.6 ppbv
$NO/NO_2/NO_x$[3,4)]	Chemiluminescence	T-API 200E		0.5 % > 50 ppb	0.4 ppbv
$NMHC/CH_4$[3,4)]	Flame Ionization Detection	Baseline-Mocon Series 9000 $NMHC/CH_4$ analyzer	± 5%	± 5%	0.1 ppmv

1) hourly data, 2) available as integrated 24 h measurements, 3) available on IOP days

4) surface-based instrumentation collecting data through a system of solenoid valves in the balloon inlet package which allowed the measurements to cycle between tethersonde height levels (4 m, 33 m, 67 m, and 100 m) and provided a measurement at each level every 12 minutes.

*) Reidmiller et al. (2010), **) Heland et al., 2001; Kleffmann et al., 2002, Ródenas et al., 2011, ***) Rappenglück et al., 2010

S2. Results for selected time periods for the Boulder site. Data in [ppbv], except for CH_4 and NMHC [ppmv]. Hourly data presented.

IOP days

	0500-0900 MST				1100-1700 MST				2100-0500 MST			
	Q_1^*	$Q_2^\#$	Q_3^+	Max.	Q_1^*	$Q_2^\#$	Q_3^+	Max.	Q_1^*	$Q_2^\#$	Q_3^+	Max.
O_3	42.7	46.6	48.7	50.9	63.2	73.0	119.6	165.8	46.3	51.0	58.7	87.7
NO	0.019	0.310	1.408	23.535	0.315	0.575	2.093	18.681	BDL	0.002	0.012	0.550
NO_2	1.416	5.362	10.862	25.815	0.791	1.863	3.229	29.012	1.899	3.353	9.748	29.648
NO_x	1.523	7.107	13.457	49.350	1.213	2.710	5.757	42.367	1.904	3.355	9.757	29.666
NO_y	3.045	9.587	15.977	55.398	5.902	11.287	19.498	66.443	4.914	7.848	13.170	30.493
HNO_3	0.283	0.893	2.549	10.906	1.225	2.484	5.951	15.795	0.481	1.295	2.477	6.525
HONO	0.130	0.317	0.442	1.360	0.201	0.510	0.972	1.397	0.093	0.164	0.363	0.908
HCHO	0.100	0.401	0.603	2.180	0.295	0.855	1.252	1.995	0.137	0.313	0.577	1.182
CH_4	2.00	2.65	3.40	9.30	2.00	2.80	3.90	6.1.	2.00	2.30	2.80	6.10
NMHC	0.10	0.45	0.73	1.20	0.20	0.60	1.20	2.20	0.20	0.30	0.50	2.00

*) Q_1: first quartile (25th percentile)
#) Q_2: second quartile (median)
+) Q_3: third quartile (75th percentile)
BDL: below detection limit

S2. continued.

non-IOP days

	0500-0900 MST				1100-1700 MST				2100-0500 MST			
	Q_1^*	$Q_2^\#$	Q_3^+	Max.	Q_1^*	$Q_2^\#$	Q_3^+	Max.	Q_1^*	$Q_2^\#$	Q_3^+	Max.
O_3	40.1	45.4	49.1	59.5	53.3	65.0	81.9	116.4	47.6	50.0	53.6	77.4
NO	0.038	0.399	1.778	6.591	0.181	0.672	1.376	20.737	BDL	0.002	0.007	0.053
NO_2	2.199	3.399	5.804	22.054	0.573	0.970	2.366	17.994	0.953	1.516	2.420	9.674
NO_x	2.255	4.455	6.243	25.725	0.817	1.617	3.685	38.730	0.962	1.516	2.446	9.677
NO_y	4.300	7.961	10.569	26.068	4.460	7.226	13.191	43.660	3.401	4.381	6.621	12.383
HNO_3	0.509	1.044	1.300	4.383	0.682	1.295	3.050	8.556	0.180	0.544	0.869	2.398
HONO	0.062	0.150	0.255	0.590	0.065	0.135	0.250	1.030	0.045	0.083	0.128	0.628
HCHO	0.126	0.209	0.360	0.926	0.219	0.316	0.593	1.346	0.110	0.191	0.286	1.105
CH_4	2.00	2.25	2.65	4.30	2.00	2.25	2.80	6.10	2.00	2.10	2.30	4.30
NMHC	0.10	0.20	5.25	1.40	0.10	0.25	0.60	1.60	0.10	0.20	0.30	1.00

*) Q_1: first quartile (25th percentile)
#) Q_2: second quartile (median)
+) Q_3: third quartile (75th percentile)
BDL: below detection limit

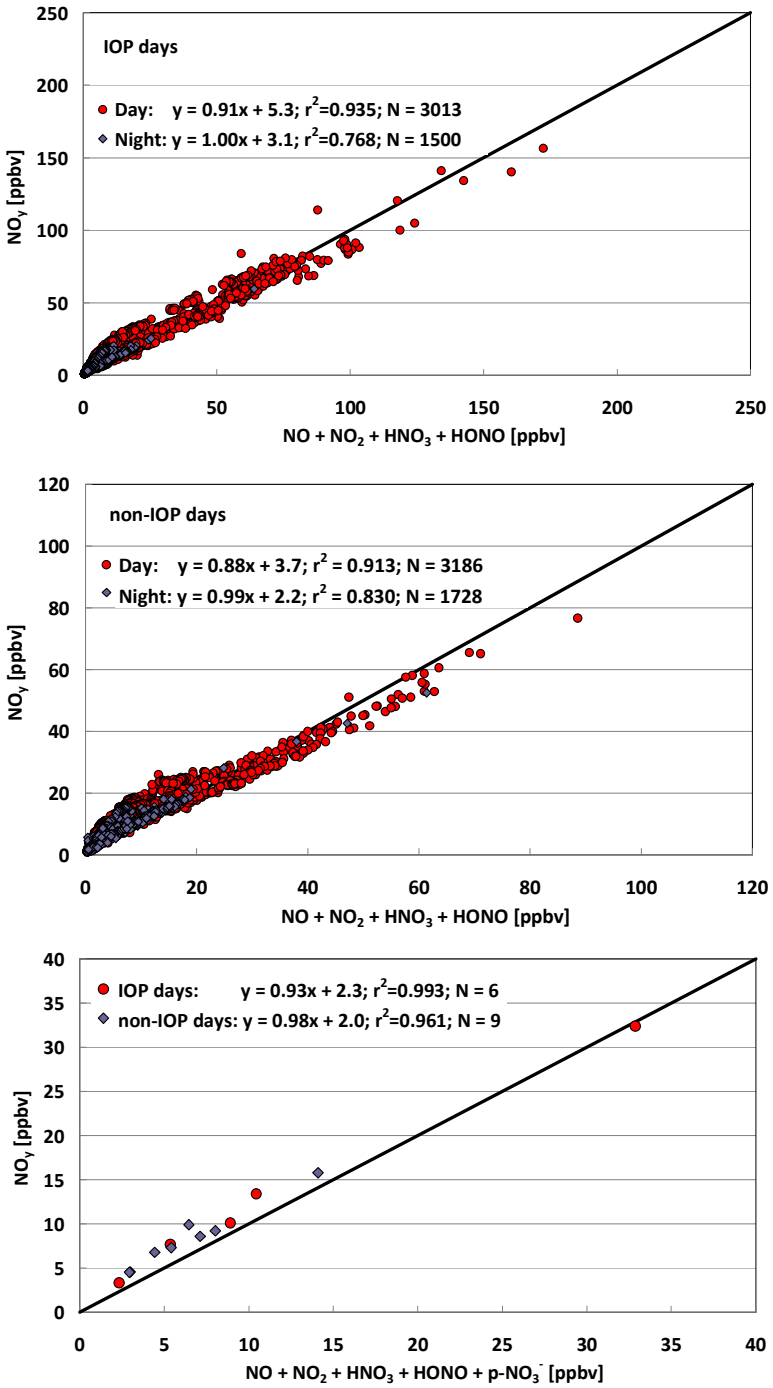

S3. NO_y mixing ratios versus sum of mixing ratios of individual NO_y compounds NO, NO_2, HNO_3, HONO, and particulate NO_3. N denotes number of data points.

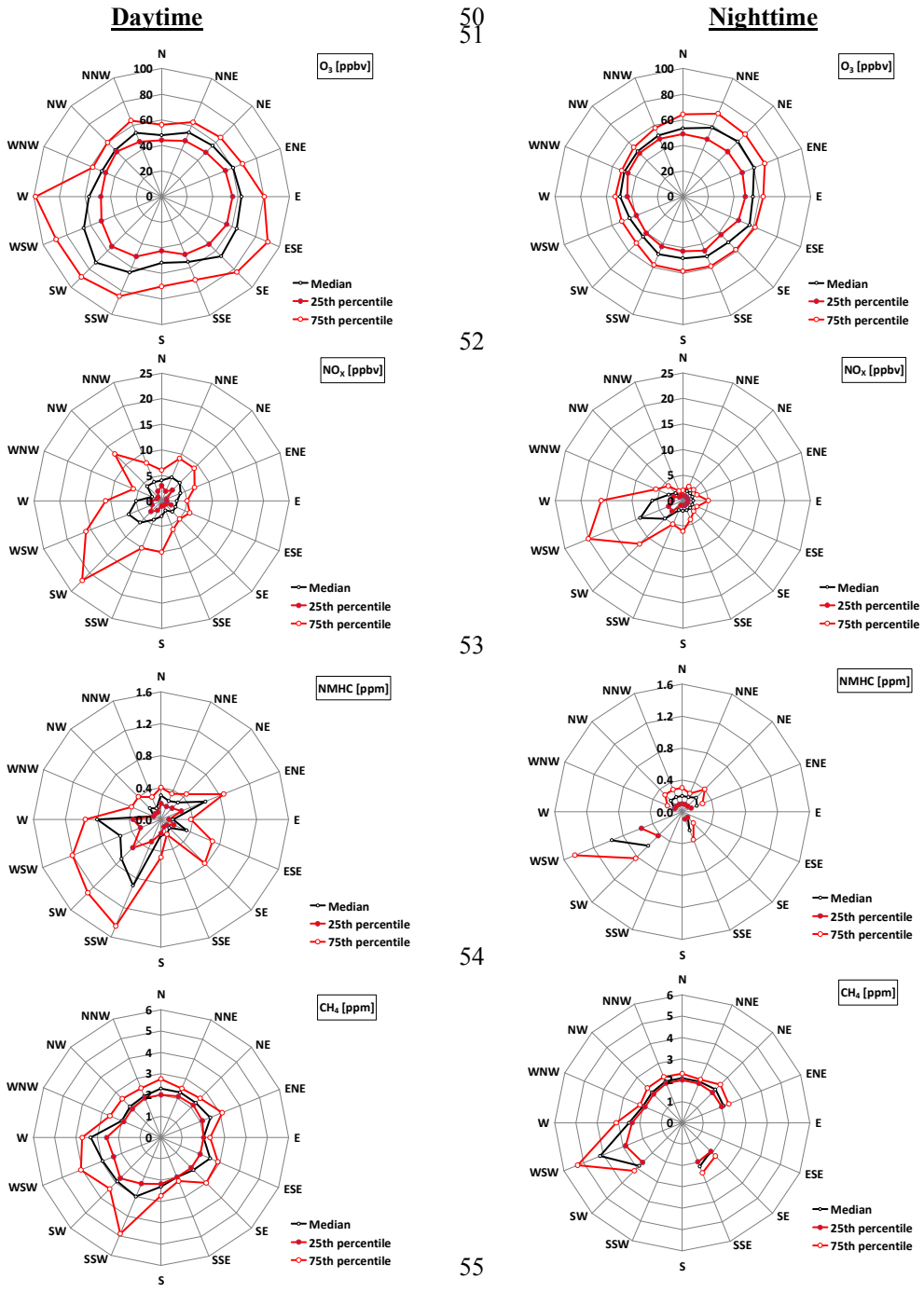

S4a. Wind directional dependence of selected trace gases for day- and night-time conditions (night-time defined as time periods with solar radiation less than 1 W/m^2). Units shown in brackets refer to the radial direction of the corresponding trace gas plot.

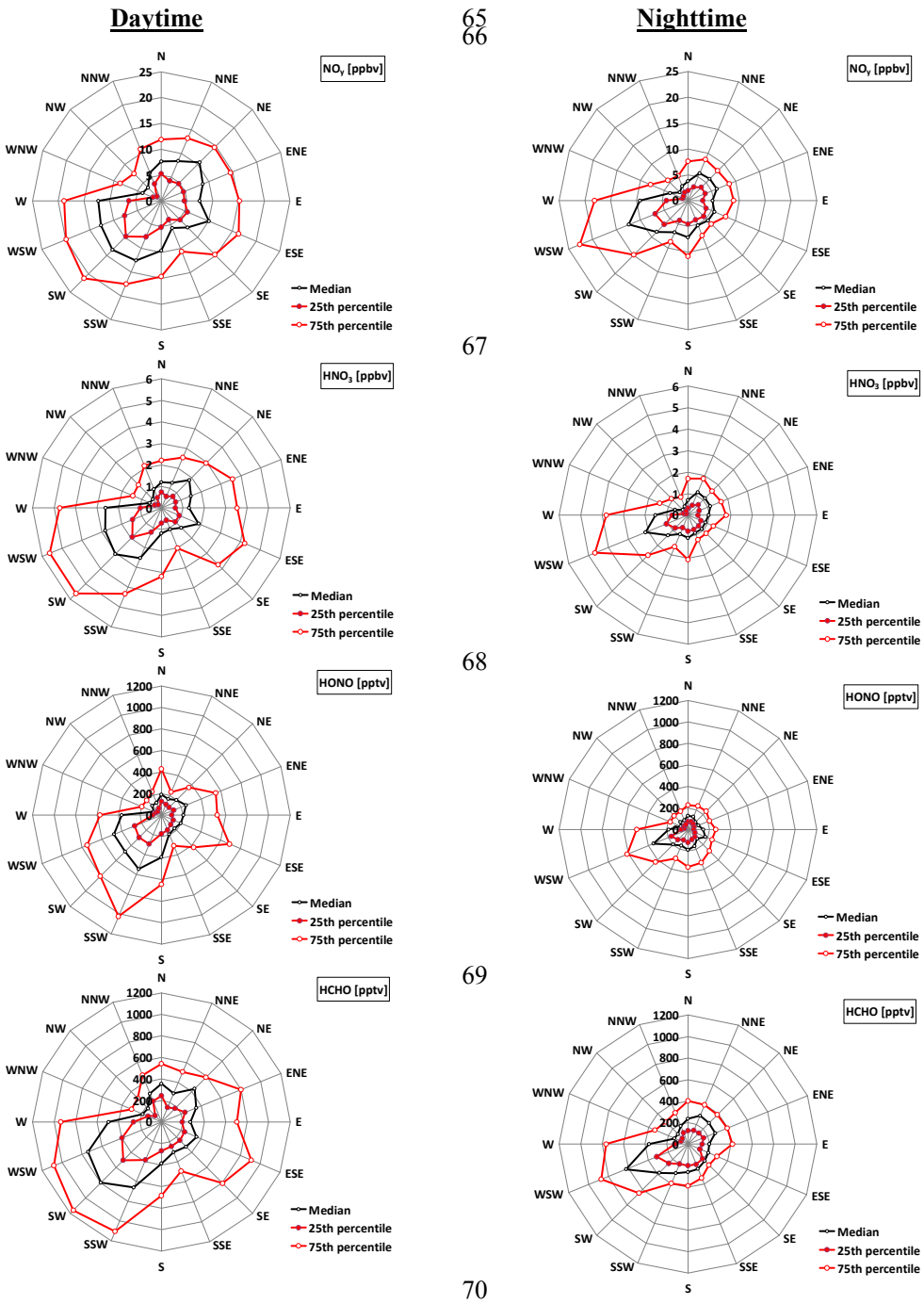

S4b. Wind directional dependence of selected trace gases for day- and night-time conditions (night-time defined as time periods with solar radiation less than 1 W/m^2). Units shown in brackets refer to the radial direction of the corresponding trace gas plot.

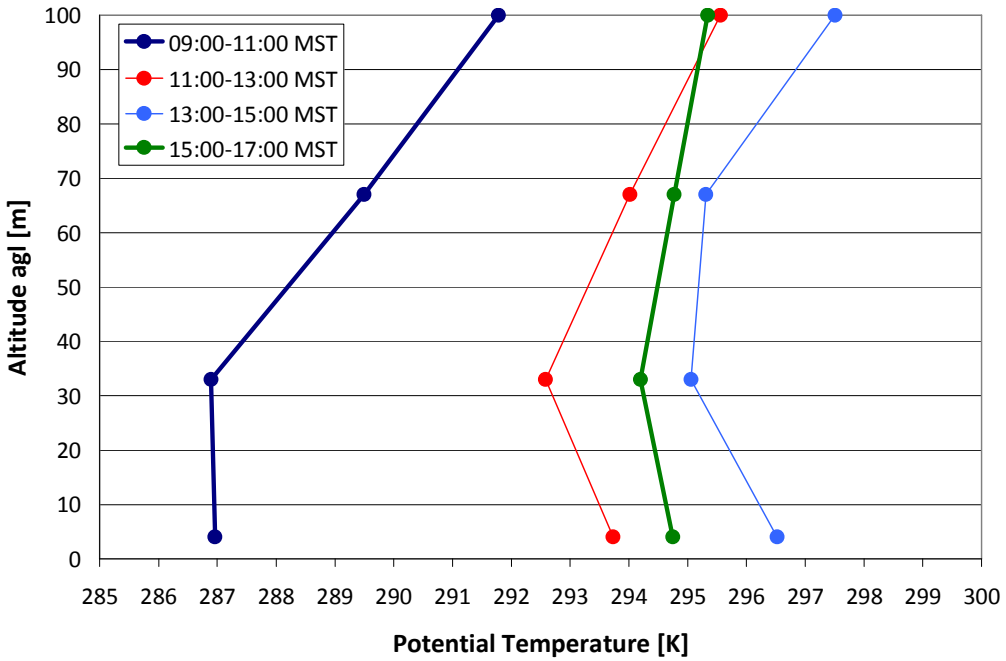

S5. Potential temperature profiles on IOP days based on tethersonde measurements segregated into selected time frames.

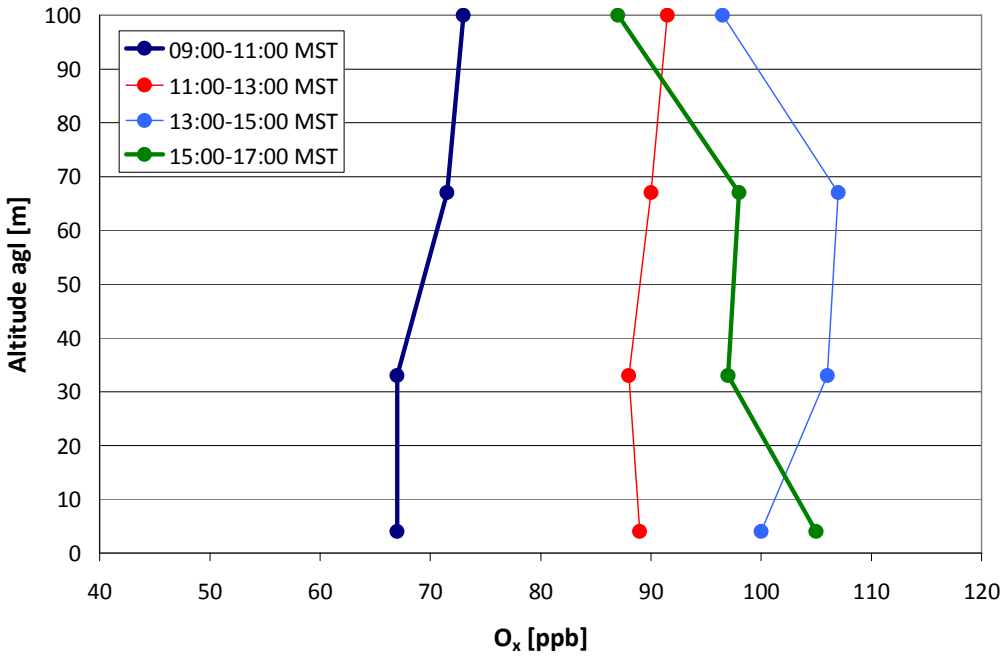

S6. Profiles of potential ozone O_x (O_x=O_3+NO_2) on IOP days based on tethersonde measurements segregated into selected time frames.

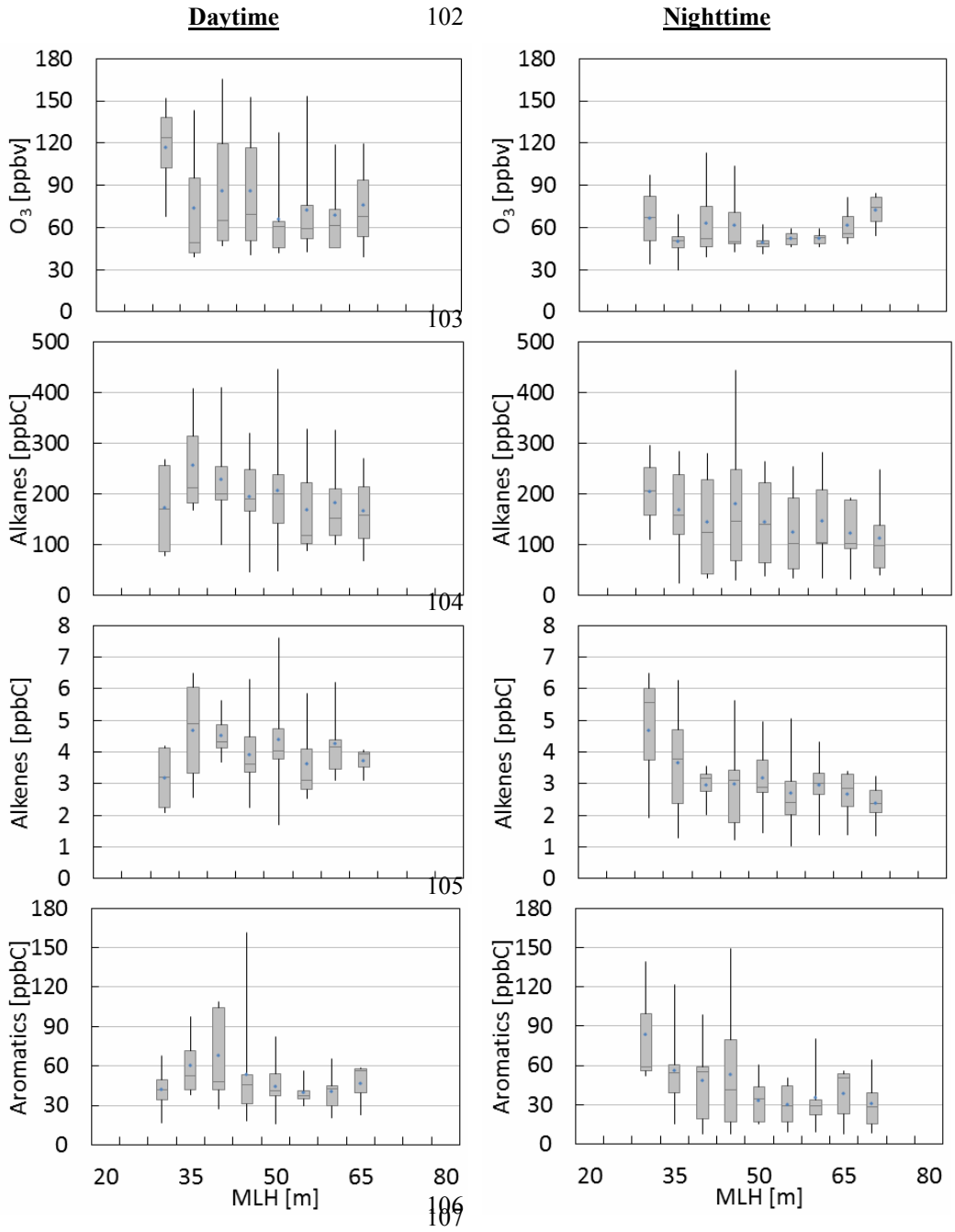

S7. Selected trace gas mixing ratios versus mixing layer heights (MLH) for day- and night-time conditions on IOP days (night-time defined as time periods with solar radiation less than 1 W/m^2). Speciated NMHC, CO, and NO_x data from the Boulder South Road site.

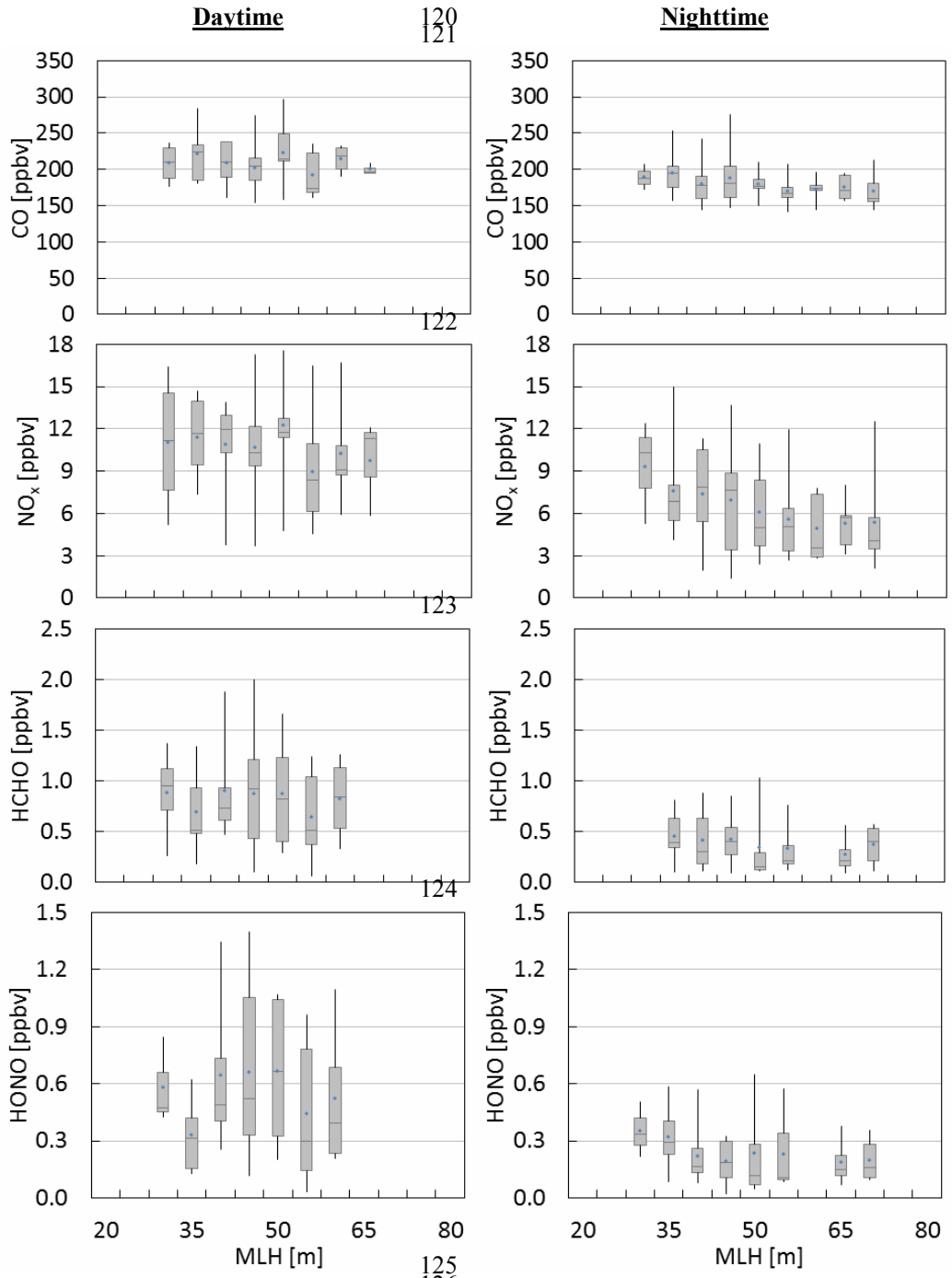

S7. continued.

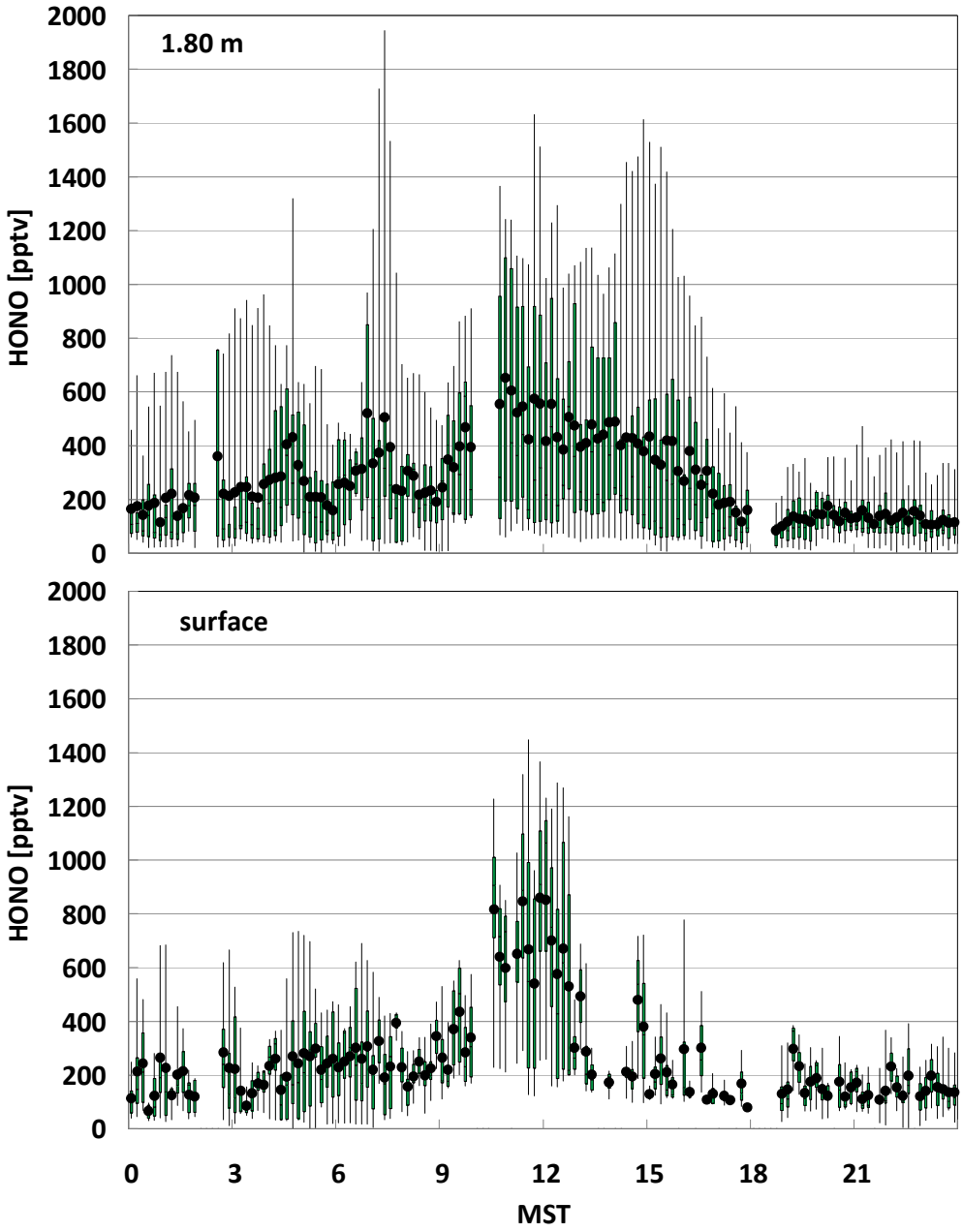

S8. Box-Whisker plots for the mean diurnal variations of HONO mixing ratios at 1.80 m above ground and close to the surface (10 cm above the ground) during the period 28/2 - 3/16/2011.

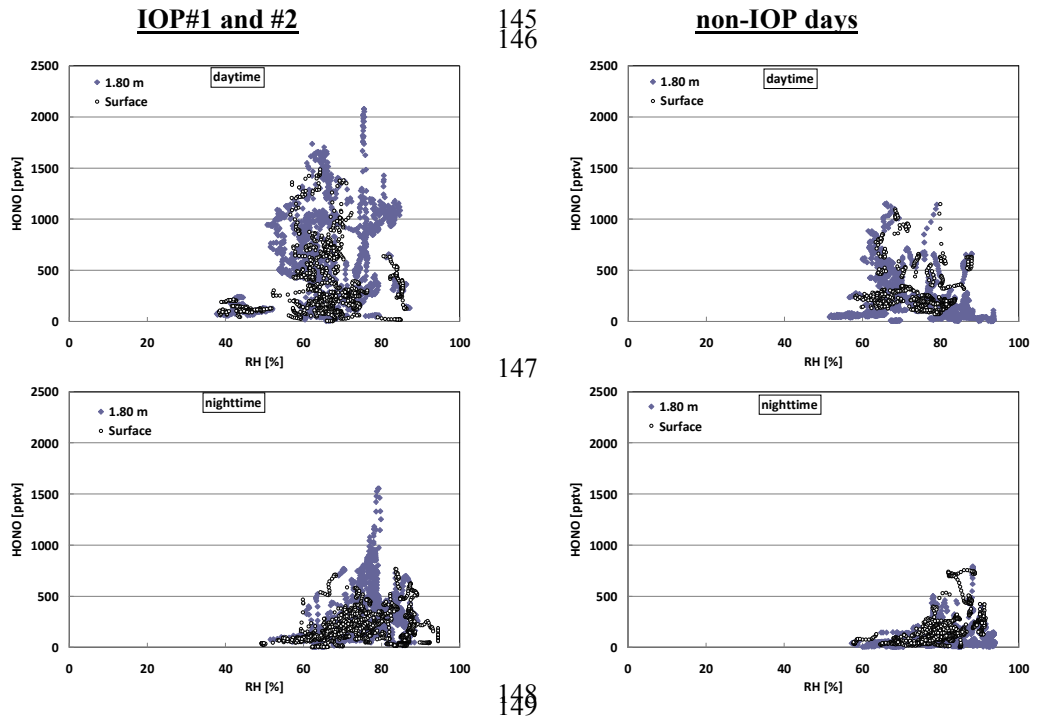

S9. HONO mixing ratios versus relative humidity for day- and night-time conditions on IOP and non-IOP days (night-time defined as time periods with solar radiation less than 1 W/m^2).

S10. Results of correlation analysis of HCHO and HONO versus selected other trace gases at the Boulder site for nighttime conditions and wind direction 180°-270°. All data 10-min values, apart from correlations which include NMHC or CH_4, which are hourly values.

	a*)	b**)	r^2
HCHO vs CH_4	0.223 (±0.040)	-148.4 (±158.7)	0.71
HCHO vs NMHC	0.493 (±0.098)	258.3 (±102.6)	0.66
HCHO vs NO_x	15.44 (±1.45)	324.7 (±31.2)	0.60
HONO vs CH_4	0.188 (±0.036)	-225.9 (±138.5	0.70
HONO vs NMHC	0.441 (±0.070)	91.2 (±69.2)	0.77
HONO vs NO_2	16.82 (±0.95)	148.5 (±19.1)	0.80
HONO vs NO_x	15.20 (±0.88)	161.5 (±19.1)	0.79
HONO vs HNO_3	100.92 (±5.95)	88.1 (±22.6)	0.80

***) a: slope in [pptv/ppbv]**
****) b: intercept in [pptv]**

S11. Values of indicator ratios for NO_x-sensitive, transitional, and VOC-sensitive conditions according to Sillman (2002) and Sillman and He (2002). Photochemical indicators for the moderately polluted case (80 ppbv < O_3 < 200 ppbv), unless otherwise stated.

Formatted: Subscript

Indicator	Median VOC sensitive	Transition (O_3 < 80 ppbv)	Transition	Median NO_x sensitive
O_3/NO_y	5	11-15	6-8	11
O_3/NO_z	6	15-20	8-10	14
O_3/HNO_3	9	n.a. **)	12-15	20
EOR*)	EOR < 0.6	n.a. **)	0.6 < EOR < 0.9	EOR > 0.9

Formatted Table

Formatted: Subscript

*) Extent of Reaction

**) no information given by Sillman and He (2002), but presumably higher than for the moderately polluted case.

S12. Average minimum values of photochemical indicators at the Boulder site and time periods and wind directions associated with these minimum values.

Indicator	Average minimum median values and time of occurrence	Average minimum median values and wind direction of occurrence
O_3/NO_y	3.1 (09:00 MST)	3.2 (SSW)
O_3/NO_z	10.1 (14:00 MST)	9.2 (SSW)
O_3/HNO_3	14.1 (09:00 MST)	11.0 (W)
EOR*)	0.53 (08:00 MST)	0.55 (WSW)

*) Extent of Reaction

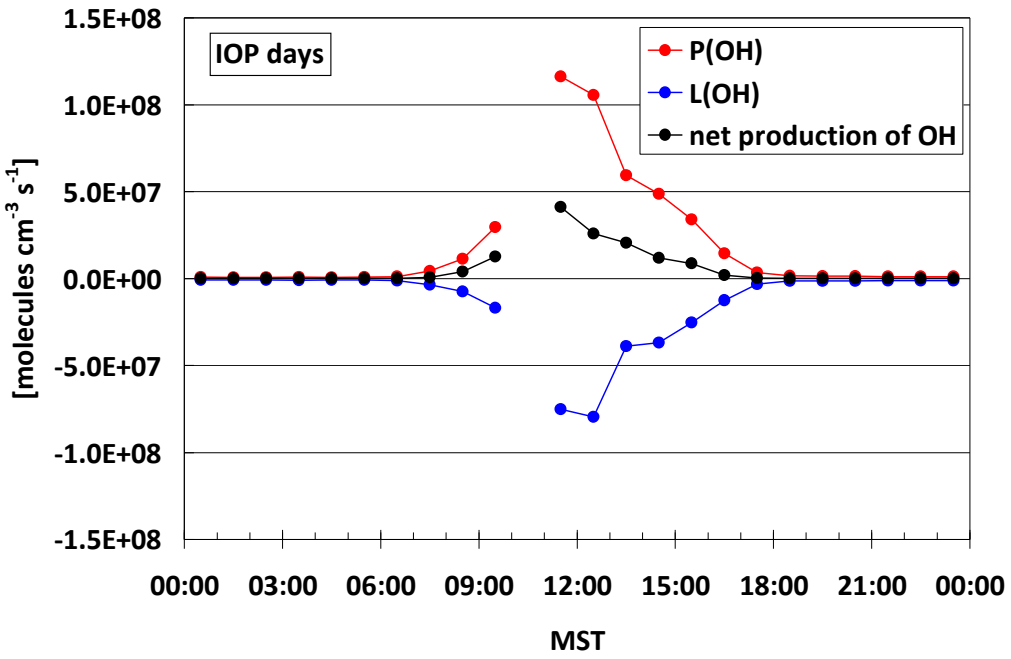

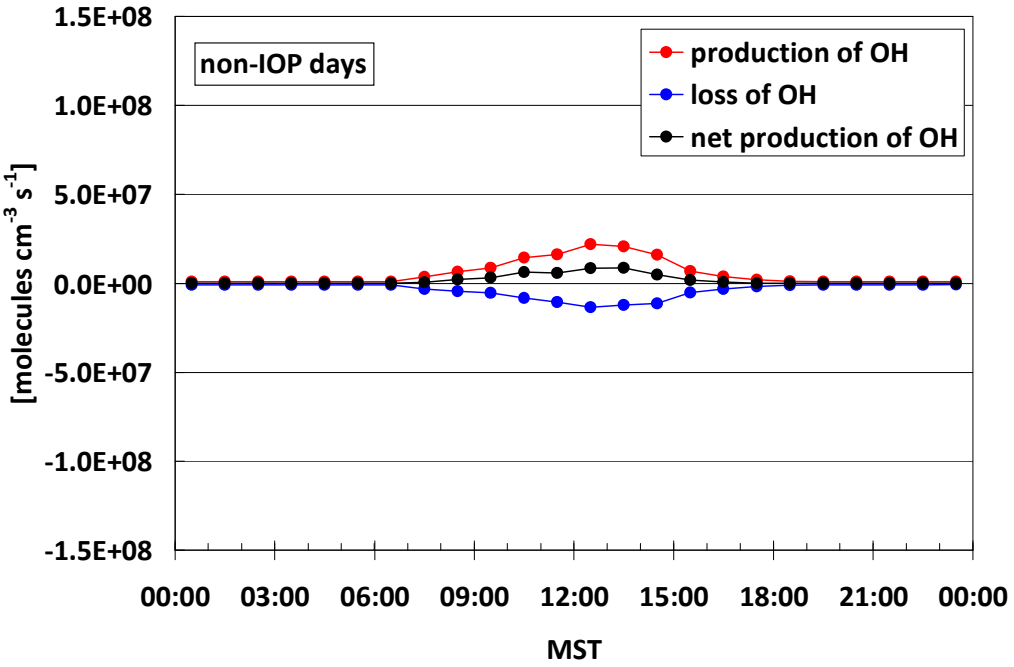

S13. Calculated production and loss rates of OH production, as well as net production rate of OH on IOP and non-IOP days.

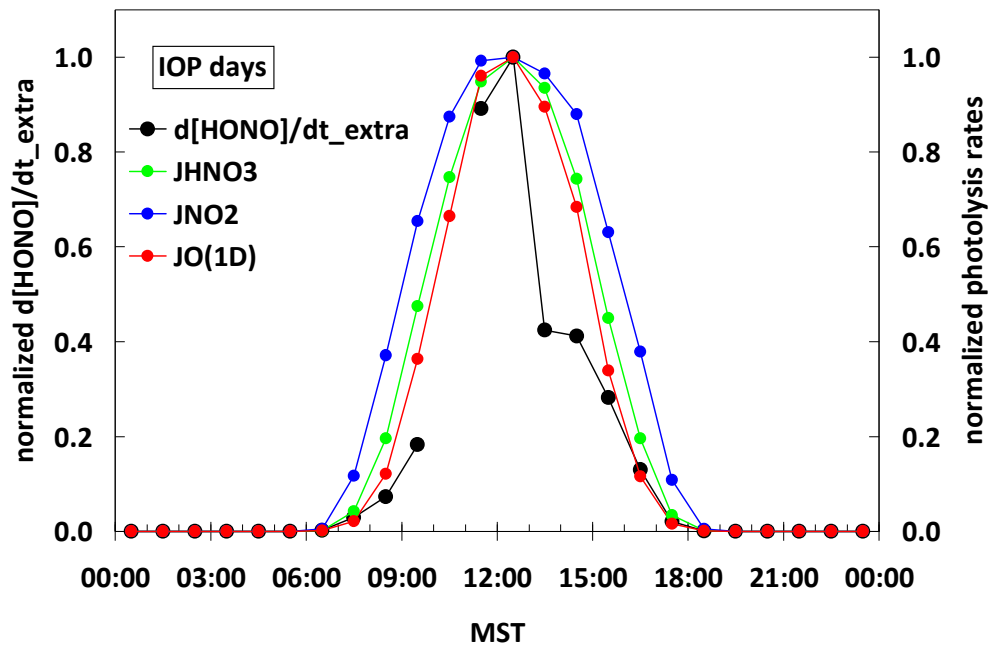

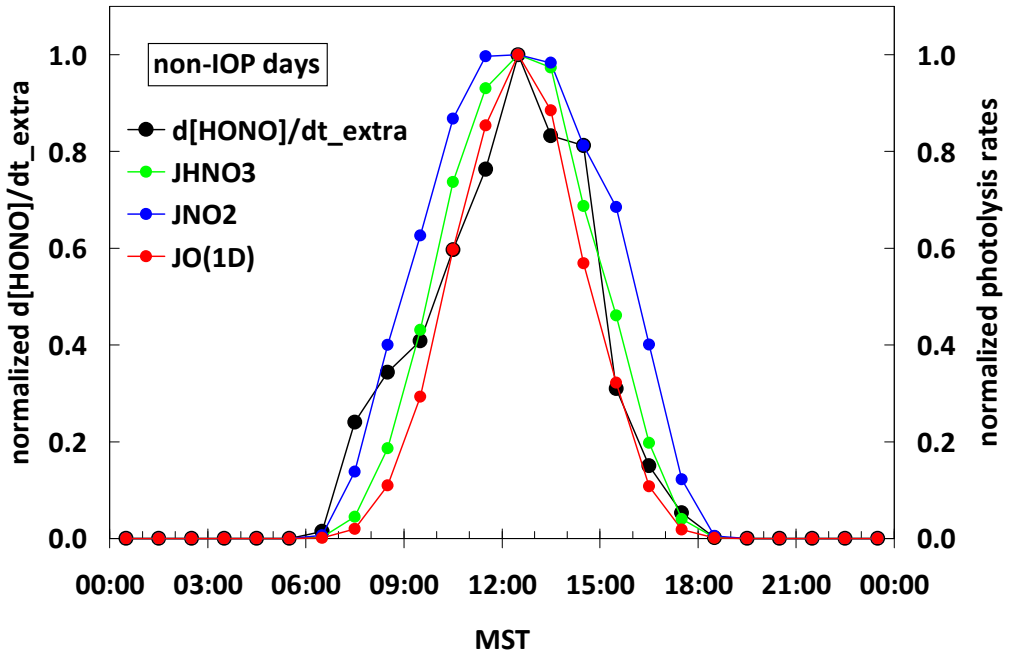

S14. Median diurnal variation of HONO extra source and J_{HNO3}, J_{NO2}, and $J_{O(1D)}$, normalized to their corresponding daily maximum median value on IOP and non-IOP days.

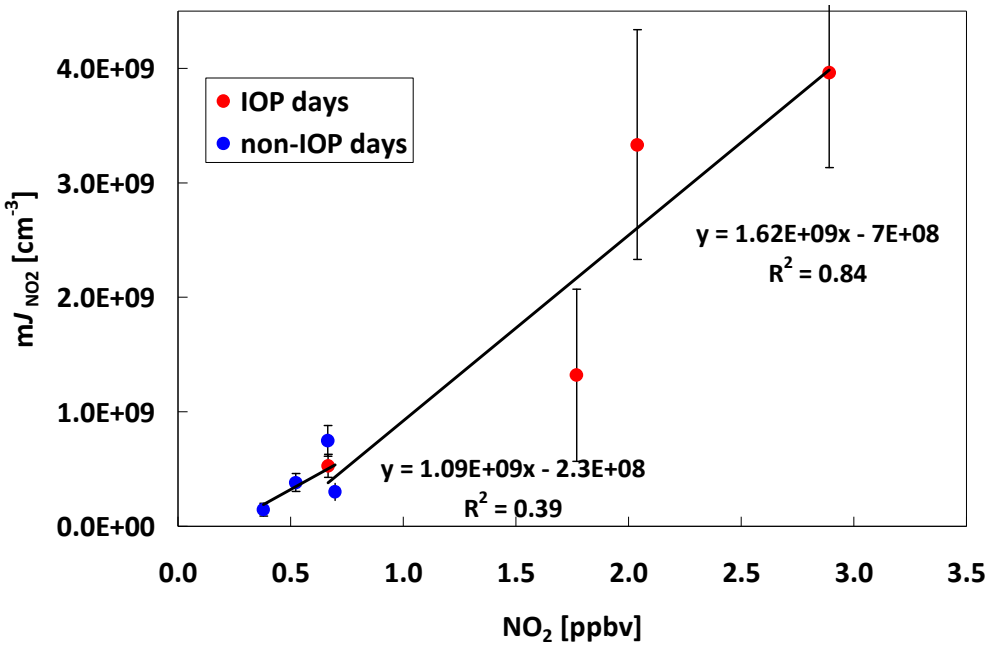

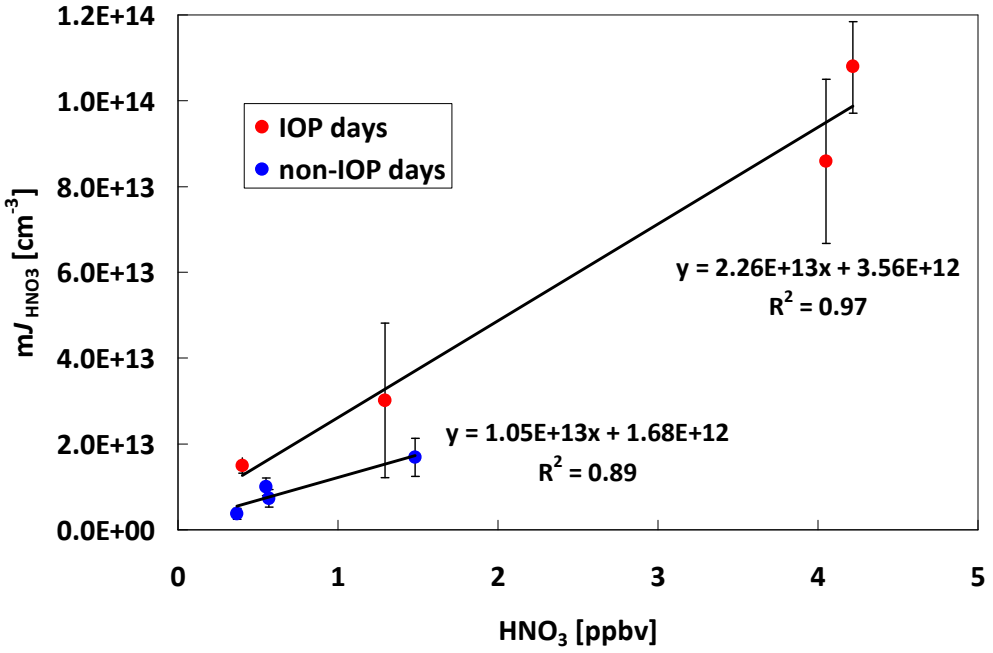

S15. Correlations of mJ_{NO2} and mJ_{HNO3} versus daily median NO_2 and HNO_3 mixing ratios on IOP and non-IOP days. Days with daily median NO mixing ratios greater than 500 pptv were excluded.